DOCTORAL THESIS

Experimental study and reaction kinetics of 1,3-butadiene synthesis from bioethanol over an Hf-Zn/SiO_2 catalyst

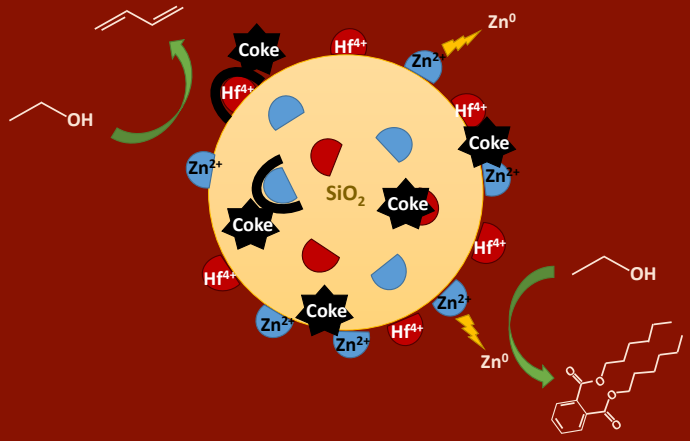

Author: Gracia María Cabello González

Thesis supervisors: Dr. Ángel L. Villanueva Perales

Dr. Fernando Vidal Barrero

Dr. Manuel Campoy Naranjo

Departamento de Ingeniería Química y Ambiental

Escuela Técnica Superior de Ingeniería

Universidad de Sevilla

2020

Doctoral Thesis

Experimental study and reaction kinetics of 1,3-butadiene synthesis from bioethanol over an Hf-Zn/SiO_2 catalyst

Author:

Mrs. Gracia María Cabello González

Thesis supervisors:

Dr. D. Ángel L. Villanueva Perales

Dr. D. Fernando Vidal Barrero

Dr. D. Manuel Campoy Naranjo

Dpto. de Ingeniería Química y Ambiental

Escuela Técnica Superior de Ingeniería

Universidad de Sevilla

Sevilla, 2020

Not all those who wander are lost

Acknowledgements

This work would have never been possible without my thesis supervisors, Dr. Fernando Vidal, Dr. Manuel Campoy and Dr. Ángel L. Villanueva, for their guidance and dedication. They have been the helm in the storm. I wish also to acknowledge the invaluable help provided by Agustín Martinez and his group from the *Instituto de Tecnología Química (ITQ-UPV-CSIC)* for the collaboration in the realization of this study.

I am particularly grateful to my family, for their unconditional support along the years, as well as to Luis, for his patience, affection and understanding. Also to my friends since always. Sergio, for being the hammer, the edge of my sword, the tip of my spear, the mail about my fist and the flight of my arrows. Thanks to Javi and Marichu for fighting alongside me against leaks and glass wool. To Sara and Bego, for being always there.

I would like to express my very great appreciation to those people who have lately managed to sneak out in my life without me noticing. To Emilio for his intense conversations about time travel and cat behaviour; Isa and Max, experts in making me re/disconnect; Jose "the kinetic guy", buen clima; Chris, for being an human grammar corrector and the best Penguin bars provider ever; Ivan, for letting me take him out of home from time to time; and last but not least, Pedro, Mr. Blue Caterpillar, for filling my mornings and afternoons with laughs.

Thanks to my colleagues from L13 and other places of the ETSI, Fernando Castaño, Mari Ángeles, Miguel, Paco, and Camilo. Also Maite, Diego and Rafael. Days go faster with you.

Finally, I would like to offer my special thanks to my *sabonims* Javier and Alejandro, and to my comrades in arms, especially to my *nakamas* Fran and David, but not forgetting Jesús, Natacha, Anika, Galván, Ricardo and everyone else. They taught me other ways to face the roads. Hai dong!

Abstract

In recent years, considerable interest in bio-1,3-butadiene has been aroused by the reduced 1,3-butadiene supply, due to the shift from oil-based naphtha cracking to shale gas-based ethane cracking as a consequence of the extreme volatilities in fossil oil price and low shale gas cost in the United Stated. Besides, the steam cracking process is associated to a high energy consumption and release considerable amount of greenhouse effect gases to the atmosphere. These facts have stimulated the interest in robust cost-efficient alternative systems that can be adapted to the new environmental policies in order to mitigate climate change and reduce dependency on importations.

In this framework, ethanol raises as an attractive and environmentally friendly feedstock for the production of 1,3-butadiene as a chemical product at commercial scale as it can be cost-efficiently produced from a variety of renewable biomass and waste sources and its production is growing worldwide, what makes it the perfect candidate for integrated biorefining systems.

The process includes two routes: the two-step pathway where, in the first step, acetaldehyde is generated from ethanol and, in the second step, the acetaldehyde/ethanol mixture is converted to 1,3-butadiene; and the one-step method where both reactions occur over the same catalyst.

This thesis focuses on the fundamental and practical aspects of the one-step process over a bimetallic Hf-Zn catalyst. First, the elucidation of the main reactions leading to 1,3-butadiene and by-products was made by means of kinetic curves and catalytic tests where intermediates were individually fed. Besides, the convenience of by-product separation from unreacted ethanol in an industrial process was studied by performing experiments where ethanol was co-fed with intermediates. Furthermore, the causes of catalyst deactivation and the impact on catalyst structure and performance of regeneration by air calcination were assessed. Also, the combined effect of the reaction conditions and the quality of the feedstock on the catalyst performance was investigated. Finally, a kinetic model was developed assuming a power-law model with an extra term to consider the effect of water on the reactions.

Our results show that the pathway from ethanol to 1,3-butadiene over the Hf-Zn catalyst involves the following reactions: (i) ethanol dehydrogenation to acetaldehyde; (ii) aldol condensation of acetaldehyde to crotonaldehyde (iii) crotonaldehyde reduction to crotyl alcohol with ethanol; (iv) 1,3-butadiene formation by crotyl alcohol dehydration. Also, numerous side-products are formed over the catalyst. When designing the separation system of the one-step process, the recycling to the reactor of unreacted ethanol along with some side-products, such as butanal and acetone, should be avoided, since they are further transformed into undesired ones, such as heavy compounds, which cause catalyst deactivation and equipment fouling.

The presence of water in the ethanol feed induces the generation of Brønsted acid sites on the catalyst surface, which results in (i) lower ethanol conversion, as some Zn^{2+} Lewis acid sites, active for the dehydrogenation of ethanol, are transformed into Brønsted acid sites and (ii) higher selectivity to dehydration products catalyzed by Brønsted acid sites and favoured by the higher ethanol partial pressure. Besides, water inhibits aldol condensation reactions by blocking Hf^{4+} active sites. This effect is beneficial at a high operating temperature, where acetaldehyde is so reactive that it is rapidly converted to heavy compounds unless water is present.

A power-law kinetic model of the synthesis of 1,3-butadiene from ethanol over the Hf-Zn/SiO_2 catalyst was built and validated with experimental data of catalyst performance. The kinetic model is capable to predict the formation of the main reaction products and adjust catalyst performance if water is present in the ethanol feed. This kinetic model is useful to optimize the design of the one-step process, considering the interactions between the reactor and the separation area.

Finally, catalyst deactivation is mainly caused by the retention of oxygenated aromatic-type coke species, preferentially formed on the dehydrogenating Zn^{2+} sites associated with the hemimorphite component of the catalyst, and also by a loss in Zn^{2+} sites due to the reduction to Zn^0 during catalysis. The presence of water in the feedstock drastically reduces the catalyst deactivation as it hinders heavy compounds production. Also, regeneration by calcination with air removes coke and re-oxidizes a fraction of Zn^0 back to Zn^{2+}, but it does not fully re-establish the original Zn^{2+}/Hf^{4+} balance.

Resumen

En los últimos años, el proceso de steam cracking para producir eteno ha cambiado, dejando de utilizar como materia prima naftas procedentes del crudo petrolífero para alimentar gas de esquisto. Esto ha sido debido a la alta volatilidad en el precio del petróleo y al bajo costo del gas de esquisto en los Estados Unidos. Como consecuencia, la producción de 1,3-butadieno, principal coproducto del steam cracking de naftas, se ha visto reducida drásticamente. Además, el steam cracking está asociado a un alto consumo energético y libera una considerable cantidad de gases de efecto invernadero a la atmósfera. Estos hechos han estimulado el interés en desarrollar sistemas alternativos, robustos y económicamente rentables que se adapten a las nuevas políticas ambientales que surgen para mitigar el cambio climático y reducir la dependencia del petróleo.

En este marco, el etanol surge como una materia prima, atractiva y respetuosa con el medio ambiente, para la producción de 1,3-butadieno. El bioetanol es actualmente un producto químico que se produce de manera rentable a gran escala a partir de una gran variedad de fuentes renovables de biomasa y desechos. Además, su producción está creciendo en todo el mundo, hecho que lo convierte en el candidato perfecto para desarrollar sistemas de biorrefinerías integradas.

El proceso para convertir etanol en 1,3-butadiene incluye dos rutas: la ruta de dos pasos donde, en el primer paso, se genera acetaldehído a partir de etanol y, en el segundo paso, la mezcla de acetaldehído / etanol se convierte en 1,3-butadieno; y el método de un paso, donde ambas reacciones ocurren sobre el mismo catalizador. Esta tesis se centra en los aspectos fundamentales y prácticos del proceso de un paso sobre un catalizador bimetálico Hf-Zn.

En primer lugar, se realizó el estudio de las principales reacciones que conducen a 1,3-butadieno y al resto de subproductos mediante curvas cinéticas y pruebas en las que los posibles productos intermedios de reacción se alimentaron individualmente. Además, se estudió la conveniencia de separar los subproductos que acompañan al etanol recirculado al reactor mediante la realización de experimentos en los que el etanol se alimentó junto con productos intermedios, susceptibles de ser también recirculados.

Por otra parte, se evaluaron las causas de la desactivación, el impacto sobre la estructura del catalizador y el rendimiento de la regeneración por calcinación con aire. Asimismo, se investigó el efecto combinado de las condiciones de reacción y la calidad de la materia prima sobre el rendimiento del catalizador. Finalmente, se desarrolló un modelo cinético asumiendo un modelo potencial con un término adicional para considerar el efecto del agua en las reacciones.

Los resultados obtenidos muestran que la ruta para dar 1,3-butadieno a partir de etanol sobre catalizadores de Hf-Zn incluye las siguientes reacciones: (i) deshidrogenación de etanol a acetaldehído; (ii) condensación aldólica de acetaldehído a crotonaldehído (iii) reducción de crotonaldehído a alcohol crotílico con etanol; y (iv) formación de 1,3-butadieno mediante deshidratación de alcohol crotílico. Por otra parte, debe evitarse la realimentación al reactor de algunos subproductos como el butanal y la acetona, ya que favorecen algunas reacciones secundarias no deseadas transformándose en compuestos pesados que causan la desactivación del catalizador y ensucian los equipos.

La presencia de agua en la alimentación de etanol induce la generación de centros ácidos de Brønsted en la superficie del catalizador, lo que resulta en (i) una menor conversión de etanol, ya que algunos centros ácidos de Lewis (Zn^{2+}), activos para la deshidrogenación de etanol, se transforman en centros ácidos de Brønsted y (ii) una mayor selectividad a los productos de deshidratación catalizados por los centros ácidos de Brønsted y favorecida por una mayor presencia de etanol en el medio. Asimismo, el agua inhibe las reacciones de condensación aldólica al bloquear los centros activos de Hf^{4+}, lo que es beneficioso a altas temperaturas de operación, donde el acetaldehído es tan reactivo que se convierte rápidamente en compuestos pesados a menos que haya cierta cantidad de agua presente en el medio.

Además, se propuso y validó, a través de resultados experimentales, un modelo cinético de la síntesis de 1,3-butadieno a partir de etanol sobre el catalizador Hf-Zn/SiO_2. El modelo es capaz de predecir la formación de los principales productos de reacción y ajustar el rendimiento del catalizador para el caso de que haya agua presente en la alimentación de etanol. Por lo tanto, es útil para optimizar el diseño del proceso de un solo paso, considerando las interacciones entre el reactor y el área de separación.

Por último, la principal causa de desactivación del catalizador es la generación y deposición de especies de coque formadas en los centros deshidrogenantes asociados con la hemimorfita del catalizador (Zn^{2+}), pero también por una pérdida de esos centros debido a la reducción de Zn^{2+} a Zn^0. En este sentido, una mayor presencia de agua en el medio alarga la vida del catalizador, ya que inhibe la formación de compuestos pesados precursores del coque. La regeneración por calcinación con aire elimina el coque y reoxida una fracción de Zn^0 a Zn^{2+}, pero no restaura completamente el equilibrio original de centros.

Summary

LIST OF FIGURES

LIST OF TABLES

Nomenclature

a	Fitting parameters of the water corrective terms (bar^{-1})
A	Pre-exponential factor (mol/g h $bar^{\Sigma ni}$)
Ac	Acetaldehyde
b	Fitting parameters of surface response model
BD	1,3-Butadiene
But	Butenes
ButA	Butanal
ButOH	Butanol
C	Total number of compounds
CP-MAS NMR	Cross Polarization Magic Angle Spinning Nuclear Magnetic Resonance
C_4	Butenes
C_{6+}	Heavy compounds
d	Diameter (mm)
D	Diffusion coefficient
DEE	Diethyl ether
e	residual
Ea	Activation Energy (kJ/mol)
Et	Ethene
EtOH	Ethanol
F	Total molar flow (mol/h)
F_k	Molar flow of compound k (mol/h)
FID	Flame Ionization Detector
H	Hydrogen
HC	Heavy Compounds
ICP-OES	Inductively coupled plasma – optical emission spectrometry
IR	Infrared radiation
J	Jacobian matrix of parameters
k	Mass transfer coefficient (m/s)
L	Length (mm)
m	Exponent of the water corrective term

MPVO	Meerwein-Ponndorf-Verley-Oppenauer reduction
n	Reaction order
N	Total number of tests
Ndf	Number of degrees of freedom
NR	Number of reactions in the kinetic model
OC	Oxygenated Compounds
P	Total pressure (bar)
P_k	Partial pressure of compound k (bar)
r	Reaction rate (mol/h g)
R	Ideal gas constant (8.314 J/mol K)
RSM	Response surface methodology
S_k	Carbon selectivity to compound k
SSEf	Sum of the squared errors of molar flow rates
$SSEr_i$	Sum of the squared errors of the reaction rates for reaction i
STEM-EDX	Scanning transmission electron microscopy – Energy-dispersive X-ray
t	Student's t-distribution
T	Reaction temperature (°C or K)
TCD	Thermal conductivity detector
TOS	Time-on-stream (h)
Tr	Trace of a matrix
V	Covariance matrix of parameters
W	Mass of catalyst (g)
Wat	Water
Wc	Water content (wt %)
WHSV	Weight hourly space velocity (h^{-1})
X_k	Conversion of compound k
XPS	X-ray photoelectron spectroscopy
XRD	X-ray powder diffraction
y_k	Mole fraction of compound k
Y_k	Carbon yield of compound k

Subscripts/ Superscript

b	bulk
c	catalyst
e	effective
i	reactions
j	experiments
k	compounds
obs	observed
p	pellets
ref	reference
regen	regenerated
S	surface of the catalyst
^	predicted by the model

Greek letters

α	confidence level
ρ	density (kg/m^3)
σ	standard deviation
θ	vector of kinetic model parameters
υ	stoichiometric coefficient

Outline

This document is organized into the following sections

- **Introduction:** in this chapter, some background information will be given to set the framework for this research. The importance, applications and fields of study of the ethanol to 1,3-butadiene route will be also commented.

- **Background and scope**: this thesis is put into context with the investigation lines of the Bioenergy Group (Chemical and Environmental Engineering Department of the University of Seville), namely, thermochemical conversion of biomass, synthesis of biofuels and bioproducts as well as about the design, simulation, evaluation and optimization of those processes.

- **Objectives**: this section defines the aims of this thesis and lists the specific goals to be achieved at the end of this work.

- **Methodology**: it includes the actions taken to reach the aforementioned objectives. The experimental laboratory facility is described as well as the specific procedures used to analyse the test results. Also, the kinetic model development is explained in detail.

- **Results and discussion**: the results of the experimental tests are presented and discussed in this section, along with the determination of the parameters of the kinetic model and its validation.

- **Conclusions**: the main findings of the research work are presented and future lines of work are proposed.

- **References**: it gathers all the bibliographic information consulted in the development of this document.

1. INTRODUCTION

Conjugated dienes are extensively used as monomers in polymerization reactions for the plastic and synthetic rubber industry. Among them, 1,3-butadiene is a key platform compound used as a chemical intermediate and as a monomer in the manufacture of polymers to produce synthetic rubber, resins and elastomers. Its main industrial application is the production of styrene-butadiene rubber (SBR), polybutadiene rubber (PBR), acrylonitrile-butadiene-styrene (ABS) and polychloroprene (neoprene). Besides, 1,3-butadiene also plays a role in the production of adiponitrile, precursor in the manufacture of nylon. These compounds are mostly related to the automotive industry since they are mainly used in tire manufacture, plastics, hardware and other car components [1][2].

1,3-Butadiene is mostly produced by the petrochemical route as a by-product of the naphtha or gas oil steam cracking process used to obtain ethylene and other light olefins. In the last years, the use of ethane as steam cracking feedstock instead of heavier fractions has risen, leading to ethylene as the main product. Thereby, the amount of 1,3-butadiene available has been reduced while its demand continues growing at 1-4% per year due to the current boost in the automotive industry produced by the rising demand of lightweight and electric vehicles. Thus, 1,3-butadiene short-term demand will not be satisfied by the current capacity of oil refineries.

Nowadays, global 1,3-butadiene demand have shifted to Asia-Pacific, that accounted around a 50% of the global 1,3-butadiene production and consumption in 2017 [3–5].

Current 1,3-butadiene production is not environmentally sustainable as is based on fossil resources [6,7]. In the framework of the 2015 United Nations Paris Agreement, the present guidelines of the European Commission lead to a climate-neutral economy by 2050 based on an industrial decarbonisation policy [8,9]. That way, the production of 1,3-butadiene from bioethanol rises as an alternative that may solve both, demand and sustainability issues, since it is a promising low carbon technology.

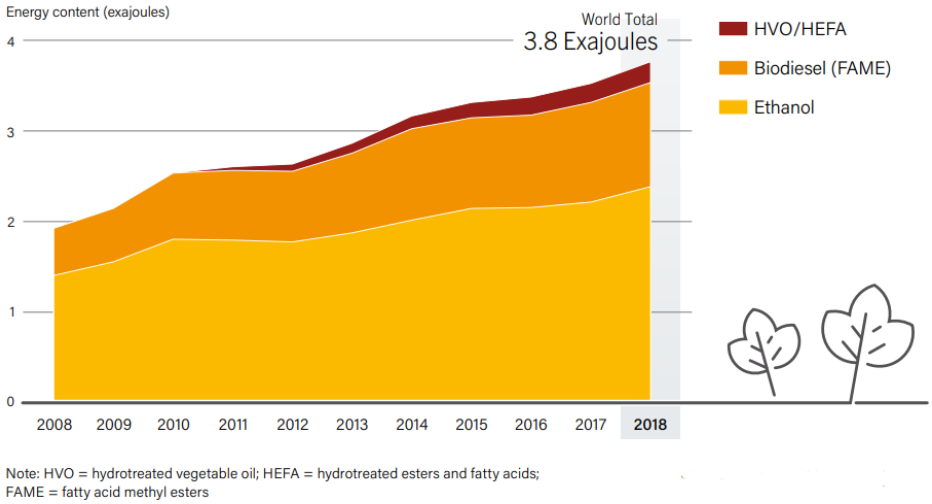

Figure 1. Global Trends in Ethanol, Biodiesel and HVO/HEFA Production [10].

The viability of the success of the ethanol to 1,3-butadiene renewable industry depends, among other factors, on the availability of bioethanol. According to the latest reports, global ethanol production increased nearly 7% in 2018 compared to 2017 (Figure 1). Currently, with around a 83% of production and use taking place in the United States and Brazil combined, bioethanol is the largest biofuel on the market and its production is expected to keep growing in the future [10,11].

The process to catalytically convert ethanol into 1,3-butadiene was industrially born in the 20th century around the time of the Second World War. The so called Lebedev process in the USSR was the first industrial process to produce 1,3-butadiene directly from ethanol (Equation 1), using a $MgO\text{-}SiO_2$ catalyst. Later, in the USA, the Union Carbide and Carbon Chemicals Corporation started the manufacture of 1,3-butadiene from ethanol based on the Ostromislensky two-step pathway to give response to the growing demand for rubber due to the Second World War conflict. In the first step, acetaldehyde is generated by ethanol dehydrogenation, while the second step involves the conversion of the acetaldehyde/ethanol mixture into 1,3-butadiene over a tantalum oxide catalyst on silica. These technologies were abandoned around 1960 due to lack of competitiveness against the petrochemical route [3,12–14].

$$2C_2H_5OH \rightarrow C_2H_6 + H_2O + H_2$$ Equation 1

The ethanol to 1,3-butadiene pathway over heterogeneous catalysts is still a subject of debate. The most accepted route nowadays comprises ethanol dehydrogenation to acetaldehyde, aldol condensation of acetaldehyde to crotonaldehyde, selective reduction of crotonaldehyde by ethanol through Meerwein-Ponndorf-Verley-Oppenauer (MPVO) reaction, and finally, the dehydration of crotyl alcohol to 1,3-butadiene (Figure 2) [3]. That way, the maximum mass yield from ethanol (EtOH) to 1,3-butadiene (BD) is 0.587 kg BD/kg EtOH.

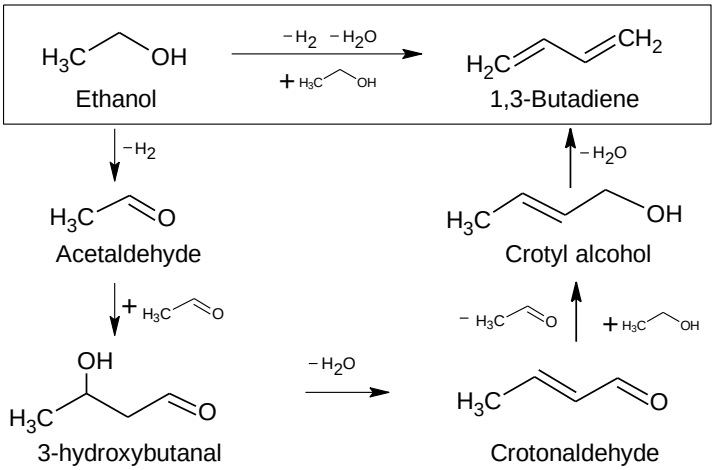

Figure 2. Generally accepted pathway for ethanol conversion to 1,3-butadiene.

Apart from 1,3-butadiene, the reaction main products are water and hydrogen, as well as acetaldehyde, product of the ethanol dehydrogenation. Other intermediate compounds, such crotonaldehyde and crotyl alcohol, are detected as traces. The main side-products are ethene and diethyl ether, direct ethanol dehydration products; ethyl acetate which is believed to be a product of the Tishchenko reaction; acetone, isopropyl alcohol, propylene, C_4-compounds such as butanal, butanol and butenes; C_6-products and heavier compounds, probably formed by the self and cross condensation of aldehydes and alcohols [3].

Although the technical feasibility of the ethanol to 1,3-butadiene route has been already demonstrated by its commercial experience, there is still room for improvement. First, the yield and 1,3-butadiene selectivity of the catalysts used in commercial plants was relatively low. Lebedev assured that the commercial catalyst reached a 1,3-butadiene selectivity carbon based of 70% but, unfortunately, they never revealed the elementary composition of the catalyst so this data could not be checked. In the two-stage process, the yield of the first stage was 92% over a copper-based dehydrogenative catalyst, while the subsequent conversion of ethanol and acetaldehyde to 1,3-butadiene reached a carbon-selectivity of 56% over a silica catalyst doped with Ta_2O_5 [3,13]. The catalyst improvement lies in finding an optimal distribution of acidic and basic centres that maximize 1,3-butadiene selectivity, minimizing the by-product formation and deactivation by coke deposition. In the last years, some catalysts exceeding the performance of old commercial ones have come to light with a 1,3-butadiene selectivity up to 90%.

The impact of this improvement on the economics of the processes is uncertain yet since there exist few techno-economic analysis published in the literature but, from these analyses, it can be concluded that, although the environmental improvement seems significant, the economy of the process still depends on several variable that makes it risky to compete with the traditional oil derived route [6,7,12,15].

In this regard, it is necessary to know how the ethanol composition and its impurities affects the catalyst performance, as well as the side-products recycle. There is currently little information about the effect of water present in the ethanol feedstock on catalyst performance [14,16–18]. This knowledge would allow to know what degree of bioethanol refinement is necessary, since the lower the refinement, the cheaper the ethanol feedstock. Also, the effect of by-product recirculation is key to determine to what extent it is convenient to recirculate to find a trade-off between operating and investment costs and 1,3-butadiene productivity. That way, it is necessary to determine a kinetic model of the catalysts in order to be able to choose the reaction conditions that optimize the whole process.

2. BACKGROUND AND SCOPE

Nowadays, the always increasing world energy and chemicals demand is mostly satisfied by the consumption of fossil resources. The main problems derived from its extensive use are the depletion of the oil reserves, the high dependence of countries with fossil resources and high supply risks, and the amount of greenhouse gas emissions in their combustion or transformation. An alternative to cope with this situation in the chemical sector is to develop biorefineries, integrated bioresources-conversion processes used to generate biobased products (ethanol, butanol, 1,3-butadiene, acetaldehyde, aromatic compounds…), as an alternative to current petroleum refineries, changing the market to competitive bioresources produced from renewable primary energy.

Within this context, the Bioenergy Group of the Chemical and Environmental Engineering Department (DIQA) of the University of Seville has collaborated on numerous research projects that contribute to the development of new processes for the conversion of bioresources in value-added products:

- **Renewable Fuels for Advanced Power Trains (RENEW)** project (SES6-CT-2003-502705. 2004-2007), a pan-European project, supported under the European Commission's 6th Framework Programme, about the development of novel ways of producing automotive biofuels from lignocellulosic biomass. DIQA worked about the catalytic route to produce ethanol from synthesis gas.

- **Production of fuel grade bioethanol via thermochemical route (BIOCOM)** project (ENE2005-08492. 2006-2008), a Plan Nacional project funded by the Ministry of Economy and Competitiveness, about the "Thermochemical Production of Bioethanol for Automotive", studied the behaviour of direct synthesis catalysts in a slurry-type reactor and the economic and life-cycle technical analysis of new process alternatives.

- **Research and development of fuel grade bioethanol (I+DEA)** project (PI-0063/2007. 2007-2010), about the "Research and Development of Ethanol for Automotive", was co-financed between the Centre for Technological and Industrial Development (CDTI) and Abengoa Bioenergy.

- **Sustainable Exploitation of CO_2 (SOST-CO_2)** project (PI-0690/2009. 2008-2011), co-funded by the Ministry of Economy and Competitiveness and the Spanish Society of Metallic Carbides in order to investigate an alternative to CO_2 confinement underground, analysing from the capture of CO_2 in emission sources, through its transportation, storage and recovery.

- **Experimental development of lignocellulosic biomass and other carbon sources transformation processes in various bioproducts in Andalusia (BIOANDALUS)** project (PI-0955/2012. 2012-2014), co-financed between the Centre for Technological and Industrial Development (CDTI) and Abengoa Bioenergy, about the transformation of ethanol into butanol and bio jet-fuel was investigated.

- **Ethanol conversion to added-value products** project (PRJ201101398. 2012-2016), financed by Abengoa Bioenergy, aimed for the design of catalytic processes for the conversion of ethanol into products with high added value.

- **Thermochemical biorefinery based on DME** project (ENE2012-31598. 2013-2015), funded by the Ministry of Economy and Competitiveness with the purpose of identifying the best reaction conditions and develop kinetic models of the catalyst deactivation.

The framework of this study is the **BIODIENE** project (Biobutadiene production from bioethanol, CTQ2015-71427-R), funded by the Ministry of Economy and Competitiveness through the European Regional Development Fund. This research is encouraged by the remarkable development of 1,3-butadiene synthesis catalysts in the last 20 years and aims to deal with research areas like process design and reaction system in order to find optimum process configurations and reaction conditions, comparing these configurations with fossil-based 1,3-butadiene production from the point of view of economics and environmental sustainability.

The project covers, on the one hand, the experimental research, with one and two-steps catalyst, focused on finding the optimum reaction conditions and developing kinetic models and, on the other hand, the conceptual design of new process configurations.

This thesis is dedicated to the experimental part of the project, being focused on the study of the industrial aspects of the one-step catalysts, such as the effect of the reaction conditions and the presence of impurities in the feed on their performance, and also their deactivation, in order to extract data for the industrial process design. That way, some catalysts were selected among those found in literature as the most promising ones and they were synthesized by the Instituto de Tecnología Química (ITQ-UPV-CSIC) in Valencia. A first screening was carried out to determine the best catalyst for the one-step route and, finally, the bimetallic $HfZn/SiO_2$ catalyst presented in the work by Trees et al. [19] was selected.

The scope of this work is to determine the best operating conditions, studying how the reaction conditions and side-products recirculation affects the catalyst performance and to determine the lifespan and catalyst regenerability. Besides, a kinetic model, including the formation of the main side-products, was created to support the development of the industrial process.

Another thesis in the context of the BIODIENE project is being developed, whose goal is the study of the technical, economic and environmental feasibility of different process alternatives for the ethanol to 1,3-butadiene production. It takes the data collected in this document as a base for the design of the process that is simulated using Aspen Plus® software. That way, investment and operating costs are being estimated, as well as Life Cycle Assessment, with the objective of identifying the most economically and environmentally promising alternatives.

3. OBJECTIVES

The main goal of this thesis is to investigate critical issues of the production of 1,3-butadiene from ethanol that can make the technology competitive against the current petrochemical route, focusing on the key aspect for its industrial application such as the influence of the operating condition, the effect of possible impurities in the feed and the catalyst lifetime and regenerability. The study will cover the Lebedev one-step process in order to find optimum reaction conditions and develop a kinetic model that will help in the future to optimize the whole process both economically and environmentally.

In order to achieve the main goal, the specific targets of this study are:

- To review the literature on the conversion of ethanol to 1,3-butadiene in order to identify the most promising catalysts for the one-step route.
- To investigate the reaction pathway from ethanol to 1,3-butadiene, as well as the possible routes to the main side-products.
- To evaluate the effect of the operating condition on the catalyst performance.
- To determine how the content of water and other reaction products in recycled ethanol affects the catalyst performance.

- To perform a study of the catalyst deactivation in order to determine the cause and the possible species involved. Also, the effect of the regeneration of the catalyst by air calcination will be assessed.
- To develop a kinetic model for the catalyst in order to assist in the design of an industrial facility.

4. METHODOLOGY

This chapter is focused on describing the methods employed for obtaining the qualitative and quantitative data necessary to achieve the aforementioned objectives. More detail information about the operation of the experimental facility for each experimental test, such as start-up procedures and operating conditions, can be found in the publications attached at the end of this document.

4.1. Description of the experimental facility

All catalytic tests were carried out in a laboratory scale facility (Figure 3) remotely controlled through a SCADA system and divided into three main zones: reactant feeding, reaction and analysis area. The reactant feeding system allows to feed gas and liquid streams into the reaction area. The gas stream, composed by nitrogen as carrier gas, is fed from a pressurized cylinder into the reactor through a mass flow controller. On the other hand, the liquid feedstock, ethanol or and ethanol-water mixture, was charged into a tank, pressurized with an inert gas (nitrogen), and fed into the reactor using an HPLC pump or a Bronkhorst® mini cori-flow. A check valve was placed at the reactor inlet to avoid reverse flow.

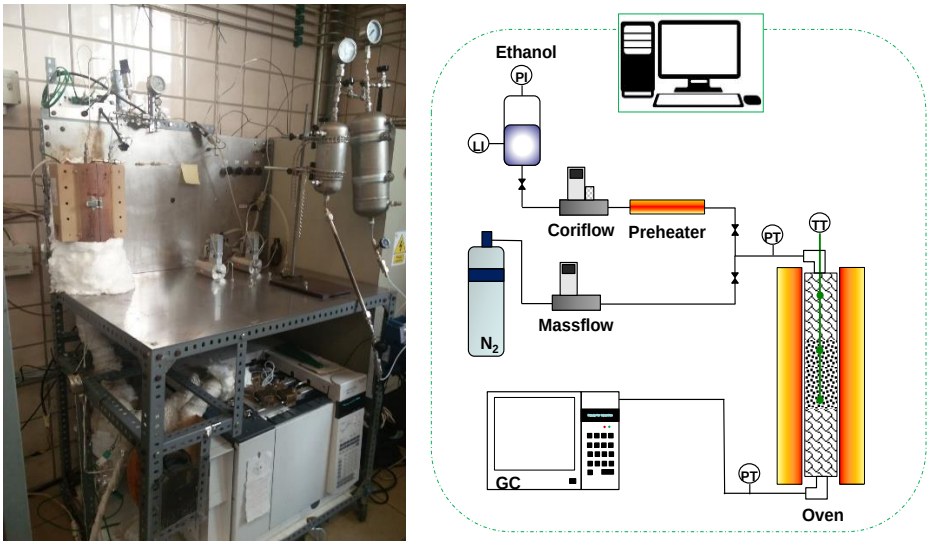

Figure 3. Simplified diagram of the experimental setup.

The reaction system includes an electric oven to set the reactor temperature, and a stainless steel continuous flow fixed-bed reactor (internal diameter = 0.83 cm and length = 25.8 cm) that contains a bed divided into three sections separated by glass wool plugs: a first bed of SiC, then the catalyst bed, and finally another SiC bed. A K-type multipoint thermocouple with three measuring points was inserted axially in the reactor in order to determine the temperature at the inlet of the reactor, and the beginning and the end of the catalyst bed. That way, isothermicity can be checked along the catalytic bed. The reactor output line is electrically traced at around 300 °C and thermally insulated to avoid any product condensations before the semi-continuous stream analysis by on-line gas chromatography (GC).

The online analyses were performed with an Agilent 7890A gas chromatograph equipped with five columns, four valves, and three detectors: two flame ionization detectors (FID), one for C_1-C_6 hydrocarbons and the other one for oxygenated compounds (alcohols, aldehydes, ketones...), and a thermal conductivity detector (TCD) for other compounds such as CO, CO_2, H_2, N_2, etc.

Finally, a gas-liquid separator was used for trapping the condensable compounds, mostly unreacted ethanol and reaction products such as alcohols, aldehydes and ketones. The gas stream, formed mostly by nitrogen and hydrocarbons, leave through the upper part of the container and are vented into the atmosphere.

The control system allows to establish the set-points for the controlled variables and includes the different control loops. It also comprises the facility security protocols and alarms that shut off the electrical supply of the resistors in case the reactor temperature exceeds the limits.

All the experimental equipment is set inside a plexiglass security screen equipped with a gas extraction system. Besides, an ethanol detector is placed near the facility to ring an alarm in the event of a leak.

4.2. Study of chemical equilibrium

Because of the complexity of the reaction system, the effect of operational parameters on the equilibrium composition was investigated in the first place by the direct minimization of the Gibbs free energy, without specifying the possible reaction pathway. Alternatively, a stoichiometric approach was proposed evaluating a set of possible reactions extracted from literature. The analysis was carried out making use of the process simulation software Aspen Plus®. The ideal gas thermodynamic method was set for all the analysis as all chemical reactions occur in gas phase and at atmospheric pressure.

A RGibbs model reactor based on free Gibbs energy minimization was used for the non-stoichiometric approach. It was used to estimate the reactor outlet composition and perform some sensitivity analysis varying pressure and temperature.

For the stoichiometric approach, the Aspen Plus® REquil model reactor was selected. This block performs chemical equilibrium analysis calculating the equilibrium constant at the outlet stream conditions based on the reaction stoichiometry. It was used to represent the Ellingham diagram of the most likely reactions involved in the process, not only for the 1,3-butadiene generation, but also for the side-products formation. These diagrams represent the Gibbs free energy change as a function of temperature and, therefore, are a measure of the thermodynamic feasibility of a reaction.

4.3. Catalysts characterization

The preparation of the catalyst, as well as its characterization, was carried out by Prof. Agustín Martínez Feliu and his group from the Instituto de Tecnología Química (ITQ-UPV-CSIC).

The mass content of Hf and Zn in the calcined catalyst was determined by Inductively Coupled Plasma-Optical Emission Spectrometry (ICP-OES). Crystalline phases in the materials were identified by powder X-ray diffraction (XRD). The textural properties of the individual hemimorphite (HM) and Hf/SiO_2 solids and the Hf-Zn catalyst were measured by N_2 physisorption.

The element distribution in fresh, spent, and regenerated catalyst samples was obtained by energy-dispersive X-ray spectroscopy (EDX). The composition and nature of the Hf, Zn, and C species present on the catalyst surface were studied by X-ray photoelectron spectroscopy (XPS).

The acidity of the calcined Hf-Zn catalyst and its components (HM, Hf/SiO_2) was studied by FTIR spectroscopy of adsorbed pyridine. Complementary characterization by low-temperature FTIR of CO adsorption was performed to investigate the different types and strength of the Brønsted and Lewis acid sites present on the surface of the Hf-Zn catalyst and its components.

Solid-state 1H-to-13C cross-polarization (CP) MAS NMR spectroscopy was performed to study the nature of the carbon compounds deposited on the catalyst during the reaction.

Thermogravimetric analysis (TGA-DTG) of the spent catalyst was carried out and the total amount of carbon in the spent and regenerated catalyst was determined by elemental analysis. The nature of the carbon species present in the spent sample was assessed by mass spectrometry (MS) after dissolving the solid in HF and subsequent extraction of the soluble coke species with CH_2Cl_2.

Besides, in situ IR spectroscopic measurements were carried out to study the possible generation of Brønsted acid sites in the mixed Hf-Zn catalyst in the presence of water at reaction conditions.

4.4. Determination of the reaction pathway

In order to investigate the reaction pathway from ethanol to 1,3-butadiene, as well as the route to the main side-products, kinetic curves (yield versus conversion) were studied to classify the different reaction products as stable/unstable and primary/secondary products according to the morphology of its curves.

Kinetics curves were obtained by carrying out several tests on the Hf-Zn catalyst at 360 °C and atmospheric pressure, varying the weight hourly space velocity (WHSV) from 1.12 to 50 h^{-1} by changing either the amount of catalyst on the bed (0.1 - 2 g) or the anhydrous ethanol flow rate to cover a wide range of ethanol conversions. Additionally, some side-product were fed and/or co-fed along with ethanol into the reactor to determine what compounds they were precursors of. The results acquired with the co-feeding tests were quantitative and it could be determined how much a certain product was enhanced by the presence of certain compounds.

4.5. Effect of operating conditions and water content in ethanol on catalyst performance

The effect of temperature, WHSV, and water content in the ethanol feedstock was studied. For all combinations of three temperatures (340, 360, and 380°C) and three water contents (0, 7.5, and 15 wt%), four space velocities (1.12, 3.2, 6.1, and either 8 or 9.8 h^{-1}) were assessed consecutively from the largest to the lowest WHSV value. Water contents were chosen as anhydrous grade ethanol (~0 wt%), industrial grade ethanol (~7.5 wt%) and crude ethanol (~15 wt%). Due to equipment limitations, for the tests where water content was 7.5 and 15 wt%, the largest space velocity studied was 8 h^{-1}, instead of 9.8 h^{-1}.

To check for catalyst deactivation, the first experiment at the highest space velocity (WHSV=9.8 or 8 h^{-1}) was repeated at the end of the run of each temperature-water content combination. Three extra tests were performed at 360 °C with a water content of 3.75 wt% in order to obtain more information about the water effect at the central temperature.

The water content in ethanol feed was obtained by adding the required amount of deionized Milli-Q water to anhydrous ethanol (Panreac ≥ 99.8% v/v). All tests were carried out with 0.5 g of catalyst at 1 bar of total pressure with ethanol partial pressure in the feed of 0.21 bar.

The nitrogen flow was adjusted to keep the ethanol partial pressure constant. When water was added to the feed, the necessary amount of nitrogen was replaced by water, therefore keeping constant the ethanol partial pressure and total volumetric flow for a given WHSV.

4.6. Response surface analysis

Response surface methodology (RSM) was used to analyse the effect of the operating condition on the catalyst performance, as well as to explore the relationship between the different variables. RSM is a statistical technique used to model and analyze systems in which one variable of interest (response variable) is influenced by others. The purpose is to design an experiment that provides values of the response variable and then determine the mathematical model that best fits the data obtained. The final objective is to establish the values of the factors that optimize the value of the response variable. Ethanol conversion, main product selectivity and 1,3-butadiene yield were set as response variables and the manipulated variables were temperature, weight hourly space velocity and the water content in the feedstock.

That way, the experimental tests proposed were carried out in the experimental facility and then, the response surface analysis was performed with the software StatGraphics®. Some experiments were set apart randomly to validate the proposed model. The response variables were fitted with a second-order equation by using linear least squares regression (Equation 2), where T is the reaction temperature in ^{0}C, Wc the water content in wt%, WHSV the weight hourly space velocity in h^{-1} and b_i the regression coefficients. The most influential factors over the response variables were determined making use of the analysis of variance (ANOVA) and the Pareto chart.

$$\hat{y} = b_0 + b_1 \cdot T + b_2 \cdot Wc + b_3 \cdot WHSV + b_4 \cdot T^2 + b_5 \cdot T \cdot Wc + b_6 \cdot T \cdot WHSV + b_7 \cdot Wc^2 + b_8 \cdot Wc \cdot WHSV + b_9 \cdot WHSV^2$$

Equation 2

The response surface analysis was finally used to find the operating conditions that maximize the ethanol conversion and 1,3-butadiene selectivity and yield.

4.7. Catalyst deactivation and regeneration

The long-term performance of the catalyst and the cause of its deactivation was determined by carrying out long-lasting tests. The evolution of ethanol conversion and main product selectivities was studied and the experiment was halted to regenerate the catalyst when ethanol conversion decreased 20 percentage points from its initial value. After regeneration the operation was resumed.

Two in-situ regeneration by air calcination were performed. That way, two experiments were carried out: the first one feeding anhydrous ethanol and the second one feeding ethanol-water azeotropic mixture (7.5% w/w of water in the feed).

4.8. Kinetic model building and validation

A kinetic model was established using the data obtained in the tests described in section 4.5, where temperature, space velocity and water content in ethanol were varied. The proposed kinetic model does not contemplate the deactivation of the catalyst by coke deposition. Some of the experiments were randomly set apart to validate the model.

A reaction network (with NR reactions) was proposed taking into account the scheme inferred from the kinetic curves, grouping some of the compounds as a simplification when necessary (lumping). A power-law kinetics was assumed for each reaction (Equation 3) and corrective terms were introduced to contemplate the inhibition and promotion of certain reactions by water.

$$r_i = A_i e^{\left(\frac{-Ea_i}{R}\left(\frac{1}{T}-\frac{1}{T_{ref}}\right)\right)} \frac{\prod_{k=1}^{C} P_k^{n_{ki}}}{\left(1+a_i P_{H_2O}\right)^{m_i}} \quad i = 1....NR \qquad \text{Equation 3}$$

In Equation 3, A_i is the kinetic constant at the central temperature for each reaction *i*, Ea_i the activation energy, n_{ki} the reaction orders and P_k the reactant *k* partial pressure. The term $(1/T - 1/T_{ref})$ is derived from expressing the kinetic constant at temperature T relative to the kinetic constant at the reference temperature (T_{ref} = central temperature, i.e., 360 ºC). In section 5.2.4, it can be experimentally observed how water affects the different reactions promoting or inhibiting the generation of some compounds. To contemplate this effect, a term has been included into the kinetic equation. The, either inhibition or enhancement term $\left(1 + a_i P_{H_2O}\right)^{m_i}$, includes a_i and m_i as fitting parameters, being $m_i < 0$ for inhibition terms and $m_i > 0$ for enhancement ones. Besides, P_{H_2O} is the water partial pressure along the reactor.

The set of laboratory-scale experiments presented in Cabello et al. [20] and summarized in table A1 and A2 (Appendix) was used to regress the 39 parameters of the model, and 10 out of the 58 catalytic tests (test number 7, 19, 22, 24, 29, 33, 39, 50, 51 and 56) were randomly set apart to validate the model. Ideal plug flow reactor was assumed for the experimental laboratory scale facility since the ratio between the length (L) and the diameter (D) of the reactor tube is greater than 20 (L/D=31.1 > 20). That simplification means that the fluid is perfectly mixed in the radial direction.

That way, the molar balance for each compound expressed as a function of the reaction rate is shown in Equation 4, being *C* the number of compounds, *W* the mass of catalyst, F_k the molar flow rate of each compound *k*, υ_{ki} the stoichiometric coefficient of each compound *k* in the chemical reaction *i*, and r_i the reaction rate.

$$\frac{dF_k}{dW} = \sum_{i=1}^{NR} \upsilon_{ki} r_i \qquad k = 1...C \qquad \text{Equation 4}$$

Regression of the kinetic parameters was carried out by applying the principle of maximum likelihood, which under the following assumptions, is equivalent to minimize an objective function [21,22]. Thus, by assuming that errors in the observations are independent, normally distributed, with constant variance for each dependent variable, and that the covariance between dependent variables is negligible, the resulting objective function is the sum of the squared errors (or residuals, *e*) of molar flow rates (SSEf) calculated as the difference between the experimental and estimated molar flow rate at the reactor outlet for each compound divided by the variance of the experimental error. In the objective function (Equation 5), F_{kj} is the molar flow rate of compound *k* at the outlet of the reactor for the experiment number *j*; σ_k^2 is the variance of the experimental error for each compound flow rate independently determined from the result of, at least, three measurements taken for each condition; *N* is the number of experiments and *C* the number of compounds.

The molar flow rate of each compound at the reactor outlet was calculated by integration of the differential equations from the molar balance in the reactor (Equation 4).

$$SSEf = \sum_{k=1}^{C} \frac{1}{\sigma_k^2} \sum_{j=1}^{N} \left(F_{kj} - \hat{F}_{kj} \right)^2 = \sum_{k=1}^{C} \frac{1}{\sigma_k^2} \sum_{j=1}^{N} \left(e_{kj} \right)^2 \qquad \text{Equation 5}$$

A good initial guess of the kinetic parameters is necessary in order to help the optimization algorithm to converge to a set of the regression parameters. For that purpose, a simplified method was carried out to estimate the parameters. Constant total molar flow rate (F) along the reactor can be assumed as the flow rate of N_2 is significantly higher than that of the reagents (Table A4). This assumption allows to avoid the integration of the differential equation system because the net reaction rate of compound k can be expressed as a function of the variation of the molar composition (y_k) (Equation 6) and, therefore, be calculated as the slope of the curve $y_k - W/F$ (such as Figure 4). Many W/F values can be chosen, and the corresponding net reaction rates be calculated from the kinetic curves of each compound.

$$\frac{dF_k}{dW} = \frac{dy_k}{d\left(\frac{W}{F}\right)} \qquad \text{Equation 6}$$

That way, the net reaction rate for each compound and every experiment was determined obtaining a large set of net reaction rates for many operating conditions and, then, the gross reaction rates (r_i) were calculated through the molar balance (Equation 4). Lastly, an initial guess of the kinetic parameters were determined separately for each reaction i, making use of non-linear regression by minimizing the sum of the squared errors of the reaction rates ($SSEr_i$) (Equation 7).

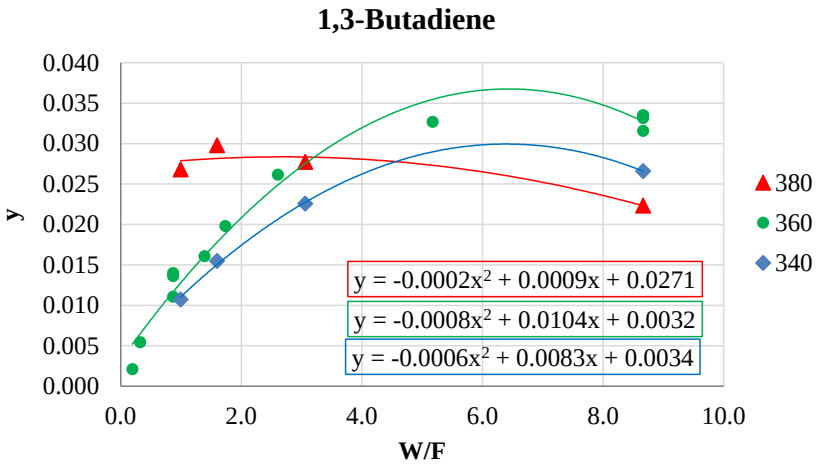

Figure 4. Molar fraction (*y*) versus *W/F* plot for 1,3-butadiene. Tests 1-30 Table A4.

$$SSEr_i = \sum_{j=1}^{N} \left(r_{ij} - \hat{r}_{ij} \right)^2 \quad i = 1....NR \qquad \text{Equation 7}$$

Once the kinetic parameters were obtained with the rigorous method, a statistical analysis based on confidence intervals was carried out to study its uncertainty. The analysis provides a range of the values in which the value of the parameter is true with a certain probability. The determination of the confidence intervals for the parameters was calculated with (Equation 8), where $\hat{\theta}$ is the estimated parameter vector, $t_{\alpha/2,Ndf}$ the t-Student value for an α confidence level and *Ndf* degrees of freedom, and $Tr\left(V_\theta\right)$ the variance-covariance matrix transpose.

$$\theta = \hat{\theta} \pm t_{\alpha/2,Ndf} \cdot \sqrt{Tr\left(V_\theta\right)} \qquad \text{Equation 8}$$

The variance-covariance matrix was estimated through the approximation to the hessian known as the Gauss-Newton approximation. That way, the variance-covariance matrix can be approached as the inverse of the product of the transpose Jacobian matrix and the Jacobian matrix itself (Equation 9).

$$V_\theta \approx \left(J^T \cdot J\right)^{-1} \qquad \text{Equation 9}$$

Finally, a significance test was carried out and the p-value was calculated for each parameter. Those parameters whose p-value was over the chosen significance level, 0.05, were considered not significant and therefore, rejected, simplifying the model. The parameters were discarded one by one and the model optimization and statistical test was repeated after each elimination until getting a model where all the parameters were found significant.

All the calculations were carried out using Matlab® software. The integration of the differential equations along the reactor was carried out with the ode45 routine. The function fminsearch, which implements the Nelder-Mead direct-search algorithm, was used to minimize the objective function (Equation 5) until a value close to the minimum. Then, the function fmincon, which make use of the interior-point algorithm and allows setting bounds for the parameters, was employed for a final parameter estimation. The lsqnonlin function was used to obtain the Jacobian matrix at the optimum point. For the simplified method, the minimization of the sum of the squared errors of the reaction rates (Equation 7) was carried out making use of the Solver Tool in MS Excel®.

Besides, an evaluation of the possible external and internal diffusion limitation was assessed to assure that the chemical reaction was the controlling resistance in the catalytic bed. Mears criterion was applied to evaluate the influence of external mass transfer effects. This criterion assures that external mass transport limitations can be neglected in the case of a Mears number (C_{Mears}) under 0.15. C_{Mears} number is defined in Equation 10, where $-r_{obs}$ is the observed reaction rate (kmol/kg·s), ρ_b is the bulk density of catalyst bed (kg/m^3), d_p is the diameter of the pellets (m), n_k is the reaction order of reactant *k*, k is the mass transfer coefficient (m/s), and C_{kB} the concentration of the reactant *k* in the bulk gas phase (kmol/m^3). It was calculated, using the reactor output values for the most unfavourable operating conditions at the three different temperatures and for each water content in the feed.

$$C_{Mears} = \frac{-r_{obs} \cdot \rho_b \cdot d_p \cdot n_k}{2 \cdot k \cdot C_{kB}}$$ Equation 10

To determine if internal diffusion is limiting the reaction, the Weisz-Prater criterion was employed. The Weisz-Prater number (C_{WP}) relates the observed reaction rate with the diffusion rate, so if C_{WP} is lower than 0.15 there are no diffusion limitations and, consequently, no concentration gradient exists within the catalytic pellets. C_{WP} number is defined in Equation 11, where $-r_{obs}$ is the observed reaction rate (kmol/kg s), ρ_c is the density of the catalyst (kg/m^3), d_P is the diameter of the pellets (m), D_e is the effective diffusion coefficient in the pores of the catalyst (m^2/s), and C_{kS} the concentration of the reactant *k* in the surface of the catalyst (kmol/m^3).

$$C_{WP} = \frac{-r_{obs} \cdot \rho_c \cdot (d_p / 2)^2}{D_e \cdot C_{kS}}$$ Equation 11

5. RESULTS AND DISCUSSION

This chapter assesses the presentation of the experimental results obtained following the method discussed in chapter 4 as well as the determination of the parameters of the kinetic model and its validation. More detail information about the discussion of the results can be found in the publications attached at the end of this document.

5.1. Study of chemical equilibrium for the ethanol conversion into 1,3-butadiene

The aim of this section is to discuss the thermodynamic aspects of the ethanol to 1,3-butadiene reaction, in order to evaluate the effect of the different process variables such as pressure and temperature, and also the presence of some species that may be found in the ethanol feed stream, such water. Besides, if the formation of unwanted side-products is not considered, the equilibrium calculations will provide an upper bound for the catalyst performance.

The overall ethanol to 1,3-butadiene reaction (Equation 1) is slightly endothermic in all the temperature range studied, from 24 kJ/mol at 50 °C to 67 kJ/mol at 500°C (Aspen Plus®). That means that the reaction is thermodynamically favoured by temperature and, therefore, ethanol conversion rises with temperature (Figure 5a). Full ethanol conversion is reached above 250-300 °C.

On the other hand, as the number of moles of the products is higher than the number of moles of reactants, the reaction is expected to be thermodynamically disfavoured at high pressure (Figure 5b).

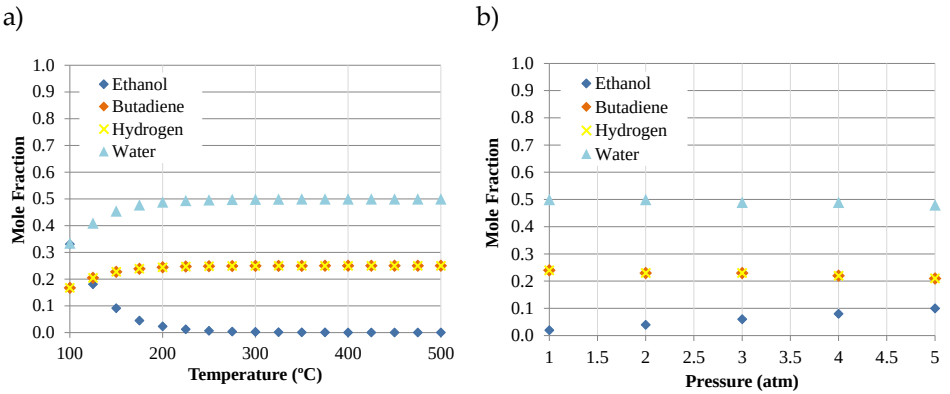

Figure 5. Variation of the equilibrium composition for the ethanol to 1,3-butadiene overall reaction: a) with temperature at 1 atm and b) with pressure at 300°C (Aspen Plus RGibbs).

When the formation of main side-products is taken into account (Figure 6), almost full conversion of ethanol is reached along the range of temperature. Nevertheless, the main product is not 1,3-butadiene but mostly butenes, which are the species most favoured thermodynamically.

As commented in the introduction chapter, the aldol condensation route (ethanol dehydrogenation to acetaldehyde, aldol condensation of acetaldehyde to croton-aldehyde, MPVO reduction of croton-aldehyde with ethanol to produce crotyl alcohol, and finally the dehydration of crotyl alcohol to 1,3-butadiene) is the most accepted pathway nowadays.

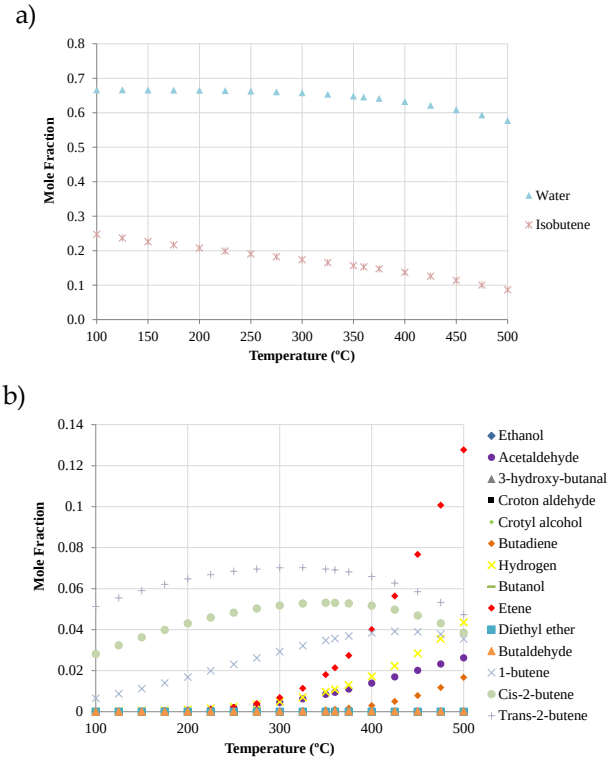

Figure 6. Variation of the equilibrium composition for the ethanol to 1,3-butadiene process with temperature at 1 atm taking into account the main secondary products. a) water and isobutene, b) rest of compounds. (Aspen Plus RGibbs)

The Ellingham diagram of this route (Figure 7) shows that the overall reaction from ethanol to 1,3-butadiene is not thermodynamically favored until 150°C at the standard state. Ethanol dehydrogenation to acetaldehyde is not thermodynamically favorable until 280°C, but the most unfavorable reaction is the aldol condensation of acetaldehyde to crotonaldehyde due to the first step of this reaction, the condensation of acetaldehyde to 3-hydroxy-butanal, which shows high values of standard Gibbs free energy. On the other hand, the Meerwein–Ponndorf–Verley (MPV) reduction of crotonaldehyde to crotyl alcohol and posterior dehydration of crotyl alcohol to butadiene always show negative values of standard Gibbs free energy, presenting this last step to 1,3-butadiene the lowest values.

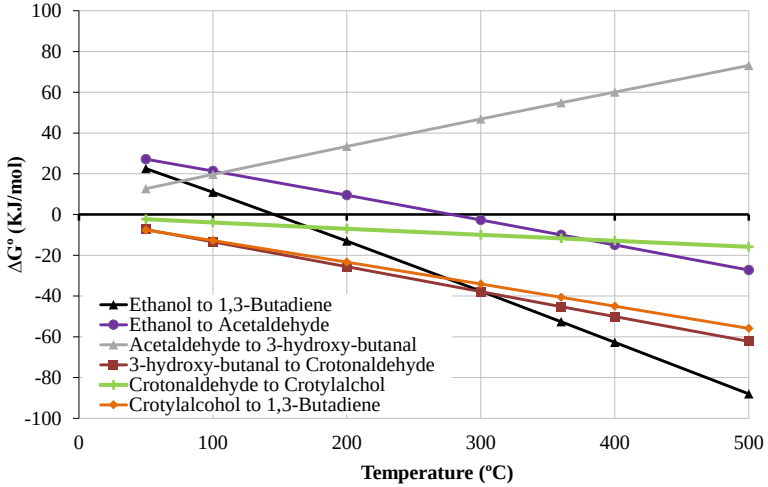

Figure 7. Ellingham diagram (1 atm) for the reaction scheme presented in Figure 2 (Aspen Plus Requil)

On the other hand, the effect of the impurities that ethanol feedstock can contain, on the chemical equilibrium, is important. In this sense, the presence of water in the feedstock slightly inhibits the 1,3-butadiene production, shifting the equilibrium and favouring acetaldehyde generation (Figure 8) as water is a reaction product of the overall reaction. Therefore, ethanol feedstock with low water content should be preferred

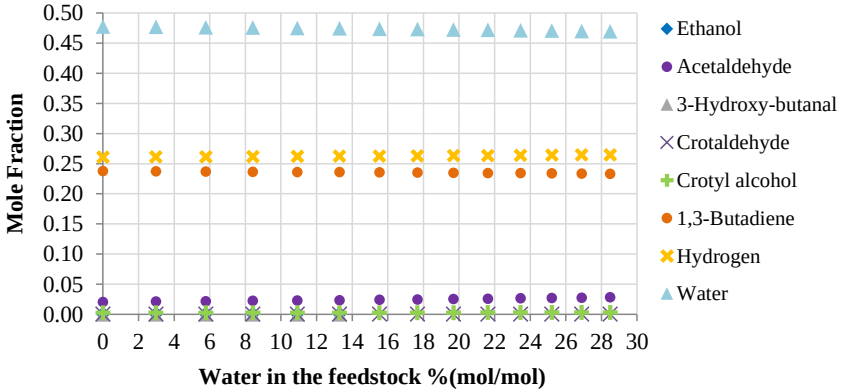

Figure 8. Equilibrium composition reached for the ethanol to 1,3-butadiene reaction while changing the water content in the feedstock at 360°C. (Aspen Plus Requil)

To sum up, since the ethanol to 1,3-butadiene reaction is not thermodynamically favoured with pressure, operation at atmospheric pressure looks like the first choice. For the selection of the operating temperature, one should bear in mind that the most thermodynamically unfavourable reactions are the dehydrogenation to acetaldehyde and the aldol reaction of acetaldehyde to 3-hydroxy-butanal. Therefore, it seems that the operating temperature should be chosen so these reactions are favoured as much as possible but limiting possible side reactions. According to the literature, the typical operating temperature sets between 350 - 430°C [3]. Finally, the presence of water in the feedstock inhibits the 1,3-butadiene production shifting the equilibrium of the dehydration reactions so ethanol feedstock with low water content may be preferred.

The acetaldehyde condensation route is the most accepted pathway. In 2013, Angelici et al. [23] compared Prins condensation, where 1,3-butadiene is formed from ethene, and aldol condensation route, concluding that the latter was thermodynamically more favourable if crotonaldehyde reduction with ethanol was considered. Later, in 2014, Makshina et al. [3] performed a thermodynamic analysis of the aldehyde condensation route with similar results to those presented here. Consequently, the aldol condensation pathway seems to be the most feasible route. However, Ochoa et al. [24] proposed an alternative route over $MgO\text{-}SiO_2$ catalysts, where acetaldehyde reacts directly to produce crotyl alcohol that further dehydrates into 1,3-butadiene. Since these route yields similar results when compared with the aldol condensation route, it would be necessary further studies to determine the most likely path towards 1,3-butadiene.

5.2. Conversion of ethanol into 1,3-butadiene over an $HfZn/SiO_2$ catalyst.

5.2.1. Catalyst selection and characterization

A bibliographic analysis was carried out with the objective of identifying the most promising catalyst for the ethanol to 1,3-butadiene one-step process. The criteria followed was to choose a cheap catalyst (absence of precious metals) with a good balance between the 1,3-butadiene selectivity and yield. That way, De Baerdemaeker et al. [19] $HfZn/SiO_2$ catalyst was selected as it does not contain precious metals and presents one of the highest 1,3-butadiene selectivity and yield in the literature (Table 1).

The $HfZn/SiO_2$ catalyst was synthesised by the ITQ (Instituto de Tecnología Química, UPV-CSIC) according to the methodology reported in Baerdemaeker et al.[19] work. The complete characterization of the synthesized catalyst, along with the images generated in the different analysis commented in this section, can be found in the work of Cabello et al. [25].

Table 1. Identified catalyst for the one-step ethanol to 1,3-butadiene process.

Doped alumina catalyst					
Catalyst	**T (ºC)**	**X (%)**	**S_{BD} (%)**	**Y_{BD} (%)**	**References**
Al_2O_3/ZnO	400	58	31	18	Lebedev et al [13,26]
20Al_2O_3/80MgO	430	91	11	10	Natta et al [27]
2PbO/98Al_2O_3	425	-	-	18	Corson et al [28]
40ZnO/60Al_2O_3	425	94.4	59	55.8	Bhattacharyya et al [29]
30ZnO/4SiO_2/4MgO/1K_2O/61γ-Al_2O_3	420	42.6	80	34.8	Tret'jakov et al [30]
40ZnO/60Al_2O_3	400	41.4	53.1	22	Ezinkwo et al [31]
Doped magnesia-silica catalyst					
Catalyst	**T (ºC)**	**X (%)**	**S_{BD} (%)**	**Y_{BD} (%)**	**References**
60MgO/40SiO_2	430	85	41	35	Natta et al [27]
2Cr_2O_5/59MgO/39SiO_2	415	82	52	43	Natta et al [27]
2Cr_2O_5/59MgO/39SiO_2	425	80	49	39	Corson et al [28]
Na_2O/MgOSiO_2	350	100	87	87	Ohnishi et al
Na_2O/MgOSiO_2	350	53	30	16	Kvisle et al [32]
NiO/MgOSiO_2	282	59	90	53	Kitayama et al [33]
Ag/MgSiO	480	85	50	42	Janssens et al [34]
CuO/MgSiO	425	80	49	39	Angelici et al [35]
MgO/SiO_2	450	95	77	73	Huang et al [36]
Other catalyst					
Catalyst	**T (ºC)**	**X (%)**	**S_{BD} (%)**	**Y_{BD} (%)**	**References**
CuZrZn/SiO_2	375	45	65	30	Jones et al. [37]
CuHfZn/SiO_2	360	98.8	70	69	De Baerdemaeker et al [19]
2Ag/4ZrO_2/SiO_2	320	55.2	71.3	39	Sushkevich et al [38]
Ag/Zr/BEA	320	30	66	21	Sushkevich et al [39]
Na/ZnZrO	350	97	47	45.6	R.Baylon et al [40]
Cr-Ba/MCM 41	450	100	30	30	La Salvia et al [41]
Zn/Talc	400	43	49	21.2	Sekiguchi et al [42]
CuTaSiBEA	325	88	73	64	Kyriienko et al [43]
1ZnO-5ZrO_2/SiO_2	400	95	41	39	Patil et al [44]
Zn0.5–ZrO_2–SiO_2	310	36	87	31	Zhang et al [45]
Ge-Talc	400	44	71	31	Akiyama et al [46]
Zn−Y/Beta	400	95	71	67.5	Yan et al [47]
1Ag/4ZrO_2/SiO_2-SBA-16	325	99	71	70	Dagle et al [48]
ZnTa-TUD-1	400	94	73	68.6	Pomalaza et al [49]

Being T temperature, X ethanol conversion, S_{BD} 1,3-butadiene selectivity and Y_{BD} 1,3-butadiene yield

The textural parameters achieved for the individual HM and Hf/SiO_2 solids and the Hf-Zn catalyst prepared by the ITQ are gathered in Table 2. As seen there, the textural properties of the Hf/SiO_2 solid showed minor deviations with respect to those of the bare SiO_2 support. In comparison, the hemimorphite (HM) exhibited much lower BET surface area and total pore volume, although higher average pore size. The Hf-Zn catalyst, prepared by physically mixing 85 wt% Hf/SiO_2 + 15 wt% HM, displayed values that are intermediate to those of the individual components, although much closer to the Hf/SiO_2 solid. According to repeated ICP-OES analyses, the Hf and Zn contents in the catalyst are, respectively, 2.5 (±0.1) wt% and 10.0 (±1.0) wt%, what means a lower Hf loading compared to the reference catalyst (2.5 < 3.5 wt% [19]).

The synthesized HM sample exhibits only the characteristic diffractions for hemimorphite XRD patterns confirming its successful preparation and high purity. On the other hand, the absence of reflections related to Hf compounds in the Hf/SiO_2 component evidences its high dispersion on the amorphous SiO_2 carrier. The Hf-Zn catalyst shows only the X-ray diffractions associated to the hemimorphite phase, albeit with a much attenuated intensity with respect to pure hemimorphite, as expected by its high dilution with Hf/SiO_2 in the physical mixture [25].

Table 2. Textural properties of the individual HM (hemimorphite) and Hf/SiO_2 solids and the Hf-Zn catalyst as measured by N_2 physisorption [25].

Sample	**BET area** (m^2/g)	**Total pore volume** (cm^3/g)	**Mean pore diameter** (nm)
Hf/SiO_2	206	1.26	26
HM	51	0.46	42
Hf-Zn	179	1.10	28

The acid properties of hemimorphite (HM), Hf/SiO_2, and Hf-Zn catalyst assessed by FTIR spectroscopy of adsorbed pyridine show that the Hf-Zn catalyst, as well as its components, exhibit essentially Lewis-type acidity, being the Lewis acid sites associated with Zn^{2+} species in hemimorphite of a slightly higher strength than those related to Hf^{4+} sites. Nevertheless, both contribute to the catalyst total Lewis acidity. The concentration of Lewis acid sites amounts to 65, 39, and 41 μmol/g for HM, Hf/SiO_2, and Hf-Zn catalyst, respectively. These results indicate that the Lewis acidity of the catalyst is mostly determined by that of its main component Hf/SiO_2. Moreover, the amount of Brønsted acid sites should be very low and/or that their strength is too low to be detected by this method. Low temperature (-170 °C) FTIR spectroscopy of CO adsorption tests confirm the presence of OH groups (i.e. Brønsted acid sites) of different acid strength [25].

Overall, the characterization results of the synthesised catalyst are in good agreement with those reported for the equivalent Hf-Zn catalyst in De Baerdemaeker et al. [19].

5.2.2. Determination of the reaction pathway

The kinetic curves (product yield vs reagent conversion) allow to distinguish stable/unstable and primary/secondary products. In order to study the reaction scheme of 1,3-butadiene formation from ethanol, kinetic curves were obtained for the main products performing several tests with different load of catalyst at several WHSV. The results of the experimental test carried out for this study are gathered in Table A1 and Table A2 of the Appendix.

Acetaldehyde is the main intermediate product of the ethanol-to-1,3-butadiene reaction. The acetaldehyde curve resembles that of a primary unstable product (Figure 9a), indicating that it is directly generated by the dehydrogenation of ethanol. This reaction takes place on the Lewis acid sites associated to Zn^{2+} species in the hemimorphite [19]. In order to study in which reactions acetaldehyde is directly involved, a set of tests was carried out feeding pure acetaldehyde. The main product obtained was crotonaldehyde, plausibly formed by the aldol condensation of acetaldehyde on Hf sites in the Hf/SiO_2 component [19]. However, almost no traces of 3-hydroxybutanal could be found among the products, probably as a consequence of its rapid dehydration to crotonaldehyde [25].

Carbon monoxide and methane were also observed in a 1:1 mole ratio, suggesting that they are formed by the decomposition of acetaldehyde. Heavy compounds (C_{6+}) were also produced in significant amount, probably through the self- and cross-condensation of acetaldehyde and crotonaldehyde [25].

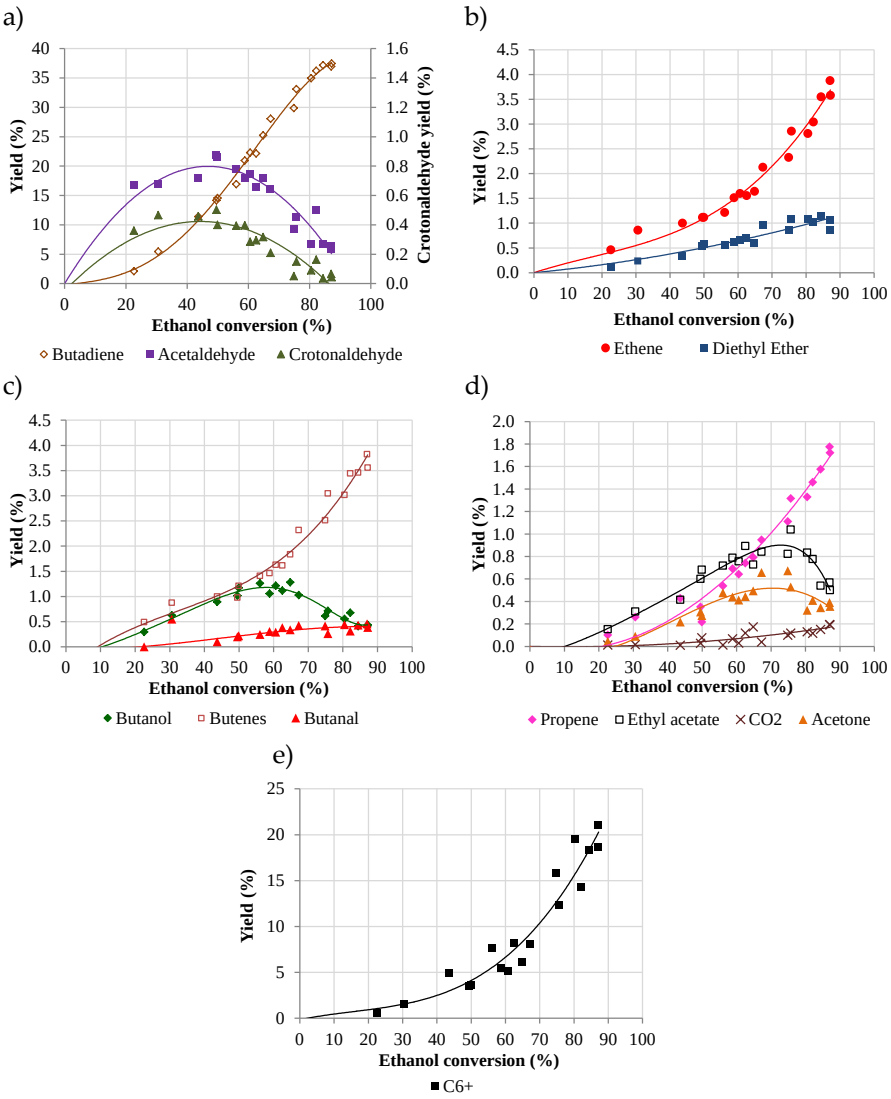

Figure 9. Ethanol to 1,3-butadiene main products yields as a function of ethanol conversion. a) 1,3-butadiene, acetaldehyde and crotonaldehyde; b) ethene and diethyl ether; c) butanol, butenes and butanal; d) propene, ethyl acetate, CO_2 and acetone; e) heavy compounds. All tests were carried out at 360 °C and atmospheric pressure.

Also, an experiment feeding pure crotonaldehyde was performed. The results of this experiment revealed the predominant formation of heavy compounds, supporting their likely formation from crotonaldehyde via self-condensation reactions, however, no traces of 1,3-butadiene were found among the products. Conversely, an increase in 1,3-butadiene selectivity was observed in experiments co-feeding crotonaldehyde with ethanol pointing to a reaction between ethanol and crotonaldehyde to produce 1,3-butadiene [25]. This observation supports the pathway where crotyl alcohol was formed through the MPVO reduction of crotonaldehyde with ethanol and subsequently dehydrated to 1,3-butadiene [27,34,50–53].

Almost no crotyl alcohol was detected during the tests feeding only ethanol, probably due to its high reactivity. The formation of 1,3-butadiene by the dehydration of crotyl alcohol and the high rate of this reaction were confirmed by individually feeding crotyl alcohol. The conversion of crotyl alcohol (360°C and WHSV of 1.12 h^{-1}) was full, with a selectivity of 60% to 1,3-butadiene [25]. Therefore, it can be concluded that, over the $HfZn/SiO_2$ catalyst, both crotonaldehyde and crotyl alcohol are directly involved in the formation of 1,3-butadiene from ethanol. Indeed, the kinetic curve of 1,3-butadiene (Figure 9a) resembles that of a secondary stable product. Its stable character was confirmed by the absence of reaction in an additional experiment performed feeding only 1,3-butadiene. Similarly, no signs for the occurrence of reactions were evidenced when 1,3-butadiene was co-fed with ethanol [25].

From literature, ethene and diethyl ether are both direct products of ethanol dehydration but ethene can also be indirectly produced from diethyl ether or, maybe, both pathways can coexist [3]. According to the obtained kinetic curves of diethyl ether and ethene (Figure 9b), they both seem to be primary stable products probably coming from ethanol dehydration. However, as the kinetic curve of ethene rises exponentially, there seems to be another reaction, besides ethanol dehydration, which leads to ethene. Prins condensation route, where ethanol dehydrogenates to acetaldehyde and dehydrates to ethene and both products react to produce 1,3-butadiene, is ruled out over this catalyst as ethene is not an intermediate product.

Several C_4 compounds were also found amid the products such as butanol, butanal and butenes. The kinetic curve of 1-butanol (Figure 9c) clearly exhibits the characteristic shape of a secondary unstable product. Although the curve of butanal also resembles that of a secondary unstable product, this seems less clear than for 1-butanol, as a net decrease in butanal yield above a certain conversion cannot be unambiguously concluded. The fact that at low ethanol conversions (< 30%) 1-butanol is detected in the products, but not butanal, may be an indication of the dehydrogenation of 1-butanol as a plausible route leading to butanal. This assumption is compatible with the results obtained in an experiment feeding only 1-butanol, where butanal was the main product formed, especially at low 1-butanol conversions, followed by butenes.

Since 1-butanal is formed from 1-butanol, crotonaldehyde hydrogenation should play a minor role as a source of butanal. Then, it seems that crotonaldehyde is mainly hydrogenated to crotyl alcohol by the MPVO reaction, which then can be further hydrogenated to 1-butanol. In fact, when only crotyl alcohol was fed, the lumped selectivity to 1-butanol and butenes was significant. This indicates that over silica doped metal catalysts, and in the absence of an external H_2 source, 1-butanol likely comes from crotyl alcohol hydrogenation by H fragments present on the catalyst surface originating from previous alcohol dehydrogenations [34,38,50].

Finally, the butenes fraction comprising 1-butene, isobutene, and cis- and trans-2-butene shows the characteristic kinetic curve of a secondary stable product (Figure 9c) which, is in line with a route involving the dehydration of 1-butanol to 1-butene and its successive isomerization to *cis*- and *trans*-2-butene and isobutene [3].

The kinetic curve of ethyl acetate (Figure 9d) indicates that it is a secondary unstable product, probably formed from acetaldehyde by the Tishchenko reaction. Indeed, ethyl acetate was observed in the products of the experiment performed feeding only acetaldehyde. Sushkevich et al. [38] proposed that further transformation of ethyl acetate leads to acetic acid, which produces acetone releasing CO_2 by decarboxylation. Finally, acetone can be reduced and dehydrated to propene. This reaction sequence is consistent with the shape and position of the kinetic curves of ethyl acetate, acetone, propene and CO_2. Acetic acid was observed in trace amounts as it is rapidly transformed into acetone and CO_2 is released.

The formation of propene from acetone was confirmed in an experiment feeding pure acetone, where isopropanol and heavy compounds (C_{6+}) were also found as main products and in experiments co-feeding ethanol and acetone, where the yield of propene was seen to increase with the acetone content in the feed. Besides acetone, the decarbonylation of crotonaldehyde is another plausible source of propene, as inferred from the results of an experiment feeding only crotonaldehyde.

In addition, compounds with more than six carbon atoms (C_{6+}) were produced in significant amounts when feeding pure ethanol. The kinetic curve of C_{6+} compounds unambiguously indicates their secondary and stable nature (Figure 9e). Some heavy products can be formed by the self and cross condensation of aldehydes such as crotonaldehyde and butanal, as can be observed in the experiments performed by feeding these compounds. Indeed, feeding only butanal lead to 2-ethyl-2-hexenal as the main product via self-aldol condensation. Moreover, when butanal was co-fed with ethanol, the selectivity to heavy compounds increased significantly. Other minor by-products like acetone have also proven to contribute to the formation of heavy compounds. The deposition of heavy compounds on the $HfZn/SiO_2$ catalyst during the course of the ethanol-to-1,3-butadiene reaction will certainly contribute to its deactivation as exposed in section 5.2.6.

The shapes of the kinetic curves found are similar to those obtained by others authors for one-step catalysts, namely, Sushkevich et al. [38] over $Ag/ZrO_2/SiO_2$ and by Shylesh et al. [12] over $Au/MgO\text{-}SiO_2$.

As a summary, a detailed reaction scheme is shown in Figure 10.

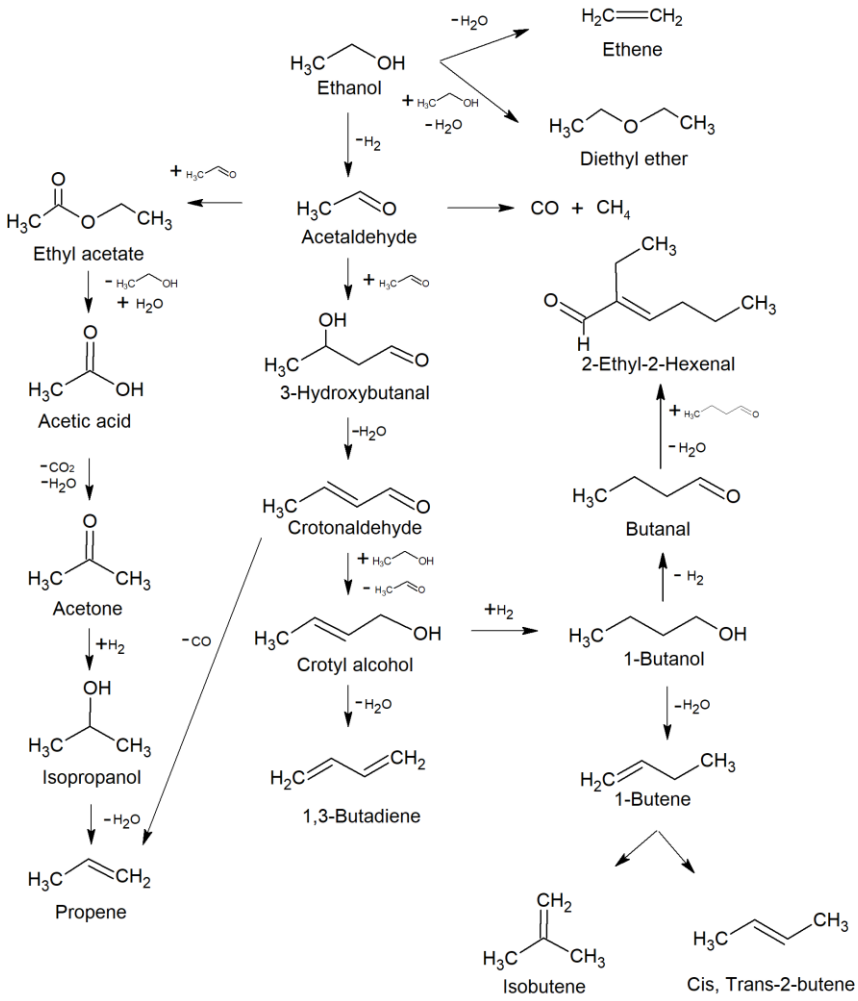

Figure 10. Proposed reaction pathway for the formation of 1,3-butadiene and side products from ethanol over a HfZn/SiO_2 catalyst.

5.2.3. Effect of operating conditions

Knowing how the different variables affect the reactor performance is crucial for the design of an industrial process. The results obtained are presented in Figure 11 and 12, while the design of experiments is shown in Table A3.

Both temperature and WHSV significantly affect the performance of the catalyst. Ethanol conversion (Figure 11) rises with temperature and linearly decreases with WHSV as the contact time diminishes in the studied range. This behaviour has also been reported for other one-step catalysts in the previous literature [34,36,44,54,55].

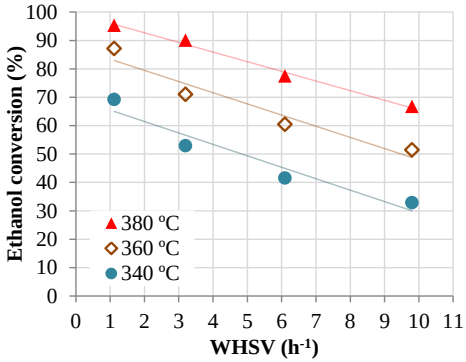

Figure 11. Effect of temperature and WHSV on the ethanol conversion over the mixed Hf-Zn catalyst. P= 1 bar, P_{EtOH}= 0.21 bar, feed is anhydrous ethanol.

At 340 and 360°C, 1,3-butadiene yield (Figure 12a) increases with ethanol conversion, that is, as WHSV decreases. On the other hand, the acetaldehyde yield (Figure 12b) shows a maximum with ethanol conversion, which confirms that acetaldehyde is an intermediate in the formation of 1,3-butadiene over the mixed Hf-Zn catalyst. At 380°C, however, the yield of 1,3-butadiene barely changes with ethanol conversion, at least in the conversion range from 65 to 95% (Figure 12a), probably because, at this temperature, acetaldehyde is so reactive that it is rapidly converted into heavy compounds (C_{6+}) through self and cross condensation (Figure 12e). The excessive formation of heavy products results in operational problems, such as faster catalyst deactivation [17,25] and lower 1,3-butadiene selectivity.

Furthermore, the formation of ethene and diethyl ether (Figure 12c), ethanol dehydration products, and of butenes (1-butene, isobutene, *cis*-2-butene and *trans*-2-butene) (Figure 12d), products of butanol dehydration, increase with temperature and contact time as reported in previous literature [34,36,56]. However, the results obtained over the mixed Hf-Zn catalyst show that these trends stop at high temperature (380°C) where the formation of heavy compounds is much more favoured than those products regardless of the WSHV.

That way, moderate temperatures and low WHSV in the reactor will maximize the 1,3-butadiene yield avoiding the formation of unwanted side-products such as heavy compounds and ethanol dehydration products.

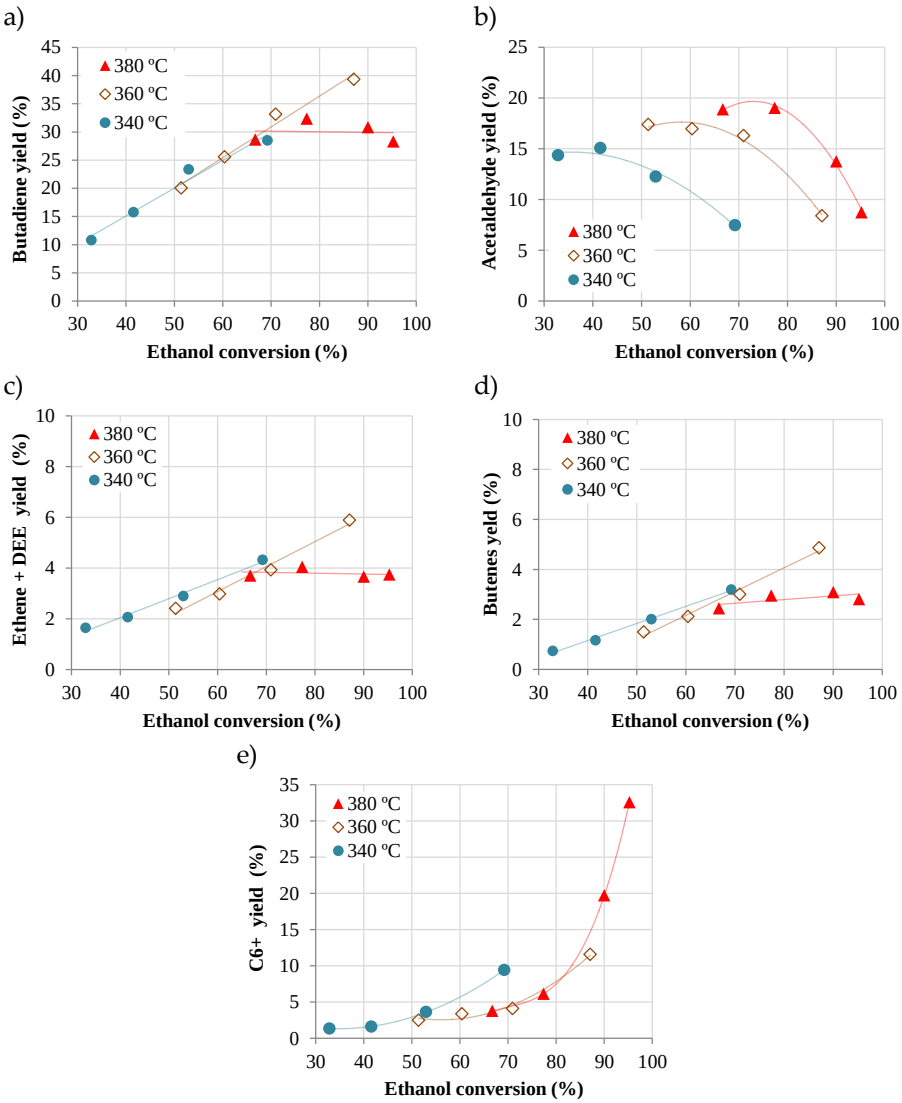

Figure 12. Effect of temperature and WHSV on the yield of a) 1,3-butadiene, b) acetaldehyde, c) ethene plus diethyl ether, d) butenes, and e) heavy products (C_{6+}), over the mixed Hf-Zn catalyst. P= 1 bar, P_{EtOH}= 0.21 bar, feed is anhydrous ethanol.

5.2.4. Effect of water content in ethanol

The consideration of water content as a process variable in the catalyst performance allows to assess the option of using a cheaper ethanol feedstock instead of anhydrous grade, and to decide to what degree water should be removed from unconverted ethanol in the conceptual design of the process in order to find a trade-off between reactor performance and separation costs. This section is part of the work of Cabello et al [20].

The presence of water in the ethanol feedstock severely affects catalyst performance. The conversion of ethanol is decreased by the presence of water (Figure 13a). The higher the water content, the lower the conversion, but this relationship is not linear. Certainly, at any temperature and space velocity, the decrease in the conversion when increasing the water content from 0 to 7.5 wt% is significantly larger than from 7.5% to 15 wt%. Also, the higher the temperature, the lower the decrease in the ethanol conversion with water content. Subsequently, operating at a high temperature partially counteracts the effect of water on ethanol conversion.

The decrease in ethanol conversion with water points to the inhibition of ethanol dehydrogenation to acetaldehyde by the competitive adsorption between ethanol and water for Zn-O Lewis acid-base pairs in hemimorphite, which are the active sites for ethanol dehydrogenation [19]. However, acetaldehyde yield increases with water content (Figure 13b).

As acetaldehyde is formed by ethanol dehydrogenation and consumed in aldol condensation reactions, the increase in acetaldehyde yield points to a larger inhibition by water of aldol condensation reactions as compared to ethanol dehydrogenation. This is supported by the decrease in the 1,3-butadiene and heavy products yield, as observed in Figure 13c (left) and Figure 14a, respectively. Inhibition of aldol condensations by water is expected to occur by blocking of Lewis acid sites active for these reactions [57] which have been associated to Hf^{4+} species [19].

Differently, at high temperature (380 °C) and low space velocity, where the formation of heavy compounds (C_{6+}) is significant for an anhydrous ethanol feedstock (Figure 14a, right), the presence of water results in an increase of the yield to 1,3-butadiene (Figure 13c, right). This fact indicates that, at 380 °C, formation of heavy products is inhibited to a larger degree than that of 1,3-butadiene. This could be explained considering that a reduction in the concentration of available active Hf^{4+} sites due to water adsorption will decrease the probability of occurrence of consecutive aldol condensation reactions through which heavy products are formed [58]. This effect can be beneficial at a high operating temperature, where acetaldehyde is so reactive that it is rapidly converted into heavy compounds unless water is present, allowing higher 1,3-butadiene yield with lower heavy compounds formation.

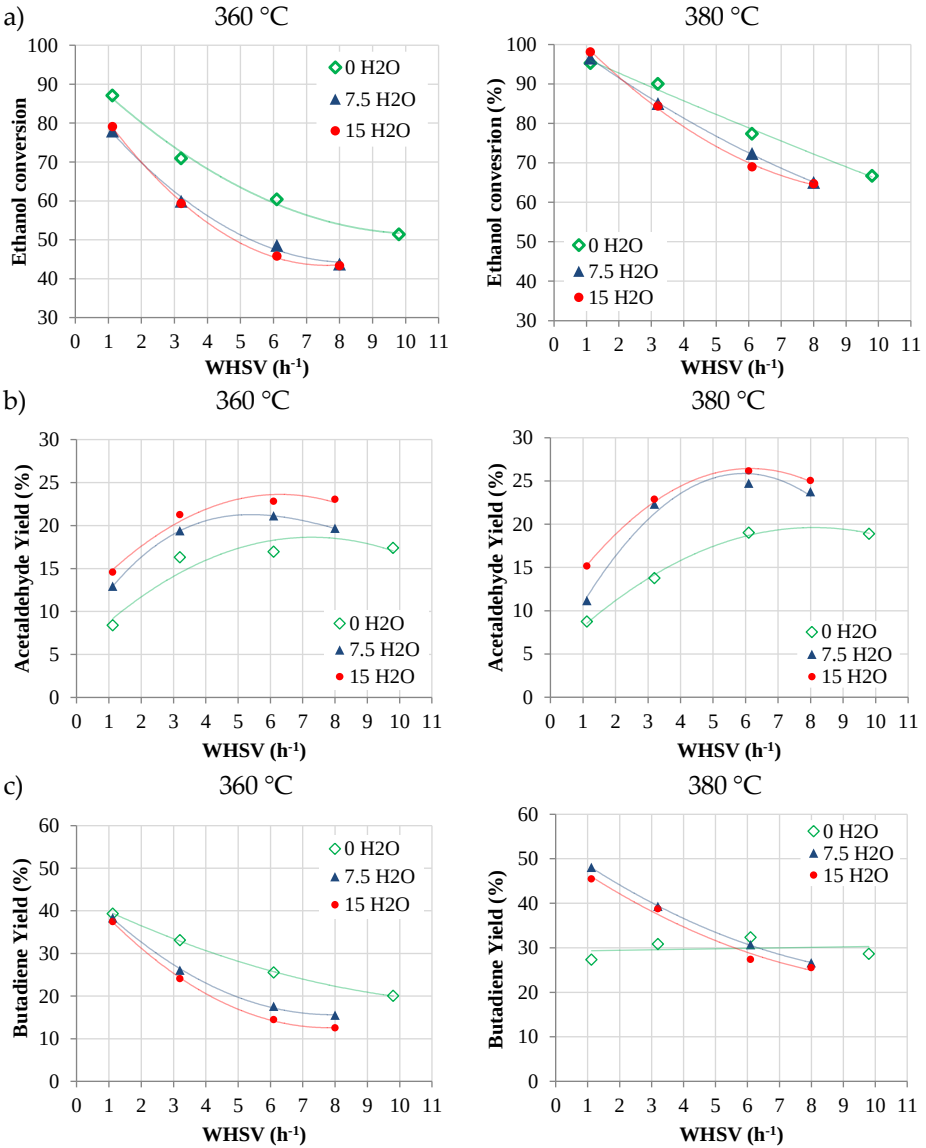

Figure 13. Effect of water content in ethanol feed on a) ethanol conversion, b) acetaldehyde yield, and c) 1,3-butadiene yield at 360 °C (left panels) and 380 °C (right panels) as a function of space velocity and water content (wt%) in ethanol.

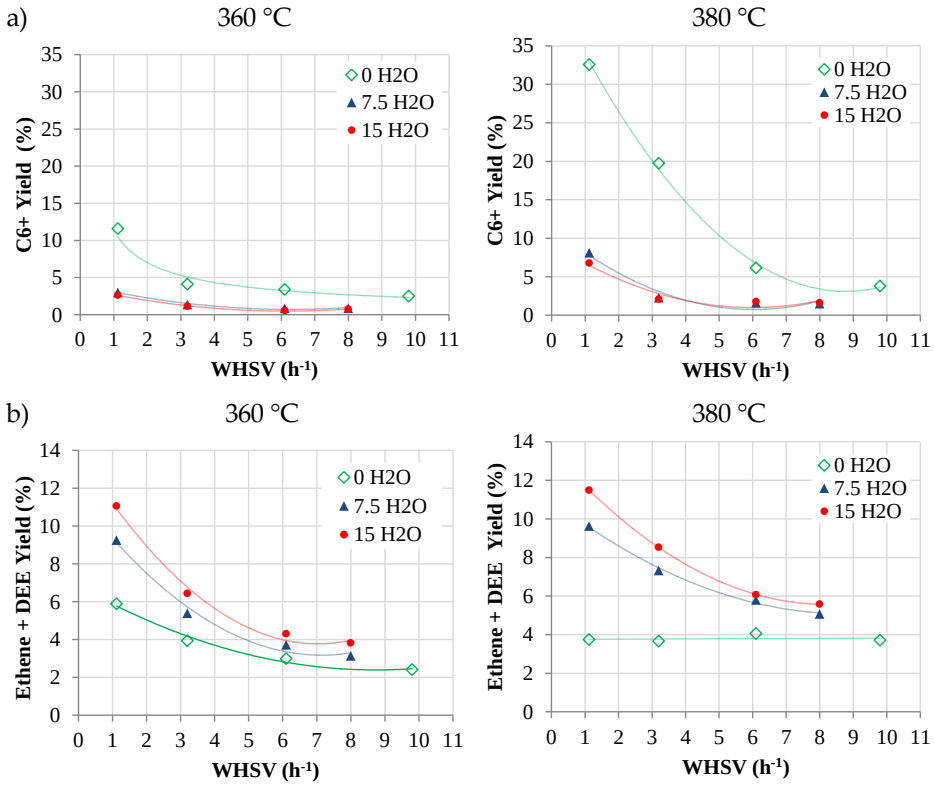

Figure 14. Effect of water content in ethanol feed on a) heavy compound yield and b) ethene + diethyl ether yield at 360 °C (left panels) and 380 °C (right panels) as a function of space velocity and water content (wt%) in ethanol.

On the other hand, the effect of water content in ethanol on the formation of butenes is, at any temperature, similar to that of 1,3-butadiene (not shown), an expectable result considering that self-condensation of acetaldehyde is also an intermediate reaction step in the formation of butenes [25].

Another observation is that, at any temperature, the presence of water increases the formation of direct ethanol dehydration products, ethene and diethyl ether (Figure 14b). This behaviour is due to an increase in the Brønsted acidity of the Hf-Zn catalyst by transformation of some of the Lewis acid sites into Brønsted acid sites by water chemisorption as demonstrated based on *in situ* IR spectroscopic experiments [20]. This alteration has been also spotted by Larina et al. [59] over Zn–La–Zr–Si oxide catalyst by situ FTIR studies and could contribute to the lower activity of the catalyst in the presence of water. Also, the inhibition of the ethanol dehydrogenation reaction results in a higher amount of ethanol available that reacts to produce ethene and diethyl ether. This last effect seems to be more noticeable as it can explain for itself the increased presence of this compounds when hydrous ethanol is fed.

5.2.5. Response surface analysis

The effect of reaction conditions (temperature, content of water in the ethanol and WHSV) on ethanol conversion (X) and product selectivity (S_i) and yield (Y_i) over the mixed Hf-Zn catalyst was studied using a response surface analysis with the statistical software StatGraphics®.

Table 3 shows the fitted parameters and the coefficients of determination (R^2) of the regressions, which are relatively high (90-98%). The selectivity to 1,3-butadiene, acetaldehyde, butenes, and heavy products as well as the yield of 1,3-butadiene were better fitted when their natural logarithm was chosen as the response variable.

Table 3. Estimated parameters for the response variables.

Parameters	X	$\ln(Y_{BD})$	$\ln(S_{BD})$	$\ln(S_{AC})$	S_{ET}	S_{DEE}	$\ln(S_{C4})$	$\ln(S_{C6+})$
a_o	-207.108	-30.456	-18.715	6.036	-190.691	16.224	-23.786	104.250
a_1	0.838	0.194	0.136	-0.012	1.105	-0.042	0.151	-0.580
a_2	-7.188	-0.475	-0.268	0.084	0.674	0.644	-0.326	-0.226
a_3	-8.619	-1.300	-0.793	0.412	-2.751	-1.286	-1.030	-0.315
a_4	-	-0.0003	-0.0002	-	-0.002	-	-0.0002	0.0008
a_5	0.016	0.0014	0.0008	-	-	-0.001	0.0009	-
a_6	-	0.0034	0.0022	-	0.005	0.004	0.0024	-
a_7	0.051	-	-0.0010	-0.0024	-0.019	-0.007		0.009
a_8	-	-0.007	-0.0053	-0.0032	-0.025	-0.005	-0.0061	-
a_9	0.421	-	-	-0.0254	0.068	-	0.0093	0.019
R^2	98.5	96.8	89.6	97.8	92.4	95.2	94.6	90.7

$$\hat{y} = b_0 + b_1 T + b_2 Wc + b_3 WHSV + b_4 T^2 + b_5 T \cdot Wc + b_6 T \cdot WHSV + b_7 Wc^2 + b_8 Wc \cdot WHSV + b_9 WHSV^2$$

Note: BD= butadiene; AC=Acetaldehyde; ET=ethene; DEE=diethyl ether; C4= butenes; C_{6+}= heavy compounds

Table 4. Prediction of response variables for the validation data set.

Op. Cond.		Value	X (%)	Y_{BD} (%)	S_{BD} (%)	S_{AC} (%)	S_{ET} (%)	S_{DEE} (%)	S_{C4} (%)	S_{C6+} (%)
T (°C)	340	Measured	41.56	15.76	37.93	36.25	3.33	1.64	2.81	3.85
W (%)	0	Estimated	40.76	15.82	36.36	33.98	2.53	1.68	2.62	4.81
WHSV (h^{-1})	6.1	Abs. Error	0.80	0.06	1.57	2.27	0.80	0.04	0.19	0.96
T (°C)	360	Measured	43.40	12.50	28.80	53.10	6.40	2.40	1.60	1.70
W (%)	15	Estimated	43.18	10.70	27.81	49.83	6.58	2.22	1.66	1.03
WHSV (h^{-1})	8	Abs. Error	0.22	1.80	0.99	3.27	0.18	0.18	0.06	0.67

BD= 1,3-butadiene; AC=Acetaldehyde; ET=ethene; DEE=diethyl ether; C_4= butenes; C_{6+}= heavy compounds

Two tests at different temperature, water content, and space velocity were set aside to validate the statistic model. As shown in Table 4, the validation data set is reasonably well predicted, being the absolute errors small. Therefore, a good generalization capability of the model is expected within the employed range of reaction conditions.

The response surface analysis allows distinguishing how reaction conditions impact variables of interest such as 1,3-butadiene yield and selectivity. For instance, when the water content in ethanol is 7.5%, the 1,3-butadiene yield is maximized at low space velocity and high operating temperature (Figure 15), which involves high ethanol conversion (Figure 16) and also high 1,3-butadiene selectivity (Figure 17).

a)

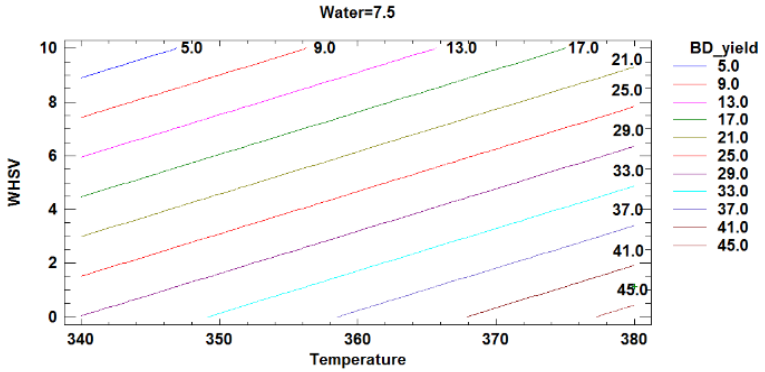

b)

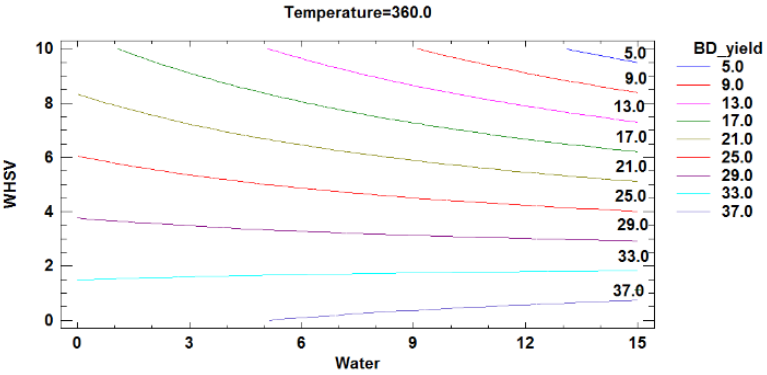

Figure 15. Parametric curves of the response surface analysis model for 1,3-butadiene yield: a) variation with temperature and WHSV, b) variation with water content and WHSV. Temperatures in °C, WHSV in h^{-1}, and water content in wt%.

a)

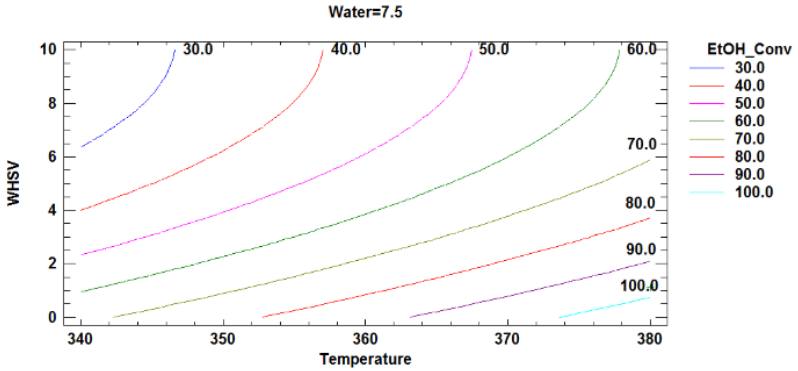

b)

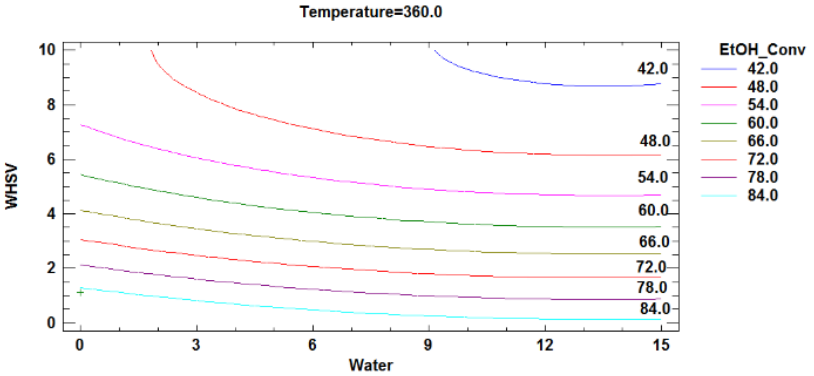

Figure 16. Parametric curves of the response surface analysis model for ethanol conversion: a) variation with temperature and WHSV, b) variation with water content and WHSV. Temperatures in °C, WHSV in h^{-1}, and water content in wt%.

a)

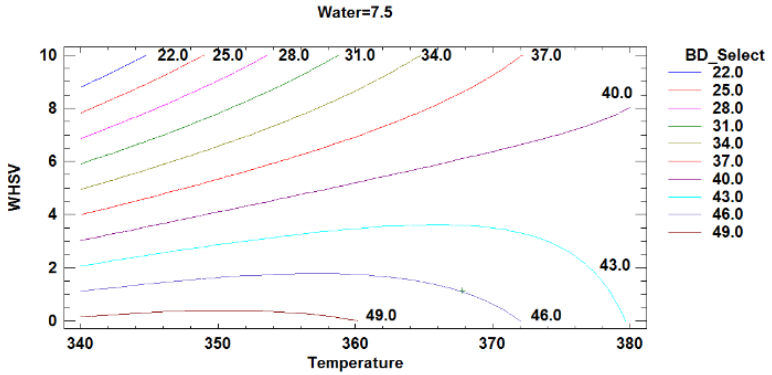

b)

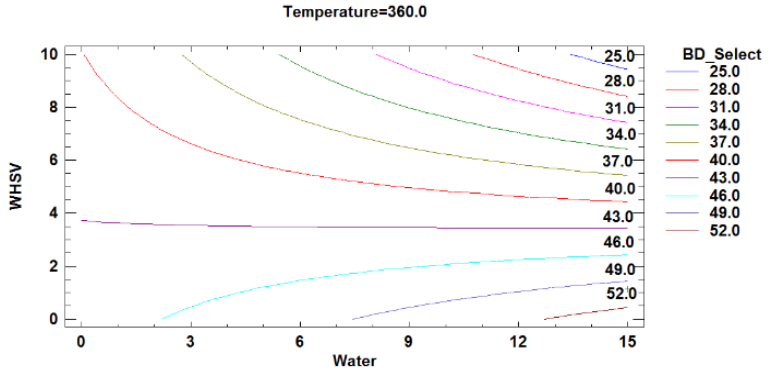

Figure 17. Parametric curves of the response surface analysis model for 1,3-butadiene selectivity: a) variation with temperature and WHSV, b) variation with water content and WHSV. Temperatures in °C, WHSV in h^{-1}, and water content in wt%.

Also, at 360 °C and relatively low space velocities (< 5 h^{-1}), the 1,3-butadiene yield is almost insensitive to the water content in ethanol (Figure 15) since contour plots are flat. This is a consequence of the fact that, at 360 °C and fixed space velocity, as water content increases ethanol conversion decreases, but 1,3-butadiene selectivity increases, and both effects counterbalance.

The statistical model was used to study which combination of operating variables maximized 1,3-butadiene selectivity or yield. As can be seen in Table 5, the highest 1,3-butadiene yield achievable within the bounds of the process variables studied is 50.62%, which involves operating at the highest temperature and lowest spatial velocity with the highest concentration of water in the feedstock (T= 380 °C, WHSV= 1.12 h^{-1} and 15 wt% water). This operating point seems to be the finest since the presence of water causes a drastic decrease in the formation of heavy compounds.

The operating conditions for maximum 1,3-butadiene selectivity (T= 368 °C, WHSV= 1.12 h^{-1} and 15 wt% water) are close to that of the maximum 1,3-butadiene yield. In fact, similar 1,3-butadiene selectivity is achieved in both scenarios but, in this case, the 1,3-butadiene yield is lower. It should be noted that the maximum yield operating point might not be the best operating condition in economic terms, as many trade-offs in the design of the process are involved such as feedstock, reactor and separation costs. Thus, selection of the best operating point of the reactor should be done within the design of the whole process with the aid of the statistical model.

Table 5. Operating conditions for maximum yield or selectivity to 1,3-butadiene.

Operating conditions	Max. yield	Max. selectivity
Temperature (°C)	380	368
Water in ethanol (%wt)	15	15
WHSV (h^{-1})	1.12	1.12
Ethanol conversion and main product selectivities (%)		
X	97.65	84.69
Y_{BD}	**50.62**	43.63
S_{BD}	50.04	**51.44**
S_{AC}	15.89	18.25
S_{ET}	10.26	10.82
S_{DEE}	1.54	2.21
S_{C4}	5.43	5.35
S_{C6+}	5.41	3.36
S_{OC}	11.4	8.57

Note: BD= butadiene; AC=Acetaldehyde; ET=ethene; DEE=diethyl ether; C4= butenes; C_{6+}= heavy compounds. OC comprises a lump of minor sub-products such as acetone, ethyl acetate, butanal, butanol, 2-ethyl-hexenal, CO, and CO_2.

5.2.6. Catalyst deactivation and regeneration.

In order to assess the deactivation behaviour and regeneration of the Hf-Zn catalyst, a long test with two intermediate in-situ regenerations was carried out. The evolution with the time-on-stream (TOS) of the ethanol conversion and the 1,3-butadiene yield and selectivity to acetaldehyde, and ethene + diethyl ether is presented in Figure 18. More data can be found in the work of Cabello et al. [25].

Catalyst deactivation resulting in a gradual loss of ethanol conversion with TOS occurred from the beginning of the reaction as well as after regeneration. In turn, the decrease in conversion is accompanied by a progressive increase in acetaldehyde selectivity and a slight decrease in 1,3-butadiene selectivity, which is more evident in the period following the second regeneration cycle.

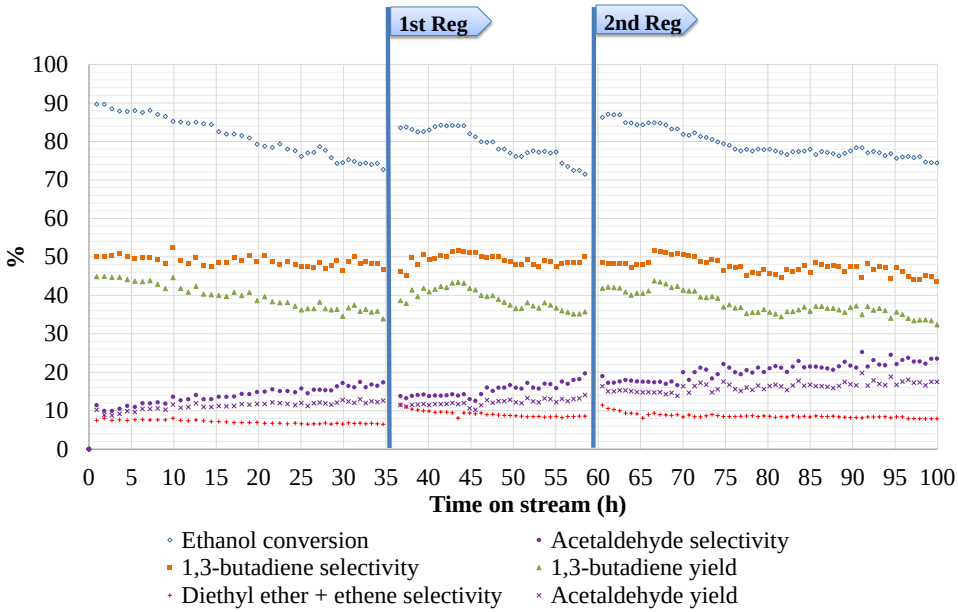

Figure 18. Effect of deactivation on ethanol conversion, main product selectivities and yields. Operating conditions: WHSV= 1.12 $g_{EtOH}/(g_{c}\cdot h)$, T= 360 °C, P_{EtOH}= 0.21 bar and P= 1bar.

Moreover, the combined selectivity to dehydration products (ethene + diethyl ether) slightly increased after the regenerations but remained nearly unaltered with TOS within each reaction period. Similar trends in activity and selectivity during the ethanol-to-1,3-butadiene conversion were observed by Baylon et al. [40] in a study reporting the deactivation and regeneration by calcination of a Na-doped Zn-Zr-mixed oxide catalyst. According to these authors, the change in 1,3-butadiene and acetaldehyde selectivity was related to the loss of active sites involved in the conversion of acetaldehyde to 1,3-butadiene.

The catalyst recovered most of its initial activity after two regenerations by calcination with air at 500 °C, what points to coke deposition as a main source of deactivation of the catalyst. The activity recovery was slightly higher after the second regeneration, lasting 8 h in contrast to the 6 h applied in the first regeneration cycle.

Besides, the deactivation rate at 360 °C decreases when feeding hydrous ethanol (7.5 wt% water) (Figure 19). The remarkably higher stability of the catalyst in the presence of water might be ascribed, in part, to the inhibited formation of heavy products which are coke precursors [60] as water blocks, on the one hand, the Zn^{2+} Lewis acid sites, generating a lesser amount of acetaldehyde, the main precursor of the heavy products; and, on the other hand, Hf^{4+} sites, were aldol condensation reactions occurs (section 5.2.4).

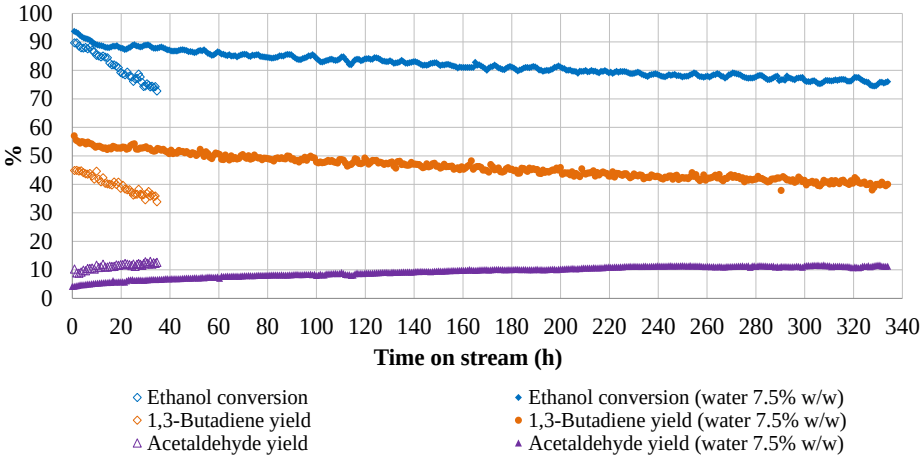

Figure 19. Effect of deactivation on ethanol conversion and 1,3-butadiene and acetaldehyde yield. Operating conditions: WHSV= 1.12 $g_{EtOH}/(g_c \cdot h)$, T= 360 °C, P_{EtOH}= 0.21 bar and P= 1bar.

The total carbon contents, measured by the elemental analysis, amounted to 2.56 and 0.17 wt% for the spent and regenerated samples, respectively. This indicates that calcination in air at 500 °C is effective in removing most of the carbon species from the catalyst and provides support for coke deposition as a main source of deactivation. The fact that still some carbonaceous material remained in the catalyst after regeneration could explain the slightly lower initial conversion observed after the regeneration cycles with respect to the fresh sample. The nature of the carbon species present in the used sample points to ethanol that remained adsorbed on the catalyst but also aromatic carbons were detected.

These results are compatible with those reported by Cavani et al. [61], who detected signs of ethanol, aldehydes and aromatic compounds adsorbed on a MgO catalyst after reaction. The most probable (> 80% probability) structures for four of the main compounds detected are shown in Figure 20.

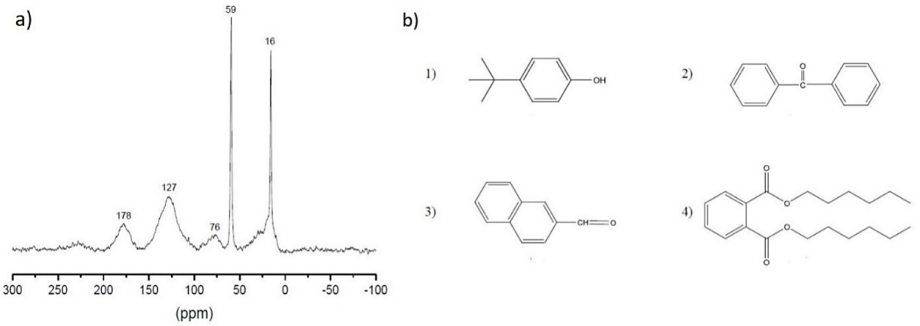

Figure 20. a) Solid-state ^{1}H-to-^{13}C CP-MAS NMR spectrum of spent Hf-Zn catalyst ($HfZn_{used}$); b) main carbonaceous species detected by GC-MS in the coke extracted from $HfZn_{used}$: 1) 4-tert-butylphenol, 2) diphenylketone, 3) 2-naphtaldehyde, and 4) dihexyl phthalate.

Some loss in crystallinity was detected in the hemimorphite (HM) phase after regeneration, pointing to a partial amorphization of the HM phase during the air calcination. The loss of the HM phase during the regeneration may expectedly induce an imbalance between Hf and Zn sites in the Hf-Zn catalyst that might account for, at least in part, the changes in activity and selectivity observed during the post-regeneration reaction periods.

Also, a reduction of the Zn^{2+} species presented in the original hemimorphite phase to Zn^0 during the ethanol-to-1,3-butadiene reaction was detected. That fact would impair the balance between the different types of active sites worsening the catalytic performance. The regeneration of the catalyst by calcination at 500 °C caused the re-oxidation of some Zn^0 species back to Zn^{2+} but it does not restore completely the balance.

The loss in hemimorphite-related Zn^{2+} centres would make Hf^{4+} sites less effective for the aldol condensation step while promoting ethanol dehydration, likely on Hf-OH sites not neutralized by Zn^{2+}. This might account for the rise in selectivity to acetaldehyde and, to a lesser extent, to ethene + diethyl ether in detriment of the 1,3-butadiene observed during the deactivation test (Figure 18) [26,27]. On the other hand, it was observed that the oxidation state and the nature of the Hf species remain the same during the course of the catalytic reaction and after regeneration.

Table 6 shows the surface composition of the catalyst in its different states. It can be seen that the carbon content on the catalyst surface almost doubles after reaction, what is consistent with the deposition of carbonaceous compounds. As a result, the surface concentration of Zn and Si in the used catalyst ($HfZn_{used}$) decreased by 50% and 40%, respectively, with respect to the fresh one ($HfZn_{fresh}$), while the concentration of Hf was much less affected. This suggests that the aromatic-type carbonaceous species were preferentially formed and retained on the dehydrogenating Zn^{2+} species in the hemimorphite component of the catalyst.

After regeneration of the catalyst, the surface contents of Zn, Si, and Hf increased, approaching the values of the fresh catalyst. Alongside, the amount of carbon decreased to levels close to those in the fresh sample, supporting the removal of most of the coke from the catalyst after regeneration by calcination in air at 500 °C.

Table 6. Atomic surface composition and metal surface ratios determined by XPS.

	Atomic surface concentration (%)				**Surface atomic ratios**		
Catalyst	Zn	Hf	Si	C	Zn/Hf	Zn/Si	Hf/Si
HfZn$_{fresh}$	0.50	0.20	32.0	24.3	2.6	0.015	0.006
HfZn$_{used}$	0.25	0.17	19.3	40.0	1.4	0.013	0.009
HfZn$_{regen}$	0.40	0.19	23.5	29.4	2.1	0.017	0.008

5.2.7. Kinetic model building and validation

The main reaction products observed in the catalytic tests were considered in the model: 1,3-butadiene, acetaldehyde, ethene, diethyl ether, and n-butanol. Besides, numerous minor compounds were grouped into three lumps, butenes, heavy compounds and oxygenated compounds, to simplify the model. 1-butene, cis-2-butene, trans-2-butene and isobutene were lumped as butenes and 1-butene was selected as characteristic compound. Heavy compounds, with more than six carbons and mostly aromatic, were grouped into one lump. Diphenyl ketone was chosen as representative compound since it was identified between those molecules absorbed over the catalyst surface after reaction [25]. It also presents a molecular formula alike to the average one of all the products considered heavy compounds. Finally, the oxygenated compounds lump comprises other compounds with a molecular formula similar to butanal. It includes a lot of minority compounds of which the main ones are: acetone, ethyl acetate, butanal and 2-ethyl-butanol.

The reaction network obtained in section 5.2.2 was used as a starting point to propose a set of reactions which could explain the formation of the selected reaction products. As crotonaldehyde and crotyl alcohol were presented in a really low concentration in the reactor outlet due to its quick transformation, acetaldehyde aldol-condensation to crotonaldehyde, crotonaldehyde reduction with ethanol, and crotyl alcohol dehydration have been unified in a global stage from ethanol to 1,3-butadiene.

These simplifications resulted in the following set of reactions: ethanol dehydrogenation to acetaldehyde (Model reaction 1), ethanol and acetaldehyde reaction to 1,3-butadiene (Model reaction 2), ethanol dehydration to diethyl ether (Model reaction 3) and ethene (Model reaction 4), butanol production from ethanol condensation (Model reaction 5), butanol dehydration into butenes (Model reaction 6), generation of heavy compounds (Model reaction 7), which are believed to be formed by acetaldehyde aldol-condensation and further dehydrogenation and cyclization reactions [58], and oxygenated compounds production (Model reaction 8). According to the experimental results shown in 5.2.2, all reactions of the kinetic model were considered irreversible in the range of operating conditions studied.

$$C_2H_5OH \rightarrow C_2H_4O + H_2$$ Model reaction 1

$$C_2H_5OH + C_2H_4O \rightarrow C_4H_6 + 2H_2O$$ Model reaction 2

$$2C_2H_5OH \rightarrow \left(C_2H_5\right)_2 O + H_2O$$ Model reaction 3

$$C_2H_5OH \rightarrow C_2H_4 + H_2O$$ Model reaction 4

$$2C_2H_5OH \rightarrow C_4H_9OH + H_2O$$ Model reaction 5

$$C_4H_9OH \rightarrow C_4H_8 + H_2O$$ Model reaction 6

$$\frac{13}{2}C_2H_4O \rightarrow C_{13}H_{10}O + \frac{11}{2}H_2O + \frac{5}{2}H_2$$ Model reaction 7

$$2C_2H_5OH \rightarrow C_4H_8O + H_2O + H_2$$ Model reaction 8

The effect of water over the catalyst performance has to be taken into account since, as commented on section 5.2.4, water inhibits aldol condensation by blocking of Lewis acid sites active for these reactions [57] which have been associated with Hf^{4+} species. Also, water blocks and/or transforms Zn^{2+} sites, where ethanol dehydrogenation undergoes. Consequently, the formation of 1,3-butadiene and most of the side-products will be hindered as the presence of water in the feed increases. In addition, water boosts the formation of ethene and diethyl ether due to a combined effect of (i) the increase in the Brønsted acidity of the catalyst by transformation of some of the Lewis acid sites into Brønsted acid sites by water chemisorption and (ii) the major presence of ethanol in the medium as a consequence of the inhibition of the ethanol dehydrogenation (section 5.2.4).

That way, as commented in section 4.8, a power-law kinetics was assumed for each reaction and a correction term was added to consider the effect of the presence of water. Model equation 6 does not include the water corrective term as it is considered that the inhibition of butenes by water is a consequence of the inhibition of butanol (Model reaction 5), since butenes are formed from butanol dehydration (Figure 10). From Model reaction 1 to 8, r_i is the reaction rate in mol/g h, A_i is the kinetic constant at the central temperature in mol/g h $bar^{\Sigma nki}$, R is the ideal gas constant in kJ/mol K, Ea_i the activation energy in kJ/mol, T the temperature in Kelvin, P_k the reactant partial pressure in bars, n_{ki} the reaction orders, and a_i (bar^{-1}) and m_i are fitting parameters.

$$r_1 = A_1 \cdot e^{\left(\frac{-Ea_1}{R}\left(\frac{1}{T}-\frac{1}{T_{ref}}\right)\right)} \frac{P_{EtOH}^{n_1}}{\left(1+a_1 P_{H_2O}\right)^{m_1}}$$ Model equation 1

$$r_2 = A_2 \cdot e^{\left(\frac{-Ea_2}{R}\left(\frac{1}{T}-\frac{1}{T_{ref}}\right)\right)} \frac{P_{EtOH}^{n_2} \cdot P_{Ac}^{n_3}}{\left(1+a_2 P_{H_2O}\right)^{m_2}}$$ Model equation 2

$$r_3 = A_3 \cdot e^{\left(\frac{-Ea_3}{R}\left(\frac{1}{T}-\frac{1}{T_{ref}}\right)\right)} \frac{P_{EtOH}^{n_4}}{\left(1+a_3 P_{H_2O}\right)^{m_3}}$$ Model equation 3

$$r_4 = A_4 \cdot e^{\left(\frac{-Ea_4}{R}\left(\frac{1}{T}-\frac{1}{T_{ref}}\right)\right)} \frac{P_{EtOH}^{n_5}}{\left(1+a_4 P_{H_2O}\right)^{m_4}}$$ Model equation 4

$$r_5 = A_5 \cdot e^{\left(\frac{-Ea_5}{R}\left(\frac{1}{T}-\frac{1}{T_{ref}}\right)\right)} \frac{P_{EtOH}^{n_6}}{\left(1+a_5 P_{H_2O}\right)^{m_5}}$$ Model equation 5

$$r_6 = A_6 \cdot e^{\left(\frac{-Ea_6}{R}\left(\frac{1}{T}-\frac{1}{T_{ref}}\right)\right)} P_{ButOH}^{n_7}$$ Model equation 6

$$r_7 = A_7 \cdot e^{\left(\frac{-Ea_7}{R}\left(\frac{1}{T}-\frac{1}{T_{ref}}\right)\right)} \frac{P_{Ac}^{n_8}}{\left(1+a_6 P_{H_2O}\right)^{m_6}}$$ Model equation 7

$$r_8 = A_8 \cdot e^{\left(\frac{-Ea_8}{R}\left(\frac{1}{T}-\frac{1}{T_{ref}}\right)\right)} \frac{P_{EtOH}^{n_9}}{\left(1+a_7 P_{H_2O}\right)^{m_7}}$$ Model equation 8

The parameters of the kinetic model were obtained by fitting data of catalyst performance from the design of experiments presented in section 5.2.3 and 5.2.4 (Table A4 and A5). Since the experiments were designed so the deactivation of the catalyst was as small as possible, the kinetic model is only valid for a fresh catalyst.

The mole balance for each compound expressed as a function of the reaction rate is presented from Equation 12 to 22, being W the catalyst mass and F_k the mole flow of each compound k, where internal and external resistance to mass transfer is neglected. The different products considered were ethanol (EtOH), acetaldehyde (Ac), water (Wat), hydrogen (H), 1,3-butadiene (BD), diethyl ether (DEE), ethene (Et), butanol (ButOH), butenes (But), heavy compounds (HC) and oxygenated compounds (OC).

Certainly, the external and internal diffusion effects were evaluated for the catalytic tests as described in section 4.8. The C_{Mears} obtained values were around $2 \cdot 10^{-3}$, which is far from 0.15 and confirms that, for all the tests, no concentration gradient exists between the bulk gas and external surface of the catalyst particle (external diffusion negligible). Also, the calculated C_{WP} values were around $1 \cdot 10^{-5}$, which is far from 0.15, confirming that internal diffusion was negligible too.

$$\frac{dF_{EtOH}}{dW} = -\left(r_1 + r_2 + 2r_3 + r_4 + 2r_5 + 2r_8\right)$$ Equation 12

$$\frac{dF_{Ac}}{dW} = -\left(-r_1 + r_2 + \frac{13}{2}r_7\right)$$ Equation 13

$$\frac{dF_{Wat}}{dW} = 2r_2 + r_3 + r_4 + r_5 + r_6 + \frac{11}{2}r_7 + r_8$$ Equation 14

$$\frac{dF_{H}}{dW} = r_1 + \frac{5}{2}r_7 + r_8$$ Equation 15

$$\frac{dF_{BD}}{dW} = r_2$$ Equation 16

$$\frac{dF_{DEE}}{dW} = r_3$$ Equation 17

$$\frac{dF_{Et}}{dW} = r_4$$ Equation 18

$$\frac{dF_{ButOH}}{dW} = r_5 - r_6$$ Equation 19

$$\frac{dF_{But}}{dW} = r_6$$ Equation 20

$$\frac{dF_{HC}}{dW} = r_7$$ Equation 21

$$\frac{dF_{OC}}{dW} = r_8$$ Equation 22

The kinetic parameters estimated with the rigorous method are shown in Table 7, along with their 95% confidence intervals. Some of the obtained reaction orders are unusually high, which might be a consequence of the simplifications made in the model building: (i) lumping of reactions and compounds; and (ii) the use of kinetic equations not derived from any reaction mechanism.

Table 7. Calculated values of kinetic parameters.

	A (mol/g h bar$^{\Sigma n_i}$)	**Ea** (kJ/mol)	**n**			**a (bar^{-1})**	**m**
			EtOH	Ac	ButOH		
r_1	49.21±0.59	162.67±0.27	$2.98\pm7.90\cdot10^{-3}$	-	-	511.06±15.65	$0.32\pm1.60\cdot10^{-3}$
r_2	7.93±0.53	170.99±0.81	1.43±0.01	0.87±0.02	-	24.46±3.51	0.57±0.04
r_3	0.68±0.23	144.91±5.82	3.51±0.18	-	-	-	-
r_4	$0.19\pm5.90\cdot10^{-3}$	193.29±0.75	1.99±0.01	-	-	-	-
r_5	$4.82\cdot10^{-3}\pm9.44\cdot10^{-5}$	197.91±0.94	0.20±0.01	-	-	20.69±0.95	1.58±0.05
r_6	1.83±0.23	230.78±1.30	-	-	1.12±0.02	-	-
r_7	$1.24\cdot10^{-2}\pm1.91\cdot10^{-4}$	69.23±4.95	-	0.63±0.01	-	3.73±1.38	3.23±1.00
r_8	$3.25\cdot10^{-2}\pm3.75\cdot10^{-4}$	205.44±0.88	$0.13\pm2.10\cdot10^{-3}$	-	-	124.12±1.36	$1.14\pm4.70\cdot10^{-3}$

The comparison between the prediction of the model and the experimental results can be observed in Figure 21, which represent the mole flows of each compound calculated by the model versus the experimental ones obtained in the catalytic tests. The model fitting is good, not only for the major compounds at the reactor outlet (ethanol, acetaldehyde, water, hydrogen and 1,3-butadiene), but also for most of the minor ones (ethene, diethyl ether, butanol and oxygenated compounds lump). Approximately 90% of the points lie within the ±20% error bands.

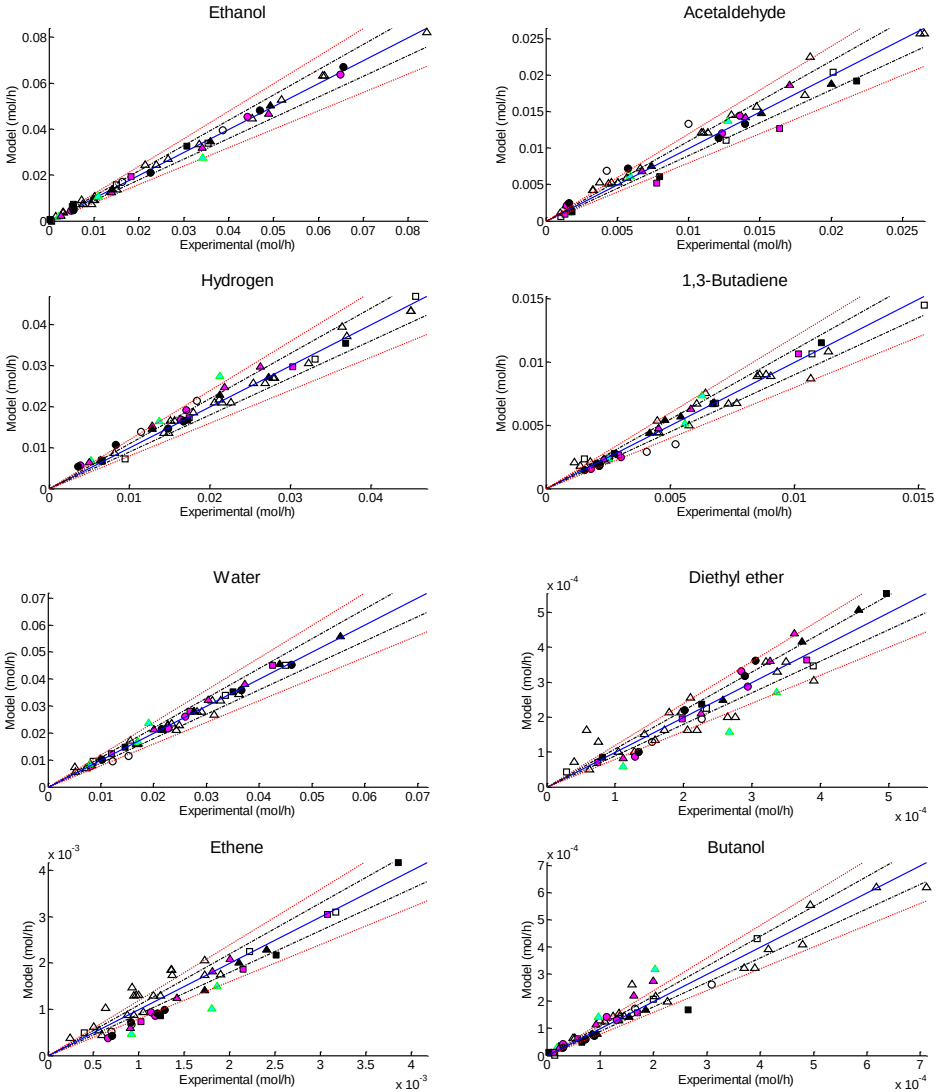

Figure 21. Comparison plots between the experimental and model flow rates. (● 340°C, ▲360°C and ■ 380°C, empty symbols 0%w/w water, green 3.75%w/w water, magenta 7.5%w/w water and black 15%w/w water) 10% error band (black dash-dot line), 20% error band (red dotted line).

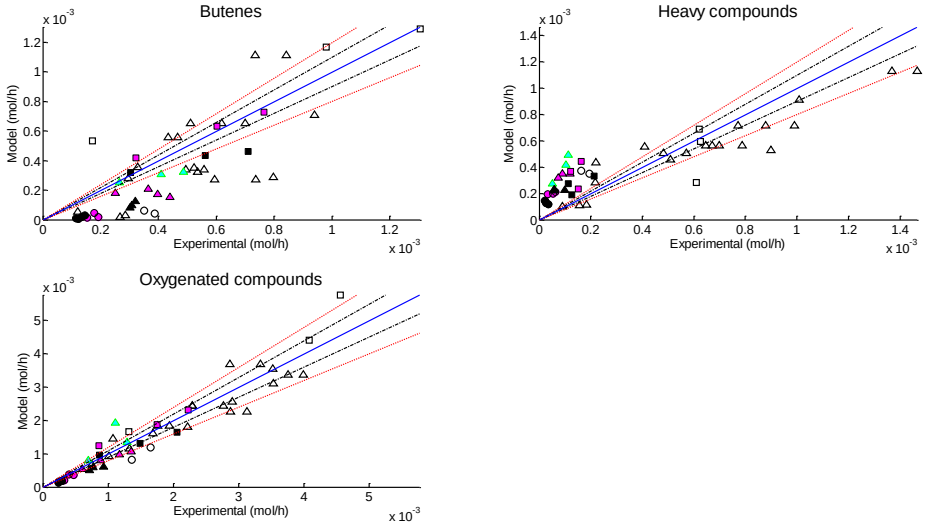

Figure 21 cont. Comparison plots between the experimental and model flow rates. (● 340°C, ▲360°C and ■ 380°C, empty symbols 0%w/w water, green 3.75%w/w water, magenta 7.5%w/w water and black 15%w/w water) 10% error band (black dash-dot line), 20% error band (red dotted line).

In order to validate the assumptions of the regression model (that the errors are independent, follow a normal distribution and have a constant variance [64]), the residuals were analyzed. As the experiments were carried out independently, the independence of the errors is satisfied. Besides, the standardized residuals are normally distributed (Figure A1) as they fairly follow the normal-distribution line, so it can be considered that the normality hypothesis is also fulfilled.

The homoscedasticity hypothesis (constant variance) was validated by plotting the standardized residuals against the estimated value of the model for each test and compound (Figure A2). The standardized residuals of the main compounds (ethanol, acetaldehyde, hydrogen, 1,3-butadiene, water, diethyl ether and ethene) do not follow any trend and also no change is observed in their spread around the zero line as one moves from left to right along the plots. Therefore, the homoscedasticity hypothesis is fulfilled for those compounds. On the other hand, the spread of the residuals of butanol and oxygenated compounds lump seems to increase with the predicted values, while the residuals of butenes lump follow a downward linear trend. Although for these minor compounds the homoscedasticity hypothesis is violated, it is fulfilled for the major compounds and therefore the model is accepted. From the residual analysis it is also observed that there are few outliers (standardized values larger than |3|), but because they are not associated to any particular test, no test was removed from the regression dataset.

The validation of the kinetic model was performed by testing it against the experimental data randomly set apart of the fitting process. Figure A3 compares the predictions by the model against the validation data. Most of the points lie within the ±20% error bands, so the generalization capability of the model is acceptable.

From the above assessment it can be concluded that, overall, the model has a good prediction capability except for butenes and heavy compounds lumps. The reason is that those are lumps, aggregations of multiple compounds, probably produced through different routes, so their prediction cannot be expected to be accurate. For instance, the use of lumps might explain why it is difficult to model the effect of water on the formation of heavy compounds (the kinetic model slightly overestimates it for hydrous ethanol feed while underestimates it for anhydrous ethanol feed). Instead, the oxygenated compounds lump is remarkable well predicted. Anyway, these compounds comprise less than 10% of the product stream on a mole basis, so the model seems acceptable for the prediction purposes. In any case, the degree of accuracy of the model for each compound should be kept in mind when using the kinetic model for the design of the industrial process.

In Table 7, it can be seen that only five of the inhibition/enhancement terms remain in the final model. Particularly, the enhancement terms for the ethene and diethyl ether production were excluded as they were found not significant according to the p-value significance test. Thus, the model can predict well the experimental data just factoring in the inhibition of some reactions, without taking into account the transformation of the active sites by water in the ethanol feed (section 5.2.4). From this, the larger generation of ethene and diethyl ether achieved with hydrous ethanol can be explained by the inhibition of ethanol dehydrogenation (Model reaction 1), which results in more ethanol available to be converted into them, rather than by the generation of Brønsted acid sites, which seems to have a minor role.

According to the Arrhenius plot (Figure 22), the limiting reaction step in the direct conversion of ethanol into 1,3-butadiene (Model reaction 1 and 2) seems to be the ethanol dehydrogenation to acetaldehyde step (Model reaction 1), whose reaction rate coefficient is the highest. This result agrees with some studies found in literature [34,35,65,66]. The lowest activation energy corresponds to the formation reaction of heavy compounds (Model reaction 7), which indicates a lower variability of the rate of this reaction with temperature. However, this seems to contradict the results reported in section 5.2.3. This fact is surely a consequence of grouping compounds of different kind.

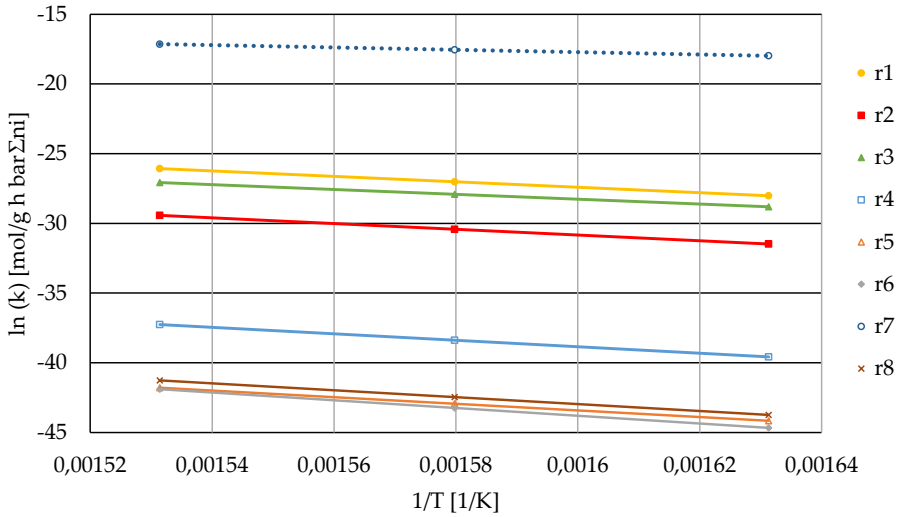

Figure 22. Arrhenius plot for the eight reactions considered in the model.

There no exists in the literature any kinetic model for this Hf-Zn/SiO_2 catalyst, so a direct comparison of the kinetic parameters with other works is difficult. Bhattacharyya et al. [52], over a ZnO/Al_2O_3 catalyst, presented an study considering the following equations: ethanol dehydrogenation to acetaldehyde, acetaldehyde aldol reaction to 3-hydroxybutanal, 3-hydroxybutanal condensation to crotonaldehyde, crotonaldehyde reduction with ethanol to produce crotyl alcohol, and crotyl alcohol dehydration. They reported an activation energy of 84 kJ/mol for the global reaction of ethanol to 1,3-butadiene, when pure ethanol was fed, which is lower to the ones obtained in this work. Other ethanol to 1,3-butadiene kinetic studies carried out over a two-step catalyst, Ta_2O_5-SiO_2, also report lower activation energies, not only for the ethanol to 1,3-butadiene reaction (around 40 kJ/mol) [67], but also for secondary reactions such as ethanol and butanol dehydration (88 and 55 kJ/mol, respectively) [68]. Also, Dussol et al. [67] report more close values of activation energy for ethanol dehydration reactions (157 kJ/mol for ethene formation and 103 kJ/mol for diethyl ether generation), but still lower ones.

5.3. Publications

The following manuscripts have been published in the framework of this thesis. Besides, other article concerning the kinetics of the process is on review.

- G.M. Cabello González, R. Murciano, A.L. Villanueva Perales, A. Martínez, F. Vidal-Barrero, M. Campoy. Ethanol conversion into 1,3-butadiene over a mixed Hf-Zn catalyst: A study of the reaction pathway and catalyst deactivation, Appl. Catal. A Gen. 570 (2019) 96–106. doi:10.1016/J.APCATA.2018.11.010.

- G.M. Cabello González, P. Concepción, A.L. Villanueva Perales, A. Martínez, M. Campoy, F. Vidal-Barrero. Ethanol conversion into 1,3-butadiene over a mixed Hf-Zn catalyst: Effect of reaction conditions and water content in ethanol, Fuel Process. Tech. 193 (2019) 263-272. https://doi.org/10.1016/j.fuproc.2019.04.036.

- G. M. Cabello González, A. L. Villanueva Perales, M. Campoy, J. R. López Beltrán, A. Martínez, F. Vidal-Barrero. Kinetic model for the one-step conversion of hydrous ethanol into 1,3-butadiene over a mixed Hf-Zn catalyst, currently under revision.

Furthermore, the following communications have been presented at international conferences:

- Poster "1,3-Butadiene synthesis from Ethanol over silica ZnHf catalysts"; 10th World Congress of Chemical Engineering, Barcelona, 1-5th October, 2017.

- Oral presentation "Effect of water content in bioethanol for its conversion into 1,3-butadiene over a HfZn catalyst"; 4th Iberoamerican Congress on Biorefineries, Jaén, 24-26th October, 2018.

- Oral presentation "A study of the effect of the reaction conditions for the ethanol and acetaldehyde conversion into 1,3-butadiene"; 3rd International Congress of Chemical Engineering, Santander, 19-21th June, 2019.

- Poster "Developing a kinetic model for the conversion of bioethanol into 1,3-butadiene over a one-step $HfZn/SiO_2$ catalyst"; 12th European Congress of Chemical Engineering, Florence, 15-19 September, 2019.

6. CONCLUSIONS AND FUTURE WORK

1,3-butadiene is a key platform compound used as a chemical intermediate and as a monomer in the manufacture of polymers to produce synthetic rubber, resins, and elastomers. Nowadays, 1,3-butadiene is mostly produced by the petrochemical route as a by-product of the naphtha or gas oil steam cracking process. The production of 1,3-butadiene from bioethanol, which was abandoned in the 1960's, rises as a sustainable and promising alternative in the framework of the new low-carbon policies due to the development of new catalysts whose performance exceed that of commercial catalysts.

This thesis is dedicated to the study of the industrial aspects of those catalysts, such as the effect of the reaction conditions and the presence of impurities in the feed on their performance, and also their deactivation, in order to extract data for the industrial process design to support the evaluation of the sustainability and profitability of this technology.

In particular, a highly selective Hf-Zn mixed catalyst was selected from the literature and its performance assessed with numerous catalytic tests to, finally, develop a kinetic model which may be used in the future to design and optimize an industrial process.

The most likely ethanol to 1,3-butadiene pathway over the one-step catalyst includes: ethanol dehydrogenation to acetaldehyde, acetaldehyde aldol-condensation to crotonaldehyde, crotonaldehyde reduction with ethanol, and crotyl alcohol dehydration, which concurs with the most accepted route in literature.

Regarding side products, ethene and diethyl ether seem to be primary stable products formed from ethanol dehydration. The decarbonylation of aldehydes has been observed over the catalyst: acetaldehyde to methane and crotonaldehyde to propene, with the associated release of carbon monoxide. Ethyl acetate is likely produced via the Tishchenko reaction and then further transformed into acetone and propene, which releases carbon dioxide.

1-Butanol seems to be formed from crotyl alcohol hydrogenation with surface H fragments originating from previous dehydrogenation reactions. 1-butanol dehydrogenation and dehydration are the main sources of butanal and 1-butene, respectively. 1-Butene can be isomerized into cis- and trans-2-butenes. The source of heavy compounds appears to be the self- and cross-condensation of C_{4+} aldehydes, like butanal and crotonaldehyde; and ketones, like acetone.

Focusing on the impurities that may be recycled along with the non-converted ethanol, the recycle of butanal and acetone should be avoided, as they are finally converted to heavy compounds by aldol condensation reactions. Heavy product formation leads to the deactivation of the catalyst, the fouling of downstream equipment and also makes it difficult to recover and recycle ethanol. Also, recycling 1-butanol should be averted, as its dehydrogenation leads to butanal and then to heavy products while 1-butanol dehydration leads to butenes, which are difficult to separate from 1,3-butadiene due to their similar boiling points, shape and polarity. Finally, the recycling of a considerable amount of diethyl ether could suppress unwanted diethyl ether formation from ethanol. The economic viability of this measure will depend on the cost of separating and recycling diethyl ether and the increase in 1,3-butadiene selectivity due to the suppression of diethyl ether formation. According to our results, this will not be practical since the needed amount of recycled diethyl ether would be quite high.

A power-law kinetic model was developed with a corrective term for water effect in order to predict the formation of the major products: acetaldehyde, 1,3-butadiene, hydrogen, water, ethene, diethyl ether, butanol, and the lumps butenes, diphenyl ketone and butanal. The predictions of the model agree with the experimental validation data, so the model can be used to predict the rates of formation of the different products, when water is present in the ethanol feedstock.

The presence of water in the ethanol feed enhances the selectivity to dehydration products, i.e., ethene and diethyl ether from ethanol and decreases ethanol conversion. The increased dehydration activity can be accounted for by the generation of new Brønsted acid sites of medium strength in the mixed Hf-Zn catalyst, as assessed by *in situ* IR spectroscopy, probably by reaction of Zn^{2+}-related Lewis acid sites (active for ethanol dehydrogenation) with water at reaction conditions. Besides, blocking of Zn^{2+} sites by water represents a loss of dehydrogenation sites resulting in a decrease in ethanol conversion and letting more ethanol available for its dehydration to ethene and diethyl ether. Indeed, the developed kinetic model explain the rise in the ethene and diethyl ether formation in the presence of water as a result of the inhibition of ethanol dehydrogenation so, although there is a transformation of the actives sites, its influence appears to be low. Moreover, water seems to hinder aldol condensation reactions to a greater degree than dehydrogenation due to blocking of Hf^{4+}-related Lewis acid sites. This effect can be beneficial at a high operating temperature, where acetaldehyde is so reactive that it is rapidly converted into heavy compounds unless water is present, allowing higher 1,3-butadiene yield with lower heavy compounds formation.

In addition, the presence of water significantly decreases the rate of catalyst deactivation, which can be ascribed to the inhibition of successive condensation and dehydrogenation reactions involved in coke formation. Catalyst deactivation is quite noticeable and mostly caused by the formation and retention of aromatic-type species preferentially on the dehydrogenating Zn^{2+} sites of the hemimorphite phase of the catalyst and by the reduction of some of these Zn^{2+} sites to Zn^{0}. The loss in Zn^{2+} sites induces an imbalance between Hf^{4+} and Zn^{2+} sites which results in a change in catalyst selectivity. Regeneration by calcination with air successfully removes coke and re-oxidizes a fraction of Zn^{0} back to Zn^{2+}, but it does not completely re-establish the Zn^{2+}/Hf^{4+} site balance as the re-oxidized Zn species are segregated from the original hemimorphite phase and provide a less favourable interaction with Hf sites.

As a general conclusion, the results presented in this work may be extrapolated for most of the ethanol to 1,3-butadiene one-step catalysts. In the first place, the elucidated pathway concurs with most of the one-step catalyst presented in the literature (i.e. $MgO\text{-}SiO_2$, $ZnO\text{-}Al_2O_3$ and $Ag\text{-}ZrO_2\text{-}SiO_2$). Besides, in the development of one-step processes the effect of co-feeding water should be taken into account since it assess the option of using a cheaper ethanol feedstock instead of anhydrous grade, and to decide to what degree water should be removed from unconverted ethanol in the conceptual design of the process in order to find a trade-off between reactor performance and separation costs. Finally, the methodology used to assess the kinetic model can be applied to any ethanol to 1,3-butadiene catalyst.

The results of this thesis suggest the following future work:

- The study of the reaction pathway, although quite complete, could be improved by conducting more feeding and co-feeding tests at different spatial velocities with other intermediate compounds whose origin is not clear.

- Since water inhibit large-chain compounds formation and deposition over the catalyst surface, limiting the catalyst deactivation, the design of experiments could be extended at higher temperatures to acquire a wider view of the effect of water over the catalyst performance.

- As the catalyst loses active centres in each regeneration, a deeper study including more regeneration cycles will be necessary to draw stronger conclusions for its industrial application suitability.

- There is also room for improvement in the kinetic model development. In the first place, to include new reaction products, especially those which can affect the separation process downstream the reactor or affect the catalyst performance when recirculated with the ethanol. This will improve the robustness of the model. For example, it is known that acetone and butanal affect negatively the catalyst performance, boosting the heavy compounds generation. Besides, it was found that when co-feeding diethyl ether, its generation was impaired so ethanol dehydration to diethyl ether may be taken as reversible.

- Also, butanal, butenes and diphenyl ketone lumps fitting may be improved by separating the main compounds they contain, adding new generation reactions for them and finding their kinetic parameters.

- Besides, the accuracy of the kinetic model should be tested on a higher scale in order to check if it is really useful for the design of an industrial process.

- The proposed kinetic model does not cover the catalyst deactivation, which is quite relevant as commented on section 5.2.6. Including the deactivation effect in the model would lead to a completer and more useful model when designing an industrial process.

- It will be also interesting to study the effect of reactor configurations and locations and distribution of ethanol feed along the reactor using the developed kinetic model.

- Finally, different scenarios of the industrial process should be proposed and analysed from an economic and environmental point of view in order to globally optimize the 1,3-butadiene production.

REFERENCES

[1] IPTS, Best Available Techniques (BAT) Reference Document for the Production of Wood-based, 2016. doi:10.2791/21807.

[2] A.J. Nizamoff, On-Purpose Butadiene On-Purpose Butadiene, (2013).

[3] E. V. Makshina, M. Dusselier, W. Janssens, J. Degrève, P.A. Jacobs, B.F. Sels, Review of old chemistry and new catalytic advances in the on-purpose synthesis of butadiene, Chem. Soc. Rev. 43 (2014) 7917–7953. doi:10.1039/C4CS00105B.

[4] Mordor Intelligence, Butadiene Market. Growth, Trends, and Forecast., (2019).

[5] M. Reporting, Argus Ethylene Annual 2018 Table of Contents Events, 2018 (2018).

[6] D. Cespi, F. Passarini, I. Vassura, F. Cavani, Butadiene from biomass, a life cycle perspective to address sustainability in the chemical industry, Green Chem. 18 (2016) 1625–1638. doi:10.1039/C5GC02148K.

[7] S. Farzad, M.A. Mandegari, J.F. Görgens, Integrated techno-economic and environmental analysis of butadiene production from biomass, Bioresour. Technol. 239 (2017) 37–48. doi:10.1016/j.biortech.2017.04.130.

[8] European Commission, Going climate-neutral by 2050, Facilities. (2018).

[9] European Commission, A clean planet for all. A European strategic long-term vision for a prosperous, modern, competitive and climate neutral economy., (2018).

[10] R.E.N. Members, Renewables 2019 Global Status Report, 2019. https://wedocs.unep.org/bitstream/handle/20.500.11822/28496/REN2019.pdf?sequence=1&isAllowed=y%0Ahttp://www.ren21.net/cities/wp-content/uploads/2019/05/REC-GSR-Low-Res.pdf.

[11] R.A. Flach B., Lieberz A., EU Annual Biofuels Annual 2017, USDA Foreign Agric. Serv. (2017) 1–44. https://gain.fas.usda.gov/Recent GAIN Publications/Biofuels Annual_The Hague_EU-28_6-19-2017.pdf.

[12] S. Shylesh, A.A. Gokhale, C.D. Scown, D. Kim, C.R. Ho, A.T. Bell, From Sugars to Wheels: The Conversion of Ethanol to 1,3-Butadiene over Metal-Promoted Magnesia-Silicate Catalysts, ChemSusChem. 9 (2016) 1462–1472. doi:10.1002/cssc.201600195.

[13] I. Lebedev, Preparation of Bivinyl directly from alcohol, Zh. Obs. Khim. 3 (1933) 698–717.

[14] A. Talalay, L. Talalay, S.K.-The Russian Synthetic Rubber From Alcohol - A Survey of the Chemistry and Technology of the Lebedev Process for Producing Sodium-Butadiene Polymers, Rubber Chem. Technol. 15 (1942) 403–429. http://rubberchemtechnol.org/doi/pdf/10.5254/1.3543128.

[15] G. Pomalaza, M. Capron, V. Ordomsky, F. Dumeignil, Recent Breakthroughs in the Conversion of Ethanol to Butadiene, Catalysts. 6 (2016) 203. doi:10.3390/catal6120203.

[16] Q. Zhu, B. Wang, T. Tan, Conversion of Ethanol and Acetaldehyde to Butadiene over MgO–SiO 2 Catalysts: Effect of Reaction Parameters and Interaction between MgO and SiO 2 on Catalytic Performance, ACS Sustain. Chem. Eng. 5 (2017) 722–733. doi:10.1021/acssuschemeng.6b02060.

[17] M. Zhang, X. Tan, T. Zhang, Z. Han, H. Jiang, The deactivation of a ZnO doped ZrO 2 –SiO 2 catalyst in the conversion of ethanol/acetaldehyde to 1,3-butadiene, RSC Adv. (2018). doi:10.1039/C8RA06757K.

[18] O. V. Larina, P.I. Kyriienko, D.Y. Balakin, M. Vorokhta, I. Khalakhan, Y.M. Nychiporuk, V. Matolín, S.O. Soloviev, S.M. Orlyk, Effect of ZnO on acid–base properties and catalytic performances of ZnO/ZrO 2 –SiO 2 catalysts in 1,3-butadiene production from ethanol–water mixture , Catal. Sci. Technol. 9 (2019) 3964–3978. doi:10.1039/c9cy00991d.

[19] T. De Baerdemaeker, M. Feyen, U. Müller, B. Yilmaz, F.S. Xiao, W. Zhang, T. Yokoi, X. Bao, H. Gies, D.E. De Vos, Bimetallic Zn and Hf on silica catalysts for the conversion of ethanol to 1,3-butadiene, ACS Catal. 5 (2015) 3393–3397. doi:10.1021/acscatal.5b00376.

[20] G.M. Cabello González, P. Concepción, A.L. Villanueva Perales, A. Martínez, M. Campoy, F. Vidal-Barrero, Ethanol conversion into 1,3-butadiene over a mixed Hf-Zn catalyst: Effect of reaction conditions and water content in ethanol, Fuel Process. Technol. 193 (2019) 263–272. doi:10.1016/j.fuproc.2019.04.036.

[21] C.D. Knightes, C.A. Peters, Statistical analysis of nonlinear parameter estimation for Monod biodegradation kinetics using bivariate data, Biotechnol. Bioeng. 69 (2000) 160–170. doi:10.1002/(SICI)1097-0290(20000720)69:2<160::AID-BIT5>3.0.CO;2-J.

[22] F.D. Marques-Marinho, I.A. Reis, C.D. Vianna-Soares, Construction of analytical curve fit models for simvastatin using ordinary and weighted least squares methods, J. Braz. Chem. Soc. 24 (2013) 1469–1477. doi:10.5935/0103-5053.20130187.

[23] C. Angelici, B.M. Weckhuysen, P.C.A. Bruijnincx, Chemocatalytic conversion of ethanol into butadiene and other bulk chemicals, ChemSusChem. 6 (2013) 1595–1614. doi:10.1002/cssc.201300214.

[24] J.V. Ochoa, C. Bandinelli, O. Vozniuk, A. Chieregato, A. Malmusi, C. Recchi, F. Cavani, An analysis of the chemical, physical and reactivity features of MgO–SiO $_2$ catalysts for butadiene synthesis with the Lebedev process, Green Chem. 18 (2016) 1653–1663. doi:10.1039/C5GC02194D.

[25] G.M.M. Cabello González, R. Murciano, A.L.L. Villanueva Perales, A. Martínez, F. Vidal-Barrero, M. Campoy, Ethanol conversion into 1,3-butadiene over a mixed Hf-Zn catalyst: A study of the reaction pathway and catalyst deactivation, Appl. Catal. A Gen. 570 (2019) 96–106. doi:10.1016/j.apcata.2018.11.010.

[26] Lebedev, Improvements in or relating to the preparation of diolefines directly from alcohols, GB331482A, 1929.

[27] G. Natta, R. Rigamonti, Synthesis of butadiene from ethyl alcohol. Thermodynamic studies and the specific function of catalysts, Chim. Ind. 29 (1947) 195–200.

[28] B.B. Corson, H.E. Jones, C.E. Welling, J.A. Hinckley, E.E. Stahly, Butadiene from Ethyl Alcohol. Catalysis in the One-and Two-Stop Processes., Ind. Eng. Chem. 42 (1950) 359–373. doi:10.1021/ie50482a039.

[29] 1962-Bhattacharayya- One-step conversion of ethanol to butadiene- Binary oxide catalysts.pdf, (n.d.).

[30] V.F. Tretjakov, Methods of production divinyl, RU2459788C2, 2012.

[31] G.O. Ezinkwo, V.F. Tretjakov, R.M. Talyshinky, A.M. Ilolov, T.A. Mutombo, Creation of a continuous process for bio-ethanol to butadiene conversion via the use of a process initiator, Catal. Commun. 43 (2014) 207–212. doi:10.1016/j.catcom.2013.10.015.

[32] S. Kvisle, A. Aguero, R.P.A. Sneeden, Transformation of ethanol into 1,3-butadiene over magnesium oxide/silica catalysts, Appl. Catal. (1988). doi:10.1016/S0166-9834(00)80905-7.

[33] Y. Kitayama, M. Satoh, T. Kodama, Preparation of large surface area nickel magnesium silicate and its catalytic activity for conversion of ethanol into buta-1,3-diene, Catal. Letters. 36 (1996) 95–97. doi:10.1007/BF00807211.

[34] W. Janssens, E. V. Makshina, P. Vanelderen, F. De Clippel, K. Houthoofd, S. Kerkhofs, J.A. Martens, P.A. Jacobs, B.F. Sels, Ternary Ag/MgO-SiO $_2$ Catalysts for the Conversion of Ethanol into Butadiene, ChemSusChem. 8 (2015) 994–1008. doi:10.1002/cssc.201402894.

[35] C. Angelici, M.E.Z. Velthoen, B.M. Weckhuysen, P.C.A. Bruijnincx, Effect of Preparation Method and CuO Promotion in the Conversion of Ethanol into 1,3-Butadiene over SiO2–MgO Catalysts, ChemSusChem. 7 (2014) 2505–2515. doi:10.1002/cssc.201402361.

[36] X. Huang, Y. Men, J. Wang, W. An, Y. Wang, Highly active and selective binary MgO–SiO $_2$ catalysts for the production of 1,3-butadiene from ethanol, Catal. Sci. Technol. 7 (2017) 168–180. doi:10.1039/C6CY02091G.

[37] M.D. Jones, C.G. Keir, C. Di Iulio, R.A.M. Robertson, C. V. Williams, D.C. Apperley, Investigations into the conversion of ethanol into 1,3-butadiene, Catal. Sci. Technol. 1 (2011) 267. doi:10.1039/c0cy00081g.

[38] V.L. Sushkevich, I.I. Ivanova, V. V. Ordomsky, E. Taarning, Design of a Metal-Promoted Oxide Catalyst for the Selective Synthesis of Butadiene from Ethanol, ChemSusChem. 7 (2014) 2527–2536. doi:10.1002/cssc.201402346.

[39] V.L. Sushkevich, I.I. Ivanova, E. Taarning, Ethanol conversion into butadiene over Zr-containing molecular sieves doped with silver, Green Chem. 17 (2015) 2552–2559. doi:10.1039/C4GC02202E.

[40] R.A.L. Baylon, J. Sun, Y. Wang, Conversion of ethanol to 1,3-butadiene over Na doped ZnxZryOzmixed metal oxides, Catal. Today. 259 (2016) 446–452. doi:10.1016/j.cattod.2015.04.010.

[41] N. La-Salvia, J.J. Lovón-Quintana, G.P. Valença, Vapor-phase catalytic conversion of ethanol into 1,3-butadiene on Cr-Ba/MCM-41 catalysts, Brazilian J. Chem. Eng. 32 (2015) 489–500. doi:10.1590/0104-6632.20150322s00003039.

[42] Y. Sekiguchi, S. Akiyama, W. Urakawa, T.R. Koyama, A. Miyaji, K. Motokura, T. Baba, One-step catalytic conversion of ethanol into 1,3-butadiene using zinc-containing talc, Catal. Commun. 68 (2015) 20–24. doi:10.1016/j.catcom.2015.04.023.

[43] P.I. Kyriienko, O. V. Larina, S.O. Soloviev, S.M. Orlyk, C. Calers, S. Dzwigaj, Ethanol Conversion into 1,3-Butadiene by the Lebedev Method over MTaSiBEA Zeolites (M = Ag, Cu, Zn), ACS Sustain. Chem. Eng. 5 (2017) 2075–2083. doi:10.1021/acssuschemeng.6b01728.

[44] P.T. Patil, D. Liu, Y. Liu, J. Chang, A. Borgna, Improving 1,3-butadiene yield by Cs promotion in ethanol conversion, Appl. Catal. A Gen. 543 (2017) 67–74. doi:10.1016/j.apcata.2017.05.025.

[45] M. Zhang, J. Zhuang, Y. Yu, A DFT study on ZrO2 surface in the process of ethanol to 1,3-butadiene: A comprehensive mechanism elucidation, Appl. Surf. Sci. 458 (2018) 1026–1034. doi:10.1016/j.apsusc.2018.07.115.

[46] S. Akiyama, A. Miyaji, Y. Hayashi, M. Hiza, Y. Sekiguchi, T. ru Koyama, A. Shiga, T. Baba, Selective conversion of ethanol to 1,3-butadiene using germanium talc as catalyst, J. Catal. 359 (2018) 184–197. doi:10.1016/j.jcat.2018.01.001.

[47] T. Yan, W. Dai, G. Wu, S. Lang, M. Hunger, N. Guan, L. Li, T. Yan, M. Hunger, L. Li, G. Wu, W. Dai, N. Guan, Mechanistic Insights into One-Step Catalytic Conversion of Ethanol to Butadiene over Bifunctional Zn-Y/Beta Zeolite, ACS Catal. 8 (2018) 2760–2773. doi:10.1021/acscatal.8b00014.

[48] V.L. Dagle, M.D. Flake, T.L. Lemmon, J.S. Lopez, L. Kovarik, R.A. Dagle, Effect of the SiO2support on the catalytic performance of Ag/ZrO2/SiO2catalysts for the single-bed production of butadiene from ethanol, Appl. Catal. B Environ. 236 (2018) 576–587. doi:10.1016/j.apcatb.2018.05.055.

[49] G. Pomalaza, G. Vofo, M. Capron, F. Dumeignil, ZnTa-TUD-1 as an easily prepared, highly efficient catalyst for the selective conversion of ethanol to 1,3-butadiene, Green Chem. 20 (2018) 3203–3209. doi:10.1039/c8gc01211c.

[50] V.L. Sushkevich, I.I. Ivanova, S. Tolborg, E. Taarning, Meerwein-Ponndorf-Verley-Oppenauer reaction of crotonaldehyde with ethanol over Zr-containing catalysts, J. Catal. 316 (2014) 121–129. doi:10.1016/j.jcat.2014.04.019.

[51] M. Gao, Z. Liu, M. Zhang, L. Tong, Study on the mechanism of butadiene formation from ethanol, Catal. Letters. 144 (2014) 2071–2079. doi:10.1007/s10562-014-1370-x.

[52] S.K. Bhattacharyya, Kinetic study on the mechanism of the catalytic conversion of ethanol to butadiene, J. Catal. 7 (1967) 152–158. doi:10.1016/0021-9517(67)90053-X.

[53] S.K. Bhattacharyya, B.N. Avasthi, One-step catalytic conversion of ethanol to butadiene in a fluidized bed, Ind. Eng. Chem. Process Des. Dev. 2 (1963) 45–51. doi:10.1021/i260005a010.

[54] S. Da Ros, M.D. Jones, D. Mattia, M. Schwaab, F.B. Noronha, J.C. Pinto, Modelling the effects of reaction temperature and flow rate on the conversion of ethanol to 1,3-butadiene, Appl. Catal. A Gen. 530 (2017) 37–47. doi:10.1016/j.apcata.2016.11.008.

[55] Y. Xu, Z. Liu, Z. Han, M. Zhang, Ethanol/acetaldehyde conversion into butadiene over sol–gel ZrO_2 –SiO_2 catalysts doped with ZnO, RSC Adv. 7 (2017) 7140–7149. doi:10.1039/C6RA25139K.

[56] S. Da Ros, M.D. Jones, D. Mattia, J.C. Pinto, M. Schwaab, F.B. Noronha, S.A. Kondrat, T.C. Clarke, S.H. Taylor, Ethanol to 1,3-Butadiene Conversion by using ZrZn-Containing MgO/SiO2Systems Prepared by Co-precipitation and Effect of Catalyst Acidity Modification, ChemCatChem. 8 (2016) 2376–2386. doi:10.1002/cctc.201600331.

[57] A.G. Panov, J.J. Fripiat, Poisoning of aldol condensation reaction with H2O on acid catalysts, 57 (1999) 25–32. doi:10.1023/a:1019079011862.

[58] L. Yang, M. Hunger, W. Dai, L. Li, T. Yan, G. Wu, C. Wang, N. Guan, On the deactivation mechanism of zeolite catalyst in ethanol to butadiene conversion, J. Catal. 367 (2018) 7–15. doi:10.1016/j.jcat.2018.08.019.

[59] O. V. Larina, I.M. Remezovskyi, P.I. Kyriienko, S.O. Soloviev, S.M. Orlyk, 1,3-Butadiene production from ethanol–water mixtures over Zn–La–Zr–Si oxide catalyst, React. Kinet. Mech. Catal. 127 (2019) 903–915. doi:10.1007/s11144-019-01618-5.

[60] M. León, E. Díaz, S. Ordóñez, Ethanol catalytic condensation over Mg-Al mixed oxides derived from hydrotalcites, Catal. Today. 164 (2011) 436–442. doi:10.1016/j.cattod.2010.10.003.

[61] A. Chieregato, J.V. Ochoa, C. Bandinelli, G. Fornasari, F. Cavani, M. Mella, On the chemistry of ethanol on basic oxides: Revising mechanisms and intermediates in the lebedev and guerbet reactions, ChemSusChem. 8 (2015) 377–388. doi:10.1002/cssc.201402632.

[62] A. Ramadoss, K. Krishnamoorthy, S.J. Kim, Novel synthesis of hafnium oxide nanoparticles by precipitation method and its characterization, Mater. Res. Bull. 47 (2012) 2680–2684. doi:10.1016/j.materresbull.2012.05.051.

[63] K.D. Jung, O.S. Joo, S.H. Han, S.J. Uhm, I.J. Chung, Deactivation of Cu/ZnO catalyst during dehydrogenation of methanol, Catal. Letters. 35 (1995) 303–311. doi:10.1007/BF00807187.

[64] N.R. Draper, H. Smith, Applied regression analysis, John Wiley & Sons, 1998.

[65] H. Niiyama, S. Morii, E. Echigoya, Butadiene Formation from Ethanol over Silica-Magnesia Catalysts, Bull. Chem. Soc. Jpn. 45 (1972) 655–659. doi:10.1246/bcsj.45.655.

[66] O. V. Larina, P.I. Kyriienko, S.O. Soloviev, Ethanol Conversion to 1,3-Butadiene on ZnO/MgO-SiO2 Catalysts: Effect of ZnO Content and MgO:SiO2 Ratio, Catal. Letters. 145 (2015) 1162–1168. doi:10.1007/s10562-015-1509-4.

[67] D. Dussol, N. Cadran, N. Laloue, L. Renaudot, J.M. Schweitzer, New insights of butadiene production from ethanol: Elucidation of concurrent reaction pathways and kinetic study, Chem. Eng. J. (2019). doi:10.1016/j.cej.2019.123586.

[68] M. Legendre, D. Cornet, Catalytic oxidation of ethanol over tantalum oxide, J. Catal. (1972). doi:10.1016/0021-9517(72)90218-7.

Appendix

Table A1. Catalytic tests (from 1 to 9) used to draw the kinetic curves. Ethanol conversion and carbon-based yield to products (%). All tests were performed at 360°C and an ethanol partial pressure of 0.21 bar. Only ethanol is fed.

Test	**1**	**2**	**3**	**4**	**5**	**6**	**7**	**8**	**9**	
Catalyst (g)	**1**	**1**	**1**	**1**	**1**	**1**	**0.5**	**0.5**	**0.5**	**SDmax**
WHSV (h^{-1})	**1.12**	**1.87**	**3.73**	**1.87**	**1.12**	**1.87**	**5.6**	**11.2**	**5.6**	
Ethanol conversion	87.0	75.7	67.3	82.2	87.2	74.9	58.8	49.6	64.8	1.6
					Yield					
1,3-Butadiene	36.9	33.1	28.0	36.21	37.45	29.86	25.23	14.16	20.92	1.60
Acetaldehyde	6.41	11.34	16.01	12.40	5.86	9.30	17.90	21.77	17.99	1.70
Crotonaldehyde (cis+trans)	0.13	0.12	0.20	0.16	0.04	0.05	0.32	0.50	0.40	0.10
3-Hidroxy Butanal	0.00	0.00	0.00	0.00	0.00	0.00	0.00	0.00	0.00	0.00
Crotyl alcohol	0.00	0.00	0.00	0.00	0.00	0.00	0.00	0.00	0.00	0.00
Ethene	3.91	2.90	2.10	3.04	3.58	2.33	1.64	1.12	1.51	0.20
Diethyl ether	1.11	1.14	1.01	1.01	0.86	0.85	0.59	0.53	0.62	0.10
Ethyl acetate	0.50	0.33	0.42	0.31	0.38	0.41	0.34	0.20	0.30	0.08
Propene	1.84	1.32	0.94	1.46	1.72	1.11	0.79	0.35	0.69	0.10
Propanal	2.20	2.10	1.92	2.36	2.14	2.03	1.69	0.92	1.49	0.10
Butenes	3.81	3.01	2.31	3.44	3.56	2.51	1.83	0.98	1.46	0.16
Butanol	0.43	0.73	1.04	0.67	0.44	0.61	1.28	1.01	1.06	0.10
Butanal	0.60	1.02	0.81	0.78	0.50	0.82	0.73	0.60	0.79	0.15
C6+	18.60	12.31	8.13	14.33	21.01	15.84	6.09	3.45	5.51	2.20
Hexene	0.33	0.13	0.23	0.26	0.25	0.21	0.16	0.07	0.14	0.02
Hexane	0.44	0.30	0.23	0.33	0.37	0.30	0.27	0.15	0.23	0.02
Hexanol	0.28	0.22	0.20	0.25	0.29	0.23	0.17	0.09	0.14	0.04
Methanol	0.62	0.61	0.43	0.55	0.65	0.53	0.46	0.25	0.37	0.08
Isopropanol	0.01	0.11	0.02	0.05	0.15	0.13	0.07	0.00	0.00	0.02
Acetone	0.41	0.53	0.70	0.41	0.36	0.67	0.50	0.31	0.44	0.15
CO_2	0.20	0.10	0.04	0.12	0.19	0.10	0.17	0.03	0.07	0.05
CO	0.03	0.02	0.01	0.02	0.02	0.01	0.01	0.01	0.01	0.00
CH_4	0.09	0.06	0.05	0.06	0.06	0.04	0.05	0.04	0.05	0.01

Carbon balance error < 10%

SDmax = maximum standard deviation among all catalytic tests

Table A2. Catalytic tests (from 10 to 18) used to draw the kinetic curves. Ethanol conversion and carbon-based yield to products (%). All tests were performed at 360°C and an ethanol partial pressure of 0.21 bar. Only ethanol is fed.

Test	**10**	**11**	**12**	**13**	**14**	**15**	**16**	**17**	**18**	
Catalyst (g)	**0.5**	**0.5**	**0.5**	**0.5**	**0.1**	**0.1**	**0.1**	**2**	**2**	**SDmax**
WHSV (h^{-1})	**11.2**	**5.6**	**3.73**	**7.0**	**11.2**	**30**	**50**	**1.12**	**1.12**	
Ethanol conversion	49.9	60.6	62.5	56.1	43.7	30.6	22.6	84.4	80.5	1.6
					Yield					
1,3-Butadiene	14.57	22.29	22.14	16.92	11.41	5.45	2.09	37.17	34.94	1.60
Acetaldehyde	21.54	18.68	16.32	19.40	17.97	16.91	16.69	6.75	6.80	1.70
Crotonaldehyde (cis+trans)	0.40	0.28	0.29	0.39	0.46	0.47	0.36	0.03	0.09	0.10
3-Hidroxy Butanal	0.00	0.00	0.00	0.00	0.00	0.00	0.00	0.00	0.00	0.00
Crotyl alcohol	0.00	0.00	0.00	0.00	0.00	0.00	0.00	0.00	0.00	0.00
Ethene	1.11	1.60	1.56	1.21	1.00	0.86	0.46	3.55	2.81	0.20
Diethyl ether	0.57	0.64	0.70	0.55	0.33	0.23	0.11	1.13	1.09	0.10
Ethyl acetate	0.22	0.29	0.38	0.24	0.10	0.55	0.00	0.43	0.44	0.08
Propene	0.22	0.64	0.74	0.54	0.43	0.26	0.10	1.58	1.33	0.10
Propanal	0.95	1.53	1.72	1.18	0.92	0.34	0.11	2.11	2.10	0.10
Butenes	1.21	1.63	1.62	1.41	1.00	0.87	0.49	3.46	3.01	0.16
Butanol	1.17	1.21	1.12	1.26	0.89	0.63	0.29	0.41	0.55	0.10
Butanal	0.68	0.76	0.89	0.72	0.41	0.31	0.15	0.54	0.83	0.15
C6+	3.59	5.14	8.18	7.69	4.92	1.57	0.54	18.28	19.57	2.20
Hexene	0.07	0.15	0.16	0.10	0.08	0.01	0.00	0.26	0.24	0.02
Hexane	0.16	0.24	0.24	0.19	0.15	0.06	0.02	0.33	0.29	0.02
Hexanol	0.07	0.12	0.21	0.15	0.12	0.04	0.04	0.16	0.21	0.04
Methanol	0.26	0.42	0.42	0.29	0.23	0.20	0.27	0.43	0.64	0.08
Isopropanol	0.06	0.07	0.10	0.05	0.04	0.04	0.01	0.12	0.12	0.02
Acetone	0.27	0.41	0.44	0.48	0.22	0.09	0.05	0.35	0.32	0.15
CO_2	0.08	0.03	0.12	0.01	0.01	0.02	0.01	0.15	0.13	0.05
CO	0.00	0.01	0.02	0.01	0.00	0.03	0.02	0.00	0.00	0.00
CH_4	0.04	0.04	0.06	0.05	0.04	0.11	0.06	0.03	0.04	0.01

Carbon balance error < 10%

SDmax = maximum standard deviation among all catalytic tests

Table A3. Experimental results of the conversion of ethanol to 1,3-butadiene over the one-step mixed Hf-Zn catalyst at different reaction temperatures (T), space velocities (WHSV), and water contents in the ethanol feed.

T	Water	WHSV	TOS	X	Y_{BD}	Selectivity (%)						
(°C)	(wt%)	(h^{-1})	(h)	(%)	(%)	BD	ET	DEE	C4	AC	C_{6+}	Others
340	0	1.12	19	69.2	28.5	41.2	4.6	1.6	4.6	10.8	13.6	23.5
	0	3.2	15	52.9	23.3	44.1	3.8	1.6	3.8	23.2	6.9	16.6
	0	6.1	10	41.6	15.7	37.9	3.3	1.6	2.8	36.2	3.9	14.2
	0	9.8	5	32.9	10.7	32.8	3.3	1.7	2.3	43.6	4.1	12.1
	7.5	1.12	19	59.9	29.8	49.8	9.0	3.5	4.9	19.9	2.9	9.9
	7.5	3.2	15	45.8	17.7	38.7	6.3	2.8	2.8	40.0	2.6	6.8
	7.5	6.1	10	33.4	9.1	27.3	5.3	2.6	1.7	55.7	1.8	5.5
	7.5	8.0	4.5	25.4	5.8	23.1	5.1	2.5	1.4	61.5	1.6	4.7
	15	1.12	16	54.9	25.5	46.6	10.5	4.0	4.3	24.2	2.3	8.1
	15	3.2	11	35.2	11.7	33.5	7.4	3.3	2.2	47.2	1.2	5.2
	15	6.1	7	29.2	6.5	22.3	6.2	2.9	1.2	62.5	0.9	3.8
	15	8.0	4	24.6	4.9	20.0	6.0	2.8	1.2	65.3	1.1	3.6
360	0	1.12	22	87.1	39.3	45.1	5.6	1.1	5.6	9.6	13.3	19.6
	0	3.2	16	70.9	33.1	46.7	4.2	1.2	4.2	22.9	5.7	14.8
	0	6.1	11	60.4	25.5	42.3	3.7	1.2	3.5	28.1	5.6	15.5
	0	9.8	7	51.4	20.0	38.9	3.5	1.2	2.9	33.8	4.9	14.7
	3.75	1.12	23	82.2	41.2	50.2	9.2	2.2	5.3	15.5	3.3	14.4
	3.75	3.2	19	68.5	32.1	46.9	7.6	2.2	4.1	24.7	2.8	11.6
	3.75	6.1	12	48.4	18.9	39.3	5.8	2.1	2.6	3.0	2.3	45.0
	3.75	8.0	7	44.1	16.1	36.4	5.5	2.1	2.3	44.2	1.8	7.7
	7.5	1.12	26	78.0	38.3	49.1	9.5	2.3	5.3	16.6	3.9	13.2
	7.5	3.2	18	59.9	26.0	43.5	6.8	2.1	3.5	32.4	2.3	9.4
	7.5	6.1	13	48.6	17.6	36.3	5.6	2.0	2.5	43.5	1.8	8.3
	7.5	8.0	8	43.7	15.4	35.4	5.3	1.9	2.3	44.9	2.1	8.1
	15	1.12	27	79.1	37.4	47.3	11.4	2.6	5.1	18.4	3.3	11.9
	15	3.2	21	59.4	24.0	40.5	8.4	2.5	3.1	35.8	1.9	7.8
	15	6.1	14	45.8	14.4	31.5	6.9	2.5	2.0	49.8	1.2	6.1
	15	8.0	7	43.4	12.5	28.8	6.4	2.4	1.6	53.1	1.7	5.9
380	0	1.12	23	95.2	27.4	28.7	3.4	0.5	2.9	9.2	34.2	23.0
	0	3.2	18	90.0	30.8	34.2	3.5	0.5	3.4	15.3	21.9	21.1
	0	6.1	12	77.4	32.3	41.8	4.3	0.9	3.8	24.6	7.9	16.6
	0	9.8	7	66.7	28.6	42.9	4.5	1.1	3.6	28.3	5.7	13.9
	7.5	1.12	22	96.5	48.0	49.7	8.7	1.3	5.4	11.6	8.4	14.8
	7.5	3.2	18	85.0	39.3	46.2	7.3	1.3	4.1	26.2	2.7	12.2
	7.5	6.1	12	72.3	30.7	42.4	6.4	1.6	3.2	34.2	2.2	10.0
	7.5	8.0	6	65.0	26.6	40.9	6.1	1.7	2.8	36.5	2.3	9.7
	15	1.12	18	98.1	45.4	46.3	10.3	1.4	5.1	15.4	6.9	14.6
	15	3.2	14	84.4	38.8	45.9	8.6	1.5	3.8	27.1	2.5	10.5
	15	6.1	8	69.0	27.4	39.7	7.1	1.7	2.8	37.9	2.5	8.3
	15	8.0	5	64.7	25.5	39.4	6.9	1.8	2.5	38.7	2.5	8.2

Note: TOS= time on stream, X= ethanol conversion, Y= yield, BD= butadiene; ET=ethene; DEE=diethyl ether; C4= butenes; AC=Acetaldehyde; C_{6+}= heavy compounds. "Others" comprises a mixture of minor sub-products such as acetone, ethyl acetate, butanal, butanol, 2-ethyl-hexenal, CO, CO_2 and CH_4.

Table A4. Operating condition and inlet flows of the tests gathered in Table A3.

Test	Catalyst load (g)	WHSV (h^{-1})	T (ºC)	Mole flow (mol/h)		
				Ethanol	Nitrogen	Water
1	1.0	1.12	360	0.0243	0.0911	-
2	1.0	1.87	360	0.0407	0.1527	-
3	1.0	3.73	360	0.0811	0.3027	-
4	1.0	1.87	360	0.0407	0.1527	-
5	1.0	1.12	360	0.0243	0.0911	-
6	1.0	1.87	360	0.0407	0.1527	-
7	0.5	5.60	360	0.0609	0.2277	-
8	0.5	11.2	360	0.1217	0.4554	-
9	0.5	5.60	360	0.0609	0.2277	-
10	0.5	11.2	360	0.1217	0.4554	-
11	0.5	5.60	360	0.0609	0.2277	-
12	0.5	3.73	360	0.0405	0.1527	-
13	0.5	7.00	360	0.0761	0.2839	-
14	0.1	11.2	360	0.0243	0.0911	-
15	0.1	30.0	360	0.0652	0.2438	-
16	0.1	50.0	360	0.1087	0.4071	-
17	2.0	1.12	360	0.0487	0.1821	-
18	2.0	1.12	360	0.0487	0.1821	-
19	0.5	9.80	340	0.1065	0.3964	-
20	0.5	6.10	340	0.0663	0.2464	-
21	0.5	3.20	340	0.0348	0.1286	-
22	0.5	1.12	340	0.0122	0.0455	-
23	0.5	9.80	360	0.1065	0.3964	-
24	0.5	6.10	360	0.0663	0.2464	-
25	0.5	3.20	360	0.0348	0.1286	-
26	0.5	1.12	360	0.0122	0.0455	-
27	0.5	9.80	380	0.1065	0.3964	-
28	0.5	6.10	380	0.0663	0.2464	-
29	0.5	3.20	380	0.0348	0.1286	-
30	0.5	1.12	380	0.0122	0.0455	-
31	1.0	8.00	340	0.0870	0.3054	0.0183
32	1.0	6.10	340	0.0663	0.2330	0.0139
33	1.0	3.20	340	0.0348	0.1232	0.0072
34	1.0	1.12	340	0.0122	0.0429	0.0028
35	1.0	8.00	340	0.0870	0.2866	0.0394
36	1.0	6.10	340	0.0663	0.2196	0.0300
37	0.5	3.20	340	0.0348	0.1152	0.0156
38	0.5	1.12	340	0.0122	0.0402	0.0056
39	0.5	8.00	360	0.0870	0.3080	0.0020
40	0.5	6.10	360	0.0663	0.2357	0.0016
41	0.5	3.20	360	0.0348	0.1232	0.0008
42	0.5	1.12	360	0.0122	0.0429	0.0003
43	0.5	8.00	360	0.0870	0.3054	0.0183
44	0.1	6.10	360	0.0663	0.2330	0.0139
45	0.1	3.20	360	0.0348	0.1232	0.0072
46	0.1	1.12	360	0.0122	0.0429	0.0028
47	2.0	8.00	360	0.0870	0.2866	0.0394
48	2.0	6.10	360	0.0663	0.2196	0.0300
49	0.5	3.20	360	0.0348	0.1152	0.0156
50	0.5	1.12	360	0.0122	0.0402	0.0056
51	0.5	8.00	380	0.0870	0.3054	0.0183
52	0.5	6.10	380	0.0663	0.2330	0.0139
53	0.5	3.20	380	0.0348	0.1232	0.0072
54	0.5	1.12	380	0.0122	0.0429	0.0028
55	0.5	8.00	380	0.0870	0.2866	0.0394
56	0.5	6.10	380	0.0663	0.2196	0.0300
57	0.5	3.20	380	0.0348	0.1152	0.0156
58	0.5	1.12	380	0.0122	0.0402	0.0056

Table A5. Mole flows at the reactor outlet of the tests gathered in Table A3. BD=1,3-butadiene, Ac=acetaldehyde, C_4=butenes, ButOH=butanol, Et=ethene, C_{6+}=heavy compounds, DEE=diethyl ether, ButA=butanal, EtOH=ethanol.

Test	Mole flow (mol/h)										
	BD	Ac	C_4	ButOH	Et	C6+	DEE	ButA	EtOH	H_2O	H_2
1	0.0045	0.0016	0.0005	0.0000	0.0009	0.0007	0.0001	0.0019	0.0032	0.0168	0.0143
2	0.0067	0.0046	0.0006	0.0001	0.0012	0.0008	0.0002	0.0023	0.0099	0.0228	0.0206
3	0.0114	0.0130	0.0009	0.0004	0.0017	0.0010	0.0004	0.0035	0.0265	0.0362	0.0370
4	0.0074	0.0051	0.0007	0.0001	0.0012	0.0009	0.0002	0.0023	0.0073	0.0248	0.0226
5	0.0046	0.0014	0.0004	0.0001	0.0009	0.0008	0.0001	0.0018	0.0031	0.0171	0.0148
6	0.0061	0.0038	0.0005	0.0001	0.0009	0.0010	0.0002	0.0028	0.0102	0.0226	0.0215
7	0.0064	0.0109	0.0004	0.0003	0.0009	0.0005	0.0002	0.0030	0.0250	0.0209	0.0249
8	0.0086	0.0265	0.0006	0.0006	0.0014	0.0006	0.0003	0.0040	0.0614	0.0283	0.0449
9	0.0077	0.0109	0.0006	0.0004	0.0010	0.0006	0.0002	0.0031	0.0214	0.0243	0.0268
10	0.0089	0.0262	0.0007	0.0007	0.0014	0.0007	0.0003	0.0038	0.0609	0.0291	0.0449
11	0.0068	0.0114	0.0005	0.0004	0.0010	0.0005	0.0002	0.0029	0.0240	0.0216	0.0254
12	0.0045	0.0066	0.0003	0.0002	0.0006	0.0005	0.0001	0.0022	0.0152	0.0156	0.0179
13	0.0064	0.0148	0.0005	0.0005	0.0009	0.0009	0.0002	0.0029	0.0334	0.0234	0.0322
14	0.0014	0.0044	0.0001	0.0001	0.0002	0.0002	0.0000	0.0008	0.0137	0.0052	0.0082
15	0.0018	0.0110	0.0003	0.0002	0.0006	0.0002	0.0001	0.0013	0.0453	0.0072	0.0156
16	0.0011	0.0181	0.0003	0.0002	0.0005	0.0001	0.0001	0.0011	0.0841	0.0051	0.0212
17	0.0090	0.0033	0.0008	0.0001	0.0017	0.0014	0.0003	0.0033	0.0076	0.0327	0.0280
18	0.0085	0.0033	0.0007	0.0001	0.0014	0.0015	0.0003	0.0029	0.0095	0.0312	0.0279
19	0.0057	0.0153	0.0004	0.0004	0.0012	0.0002	0.0003	0.0017	0.0715	0.0171	0.0248
20	0.0052	0.0100	0.0004	0.0003	0.0009	0.0002	0.0002	0.0016	0.0387	0.0152	0.0183
21	0.0041	0.0043	0.0003	0.0002	0.0007	0.0002	0.0002	0.0014	0.0164	0.0123	0.0114
22	0.0017	0.0009	0.0002	0.0000	0.0004	0.0002	0.0001	0.0010	0.0037	0.0063	0.0052
23	0.0107	0.0185	0.0008	0.0005	0.0019	0.0004	0.0003	0.0035	0.0518	0.0315	0.0364
24	0.0085	0.0112	0.0007	0.0003	0.0015	0.0003	0.0002	0.0028	0.0263	0.0251	0.0256
25	0.0058	0.0057	0.0005	0.0001	0.0011	0.0002	0.0002	0.0017	0.0101	0.0168	0.0151
26	0.0024	0.0010	0.0003	0.0000	0.0006	0.0002	0.0001	0.0010	0.0016	0.0083	0.0064
27	0.0152	0.0201	0.0013	0.0004	0.0032	0.0006	0.0004	0.0046	0.0355	0.0450	0.0455
28	0.0107	0.0126	0.0010	0.0002	0.0022	0.0006	0.0002	0.0041	0.0150	0.0336	0.0330
29	0.0054	0.0048	0.0005	0.0001	0.0011	0.0011	0.0001	0.0032	0.0035	0.0221	0.0229
30	0.0015	0.0011	0.0002	0.0000	0.0004	0.0006	0.0000	0.0013	0.0006	0.0086	0.0094
31	0.0026	0.0136	0.0002	0.0001	0.0011	0.0001	0.0003	0.0004	0.0649	0.0260	0.0170
32	0.0030	0.0123	0.0002	0.0001	0.0012	0.0001	0.0003	0.0005	0.0442	0.0227	0.0164
33	0.0031	0.0064	0.0002	0.0001	0.0010	0.0001	0.0002	0.0004	0.0189	0.0159	0.0105
34	0.0018	0.0014	0.0002	0.0000	0.0007	0.0000	0.0001	0.0003	0.0049	0.0081	0.0039
35	0.0021	0.0139	0.0001	0.0001	0.0013	0.0000	0.0003	0.0003	0.0656	0.0461	0.0167
36	0.0022	0.0121	0.0001	0.0001	0.0012	0.0000	0.0003	0.0003	0.0469	0.0366	0.0148
37	0.0021	0.0058	0.0001	0.0001	0.0009	0.0000	0.0002	0.0002	0.0226	0.0215	0.0083
38	0.0016	0.0016	0.0001	0.0000	0.0007	0.0000	0.0001	0.0002	0.0055	0.0102	0.0036
39	0.0070	0.0169	0.0004	0.0002	0.0021	0.0001	0.0004	0.0012	0.0486	0.0214	0.0261
40	0.0063	0.0128	0.0004	0.0002	0.0019	0.0001	0.0003	0.0011	0.0342	0.0191	0.0212
41	0.0056	0.0059	0.0005	0.0001	0.0018	0.0001	0.0003	0.0013	0.0109	0.0170	0.0137
42	0.0025	0.0015	0.0003	0.0000	0.0009	0.0001	0.0001	0.0007	0.0022	0.0079	0.0052
43	0.0067	0.0171	0.0004	0.0002	0.0020	0.0001	0.0004	0.0014	0.0489	0.0372	0.0263
44	0.0058	0.0140	0.0004	0.0002	0.0018	0.0001	0.0003	0.0012	0.0341	0.0303	0.0218
45	0.0045	0.0067	0.0004	0.0001	0.0014	0.0001	0.0002	0.0009	0.0139	0.0200	0.0128
46	0.0023	0.0016	0.0003	0.0000	0.0009	0.0001	0.0001	0.0006	0.0027	0.0099	0.0050
47	0.0054	0.0200	0.0003	0.0002	0.0024	0.0001	0.0005	0.0009	0.0493	0.0554	0.0273
48	0.0048	0.0151	0.0003	0.0002	0.0021	0.0001	0.0004	0.0008	0.0359	0.0439	0.0212
49	0.0042	0.0074	0.0003	0.0001	0.0017	0.0001	0.0003	0.0007	0.0141	0.0277	0.0128
50	0.0023	0.0018	0.0002	0.0000	0.0011	0.0000	0.0001	0.0006	0.0025	0.0127	0.0050
51	0.0116	0.0207	0.0008	0.0003	0.0035	0.0002	0.0005	0.0025	0.0304	0.0508	0.0365
52	0.0102	0.0164	0.0008	0.0002	0.0031	0.0002	0.0004	0.0022	0.0183	0.0425	0.0303
53	0.0068	0.0078	0.0006	0.0001	0.0022	0.0001	0.0002	0.0017	0.0052	0.0269	0.0174
54	0.0029	0.0014	0.0003	0.0000	0.0010	0.0002	0.0001	0.0009	0.0004	0.0121	0.0065
55	0.0111	0.0218	0.0007	0.0003	0.0039	0.0002	0.0005	0.0021	0.0307	0.0709	0.0369
56	0.0091	0.0173	0.0006	0.0002	0.0032	0.0002	0.0004	0.0017	0.0205	0.0560	0.0297
57	0.0067	0.0080	0.0006	0.0001	0.0025	0.0001	0.0002	0.0015	0.0054	0.0351	0.0172
58	0.0028	0.0018	0.0003	0.0000	0.0012	0.0001	0.0001	0.0009	0.0002	0.0146	0.0066

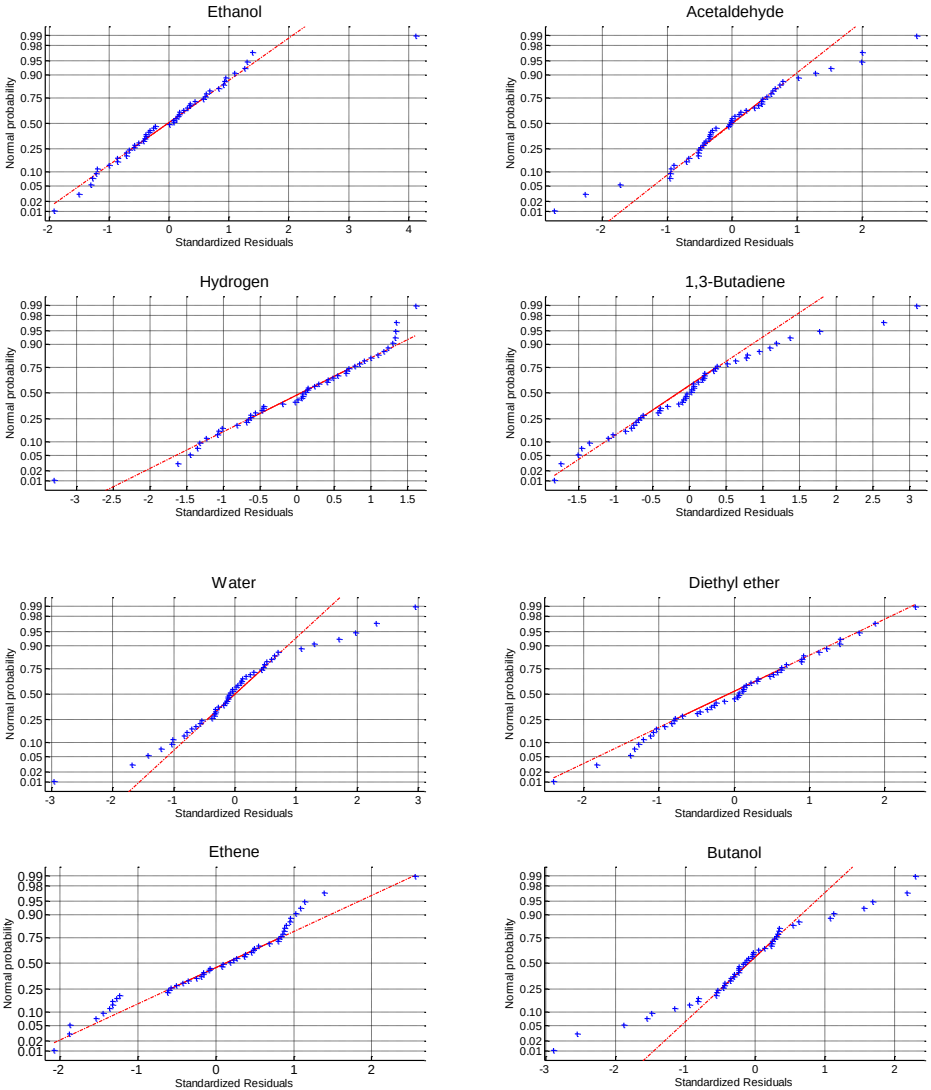

Figure A1. Normal distribution of standardized residuals.

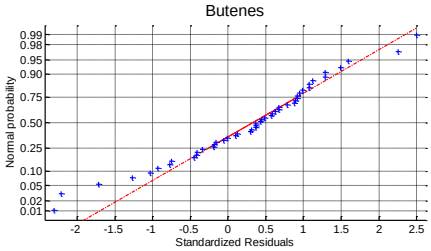

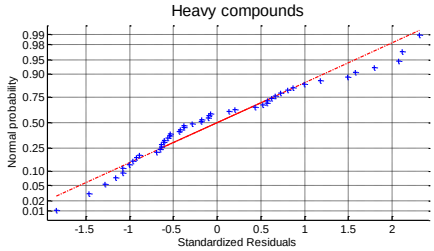

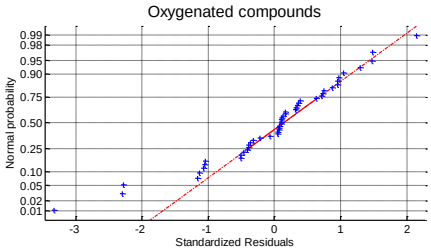

Figure A1 cont. Normal distribution of standardized residuals.

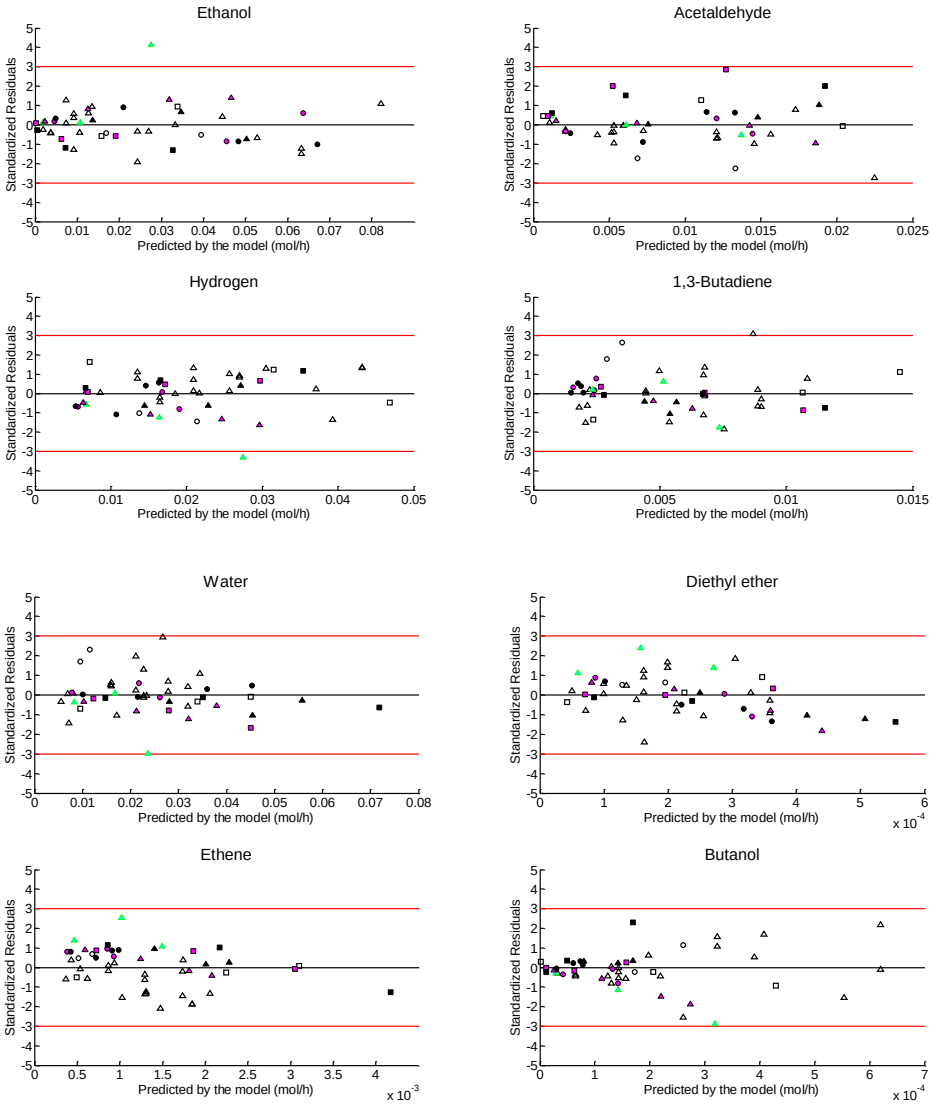

Figure A2. Standardized residuals versus predicted values. Temperature of experiments 340°C (circle), 360°C (triangle) and 380°C (square). Water content in ethanol feed: blank: 0 wt%, cyan: 3.75 wt%, magenta: 7.5 wt%, black: 15 wt%)

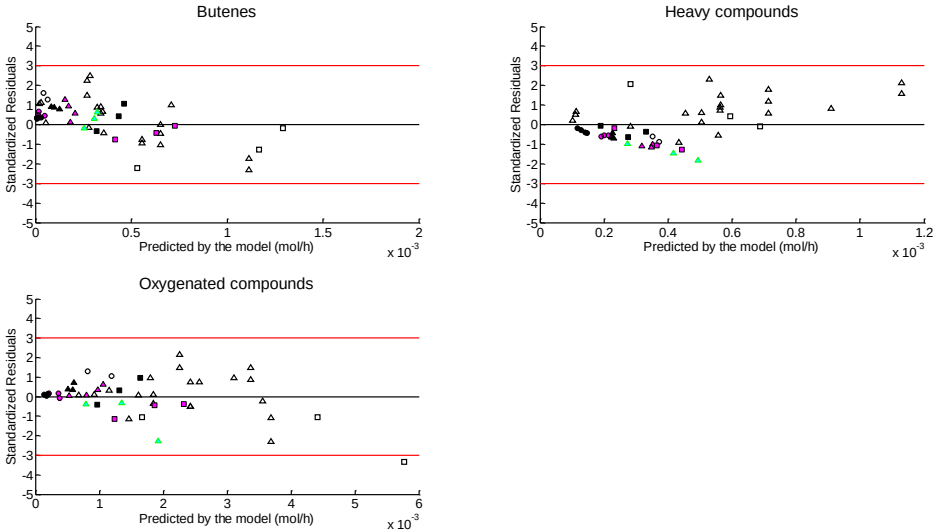

Figure A2 cont**.** Standardized residuals versus predicted values. Temperature of experiments 340°C (circle), 360°C (triangle) and 380°C (square). Water content in ethanol feed: blank: 0 wt%, cyan: 3.75 wt%, magenta: 7.5 wt%, black: 15 wt%)

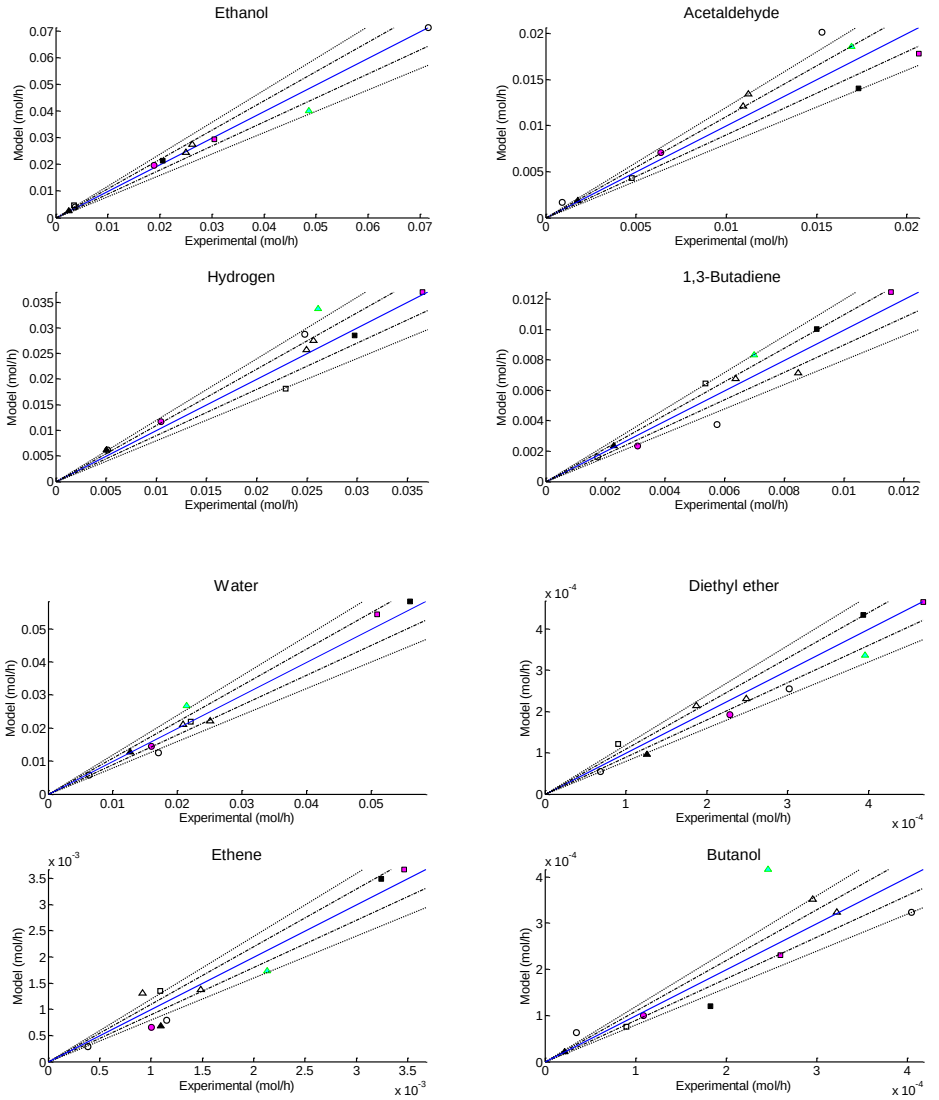

Figure A3. Comparison plots between the experimental and model flow rates. (● 340°C, ▲ 360°C and ■ 380°C, empty symbols 0%w/w water, cyan 3.75%w/w water, magenta 7.5%w/w water and black 15%w/w water). 10% error band (dash-dot line), 20% error band (dotted line).

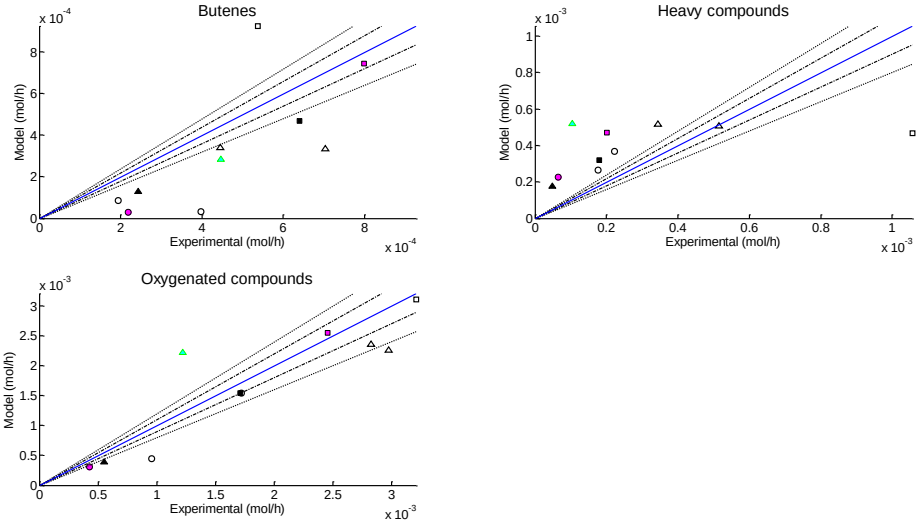

Figure A3 cont. Comparison plots between the experimental and model flow rates. (● 340°C, ▲ 360°C and ■ 380°C, empty symbols 0%w/w water, cyan 3.75%w/w water, magenta 7.5%w/w water and black 15%w/w water). 10% error band (dash-dot line), 20% error band (dotted line).

Appendix